IMPLICATIONS FROM LIQUEFACTION OBSERVATIONS IN NEW ZEALAND FOR INTERPRETING PALEOLIQUEFACTION DATA IN THE CENTRAL EASTERN UNITED STATES (CEUS)

Russell A. Green[1], Brett W. Maurer[2], Brendon A. Bradley[3], Liam Wotherspoon[4], Misko Cubrinovski[5]

U.S. Geological Society Final Technical Report
Award No. G12AP20002
Term: Dec. 2011 – Aug. 2013

Principal Investigator:

Professor Russell A. Green, Ph.D., P.E.
Department of Civil and Environmental Engineering
Virginia Tech
Blacksburg, VA 24061
P: 1-540-231-9826 F: 1-540-231-7532 E: rugreen@vt.edu

November 30, 2013

---

1 Virginia Tech, Department of Civil and Environmental Engineering, 120 B Patton Hall, Blacksburg, VA 24061. Phone: 1-540-231-9826. Fax: 1-540-231-7532. Email: rugreen@vt.edu

[2] Virginia Tech, Department of Civil and Environmental Engineering, 20 Patton Hall, Blacksburg, VA 24061. Phone: 1-315-521-1054. Fax: 1-540-231-7532. Email: bwmaurer@vt.edu

[3] University of Canterbury, Department of Civil and Natural Resources Engineering, Private Bag 4800, Christchurch, New Zealand 8140. Phone: 64-3-364-2987. Fax: 64-3-364-2758. Email: brendon.bradley@canterbury.ac.nz

[4] University of Auckland, Department of Civil and Environmental Engineering, Private Bag 92019, Auckland, New Zealand 1142. Phone: 64-9-373-7599. Fax: 64-9-373-7462. Email: l.wotherspoon@auckland.ac.nz

[5] University of Canterbury, Department of Civil and Natural Resources Engineering, Private Bag 4800, Christchurch, New Zealand 8140. Phone: 64-3-364-2251. Fax: 64-3-364-2758. Email: misko.cubinovski@canterbury.ac.nz

ABSTRACT

For liquefaction-based paleoseismic analyses, proper interpretation of paleoliquefaction evidence is critical, with the difficulty of interpretation increasing for sites of recurrent liquefaction induced by earthquakes spaced closely in time. Furthermore, even with proper field interpretations, the efficacies of numerical back-calculation techniques are unknown. The study presented herein aims to address these issues by studying sites of liquefaction induced by the 2010-2011 Canterbury (New Zealand) earthquake sequence, which resulted in a liquefaction dataset of unprecedented size and quality. The combination of well-documented liquefaction response, densely-recorded ground motions, and detailed subsurface characterization provides an unprecedented opportunity to address prevailing uncertainties related to paleoliquefaction field interpretation and back-calculation techniques. Towards this end, the objectives of this study are (1) to evaluate the accuracies of methods proposed to back-calculate paleoearthquake magnitudes by using the methods to estimate the magnitudes of the Canterbury earthquakes and comparing the results with the actual magnitudes; (2) to determine whether the recurrence of liquefaction can be discerned from earthquake-induced liquefaction structures; and (3) to determine whether liquefaction resistance is reduced following recent liquefaction.

With respect to objective (1), it is shown that when the earthquake source location and mechanism are known, back-analysis methods are capable of accurately deriving seismic parameters from liquefaction evidence. However, because the source location and mechanism are often unknown in paleoliquefaction studies, and because accurate interpretation is shown to be more difficult in such cases, new analysis techniques are proposed herein. For the "site-specific approach", an objective parameter is proposed to geospatially assess the likelihood of any source location, enabling an analyst to more accurately estimate the most likely magnitude of the causative earthquake. For the "magnitude-bound approach", consideration of liquefaction susceptibility is likewise shown to improve the accuracy of interpretation. This analysis demonstrates the challenges of applying these methods, provides insight into their potential accuracies, and provides a framework for performing paleoliquefaction analyses worldwide. With respect to objective (2), a series of trenches were dug through undisturbed liquefaction features at sites of recurrent liquefaction. The structure of blow material was mapped in detail and extensive sampling was performed to analyze spatial trends in particle size gradation. Multiple episodes of liquefaction were clearly evident, separated by silt laminations whose thickness was proportional to the fines content of the liquefied source stratum. However, there were no ubiquitous trends in the spatial sorting of grain sizes in the coarser fraction of the ejecta underlying silt seams, even though these strata were often 10 cm thick and flowed laterally up to several meters. Consequently, recurrent liquefaction cannot be disproven by a lack of trends in the spatial distribution of grain sizes or by lack of inter-event silt seams, if the liquefaction source stratum lacks sufficient fines. Lastly, with respect to objective (3), an assessment of aging-correction factors at sites of recurrent liquefaction was performed to determine whether prior liquefaction reduced liquefaction resistance. Short time-scale aging correction factors for CRR-based triggering curves (i.e., $K_{DR} < 1$) were found to be plausible at sites with prior moderate-to-severe liquefaction. However, while $K_{DR} < 1$ correction factors were found to be plausible, post-liquefaction reductions in reliquefaction resistance did not exacerbate liquefaction hazard to the built-environment. Although a modified K_{DR} relation is proposed, considerable scatter still exists in the dataset, and judicious use of aging corrections in paleoliquefaction analyses is thus advised.

CONTENTS

I. Preface

The interpretation of paleoseismic histories from liquefaction evidence requires a detailed field interpretation of numerous liquefaction features, followed by a quantitative back-analysis to estimate the causative earthquake's magnitude. At present, uncertainties exist with respect to the accuracies of both field interpretation and quantitative back-analysis methods. Owing to these uncertainties, computed seismic hazards remain controversial in regions where seismic records are inferred from liquefaction evidence, such as the central eastern U.S. (CEUS). In the study presented herein, parsed into Parts A, B, and C, data from the 2010-2011 Canterbury, New Zealand earthquake sequence is used to evaluate the accuracies of paleoliquefaction analysis techniques, and to explore the challenges and uncertainties of their application. In addition, novel paleoliquefaction interpretation and analysis techniques are proposed and evaluated.

In part A, the efficacies of numerical back-analyses are assessed assuming that liquefaction effects would be accurately interpreted in a paleoliquefaction field study. This assumption is not intended to diminish the importance or trivialize the difficulty of field interpretation; the objective of Part A is to evaluate the accuracies of quantitative back-analysis methods, where Parts B and C address nuances of interpretation. In part B, the difficulty of discerning recurrent liquefaction from the physical structure of liquefaction features is discussed. For any back-analysis method, deciphering whether liquefaction features are the result of one earthquake or multiple earthquakes closely spaced in time is critical. As such, the difficulty of field interpretation increases for spatiotemporally neighboring earthquakes [e.g., the 1811-1812 events in the New Madrid Seismic Zone (NMSZ)]. Accordingly, to better interpret recurrent paleoliquefaction in the field, liquefaction features in New Zealand were studied to determine whether episodic liquefaction can be discerned from the structure and grain size distribution of vented sediments. In Part C, "aging effects" (a nuance of performing numerical back-analyses at sites of recurrent liquefaction) are assessed. Although not yet fully understood, studies suggest reliquefaction resistance is reduced after recent liquefaction. As such, the susceptibility of liquefaction triggering and severity of liquefaction manifestation may be greater than expected for sites of repeat liquefaction closely spaced in time. Of relevance to paleoliquefaction analyses, the back-calculated magnitudes of paleoearthquake clusters may be erroneous if the time since prior liquefaction is not appropriately taken into account. Accordingly, aging correction factors are evaluated at sites of recurrent liquefaction during the Canterbury earthquakes.

Collectively, Parts A, B, and C address prevailing uncertainties pertaining to paleoliquefaction analyses using case studies from the Canterbury (New Zealand) earthquake sequence. The geomorphology of soil deposits, severity of liquefaction, and relative timing of the Canterbury events make them directly analogous to paleoearthquake clusters that occurred in the NMSZ and elsewhere. As such, the CES provides a unique modern analog for evaluating paleoliquefaction interpretation and analysis techniques.

II. Part A: Assessment and Updating of Liquefaction-Based Paleoseismic Back-Analysis Methods

Summary

Using case studies from the 2010-2011 Canterbury, New Zealand earthquake sequence, Part A assesses the accuracies of paleoliquefaction back-analysis methods, namely the "magnitude-bound" and "site-specific geotechnical" methods, and explores the challenges, techniques, and uncertainties associated with their application. While these back-analysis methods have been widely used to estimate the magnitudes of paleoearthquakes, their uncertain efficacies continue to significantly affect the computed seismic hazard in regions where they are relied upon. Accordingly, their performance is evaluated herein using liquefaction data from modern earthquakes with known magnitudes. It is shown that when the earthquake source location and mechanism are known, back-analysis methods are capable of accurately deriving seismic parameters from liquefaction evidence. However, because the source location and mechanism are often unknown in paleoliquefaction studies, and because accurate interpretation is shown to be more difficult in such cases, new analysis techniques are proposed herein. For the site-specific approach, an objective parameter is proposed to geospatially assess the likelihood the source location, enabling an analyst to more accurately estimate the most likely magnitude of the causative earthquake. For the magnitude-bound approach, consideration of liquefaction susceptibility is likewise shown to improve the accuracy of interpretation. Part A demonstrates the challenges of applying these methods, provides insight into their potential accuracies, and provides a framework for performing paleoliquefaction analyses, both globally and in Christchurch.

1. Introduction

The objective of this study is to assess the accuracies of paleoliquefaction back-analysis methods, and to explore the challenges, techniques, and uncertainties associated with their application, using case studies from the 2010-2011 Canterbury, New Zealand earthquake sequence. In recent years, the use of paleoliquefaction evidence for assessing seismic hazards has become more common, particularly in regions of infrequent but potentially damaging seismicity. This technique involves locating liquefaction features induced by prehistoric or pre-instrumental paleoearthquakes and using quantitative back-analysis methods to estimate the causative ground acceleration and/or earthquake magnitude. In some cases, the local paleoseismic record can be inferred as far back as Pleistocene time, providing data for seismic hazard analyses for engineering design and planning. For this reason, the value of paleoliquefaction evidence is widely recognized and back-analysis techniques have been applied to sites around the world, in addition to many in the United States. These include the New Madrid seismic zone (NMSZ) of Missouri, Arkansas, and Tennessee (e.g., Tuttle, 2001), the Wasbash Valley seismic zone (WVSC) of Illinois and Indiana (e.g. Obermeier, 1998), the Charleston, South Carolina coastal plain (e.g., Talwani and Schaeffer, 2001), and the Cascadia subduction zone of

Oregon and Washington (e.g., Obermeier and Dickinson, 2000), among several others (Ellis and de Alba, 1999; Tuttle et al., 2002a; Cox et al., 2004; Kuhn, 2005).

While several procedures have been proposed for estimating the magnitudes of earthquakes from paleoliquefaction data, the two most credible and widely-used are the "site-specific geotechnical analysis" procedure (e.g., Obermeier and Dickenson, 2000; Green et al., 2005) and the "magnitude-bound" procedure (e.g., Obermeier, 1998; Olson et al., 2005b; Papathanassiou et al., 2005; Pirrotta et al., 2007). The site-specific geotechnical analysis, also referred to as the cyclic stress method, is an analytical approach which uses in-situ test data (e.g. cone penetration test) in conjunction with cyclic resistance ratio curves (e.g. Youd et al., 2001) and appropriate ground motion predictive equations (GMPEs) to back calculate the minimum magnitude earthquake required to induce liquefaction at a particular site. Regional results from multiple sites are then combined to yield a best-estimate of the paleoearthquake magnitude (e.g., Green et al., 2005). The magnitude-bound procedure uses a correlation developed from modern liquefaction observations relating earthquake magnitude to the site-to-source distance of the most distal observation of liquefaction.

Although these back-analysis methods have been widely used to estimate the magnitudes of paleoearthquakes, their accuracies are unknown. Liquefaction-based paleoseismic analyses are subject to many uncertainties, including factors related to liquefaction susceptibility, ground motion attenuation, field observations, and the validity of in-situ test methods. The accuracies of these techniques are more than just an academic curiosity; the epistemic and aleatoric uncertainties inherent to paleomagnitude estimates significantly affect the computed seismic hazard in regions where these techniques are relied upon. For example, the computed seismic hazard of the central U.S. is founded largely on the paleoliquefaction record of the NMSZ (Petersen et al., 2008) and is significantly influenced by the uncertainty of paleomagnitude estimates (Vidale et al., 2011). If this uncertainty is biased toward higher magnitudes than actual, the seismic hazard is overestimated, and capital is spent superfluously on excessive seismic design of civil infrastructure. Conversely, if the seismic hazard is underestimated, infrastructure is under-designed and people are potentially at undue risk. A 2009 impact assessment of an M_w7.7 earthquake in the NMSZ projected extensive damage in Memphis, TN and St. Louis, MO, resulting in over 80,000 injuries and fatalities and direct economic losses of $300 billion (Elnashai et al., 2009). Thus, there are significant consequences associated with the accuracy of inputs to seismic hazard analyses.

The potential consequences of seismic hazard uncertainty were vividly displayed during the 2010-2011 Canterbury (New Zealand) earthquake sequence (CES), which caused widespread and severe damage throughout the city of Christchurch and surrounding area. While earthquake scenarios on the Alpine Fault and in the foothills of the Southern Alps had long been recognized and accounted for in seismic hazard analyses (e.g. Stirling et al., 2007), the fault system which ruptured beneath Christchurch during the CES was previously unmapped. As a result, in the 22 February 2011, M_w6.2 Christchurch earthquake, seismic demands in much of the Christchurch urban area were greater than the 475-year return-period design ground-motion as specified by the existing New Zealand loading standard (New Zealand Standards 1170.5 2004), where for some structures, the ground-motion displacement demands were approximately twice the seismic design level (Bradley and Cubrinovski,

2011). In March 2011, it was preliminarily determined that 77% of buildings within the central business district (CBD) required either demolition or extensive repair (Kam et al., 2011), with the final proportion likely being greater (Smyrou et al., 2011). Coinciding with the unanticipated ground motions, the CES induced widespread liquefaction. The high liquefaction susceptibility of soils in the region had been recognized (Environment Canterbury [ECan], 2004), but the only previously documented liquefaction occurred in the village of Kaiapoi, north of Christchurch, during the 1901 Cheviot earthquake (e.g., Berrill et al., 1994). In the M_w6.2 Christchurch earthquake, nearly half of the Christchurch urban area was affected by liquefaction, with the thickness of vented sediments on the ground surface exceeding 0.5 m at some sites, making it one of the most pervasive and severe liquefaction events on record (e.g., Cubrinovski and Green, 2010; Cubrinovski et al., 2011b; Orense et al., 2011).

In addition to illustrating the importance of accurate inputs for seismic hazard analyses, the CES presents a unique opportunity to assess the efficacy of liquefaction analytics. This includes an assessment of both forward-analysis methods (i.e. assessing liquefaction hazard) such as liquefaction potential index (e.g., Maurer et al., 2013), and the focus of this study: back-analysis methods (i.e., deriving seismic parameters from liquefaction evidence). The uncertain efficacies of back-analysis techniques are due, in part, to the fact that the application and accuracy of these techniques have never been assessed using modern analog earthquakes. In other words, their performance has never been evaluated using case studies from earthquakes with known magnitudes. The Canterbury earthquakes represent a best-case scenario of what could be obtained during a paleoliquefaction study (i.e., identification of numerous liquefaction features and extensive in-situ soil characterization) and present an opportunity to evaluate our capacity for estimating earthquake magnitudes from liquefaction data. Thus, the primary objective of this study is to evaluate the accuracy of magnitude back-analysis methods, namely the magnitude-bound approach and the site-specific geotechnical analysis approach, using case studies from the CES. This evaluation will be performed by studying sites of liquefaction (and non-liquefaction) from by the 4 September 2010, M_w 7.1 Darfield and 22 February 2011, M_w 6.2 Christchurch earthquakes. The study presented herein demonstrates the challenges of applying these methods, provides insight into their potential accuracies, and has implications for paleoliquefaction analyses (and thus, computed seismic hazards) worldwide.

Specific to Christchurch, this study presents a framework for analyzing paleoliquefaction evidence discovered in the region. In light of the prior inconspicuousness of local faults and the exceedance of design ground-motions during the CES, the need to reassess the return-period of large local earthquakes is obvious. Although just beginning, efforts have recently uncovered the first probable paleoliquefaction features in the region (Tuttle et al., 2012; Bastin et al., 2012; Quigley et al., 2013), but the causative earthquake source location and magnitude are unknown. Preliminary evidence indicates that a liquefaction-inducing earthquake occurred between A.D. 1000 and A.D. 1400 (Tuttle et al., 2012), but rockfall evidence suggests that no significant earthquakes have occurred on local faults within the last 8000 years (Canterbury Earthquakes Royal Commission, 2012). Thus, if and when additional paleoliquefaction evidence is discovered, the framework presented herein could

elucidate the region's paleoseismic history and aid in more accurately assessing the regional seismic hazard.

In the following, brief outlines of the paleoliquefaction back-analysis procedures are given, followed by a summary of the 2010-2011 CES. Then, the methodologies used to apply these procedures to data from the Darfield and Christchurch earthquakes are covered in detail. The results of the magnitude back-analyses are then discussed, with observations on their efficacy, and on the implications for paleoliquefaction analyses, both globally and locally.

2. Background

2.1 Paleoliquefaction back-analysis procedures

As stated previously, two approaches are commonly used to back-calculate paleoseismic parameters from liquefaction evidence (i.e., the site-specific geotechnical and magnitude-bound methods). The first employs the liquefaction triggering methodology to back-calculate the causative ground acceleration required to induce liquefaction, which, when combined with a GMPE, yields an estimate of earthquake magnitude. The second approach relies upon empirical correlations relating earthquake magnitude to the site-to-source distance of liquefaction observations. Both of these approaches are thoroughly summarized and extensively discussed by Obermeier et al. (2001) and Olson et al. (2005a), who provide guidelines for proper conduct of paleoliquefaction analyses, ranging from geologic interpretation to refinement of back-calculation techniques. In addition, Green et al. (2005) illustrate the application of these methods by estimating a paleomagnitude in the central eastern United States, and discuss in detail the uncertainties and assumptions used in the assessment. In light of this, the site-specific geotechnical and magnitude-bound approaches are briefly outlined below, and the reader is referred to the above sources, which remain authoritative, for additional information. However, as will be discernible from the following outlines, knowing or estimating the earthquake source location is critical to obtaining an accurate estimate of earthquake magnitude. Therefore, because the importance of source location is a focus of this study, and because new approaches for determining source location are demonstrated herein, the determination of site-to-source distance is also discussed following the descriptions of the back-analysis techniques.

2.1.1 Site-specific geotechnical approach

The site-specific geotechnical analysis, referred to subsequently as the "site-specific" approach for brevity, evaluates sites of liquefaction and non-liquefaction across a broad region to give a best-estimate of the causative earthquake magnitude. The most widely-used analysis of this form uses the cyclic stress approach proposed by Whitman (1971) and Seed and Idriss (1971), commonly referred to as the "simplified" liquefaction evaluation procedure. First developed using Standard Penetration Test (SPT) data, the original procedure has gone through several updates (e.g., Seed et al., 1985; Youd et al., 2001; Cetin et al., 2004; Idriss and Boulanger, 2006) and a Cone Penetration Test (CPT) based procedure has been developed (e.g., Seed and DeAlba, 1986; Stark and Olson, 1995; Robertson and

Wride, 1998; Youd et al., 2001; Moss et al., 2006; Idriss and Boulanger, 2006). In this procedure, the factor of safety against liquefaction (FS_{liq}) at a given depth in the soil profile is equal to the ratio of the cyclic resistance of the soil (CRR) to the earthquake induced cyclic stress ($CSR_{7.5}$). To use this procedure for back-analysis of a liquefaction investigation site, the strata within the soil profile with depth-thickness-density combination consistent with the observed liquefaction response of the site (i.e., the "critical layer") is identified and assumed to have an FS_{liq} of 1.0 (Eq. 1).

$$FS_{liq} = \frac{CRR}{CSR_{7.5}} = 1.0 \quad (1)$$

By substituting for CRR and $CSR_{7.5}$ as defined by the simplified liquefaction evaluation procedure for CPT data, the minimum PGA required to induce liquefaction may be expressed as:

$$a_{max} = CRR(q_{1N,cs})MSF(M_w)K_\sigma \frac{g\sigma'_{vo}}{0.65\sigma_{vo}r_d} \quad (2)$$

where a_{max} = peak geometric-mean horizontal ground acceleration (PGA); $q_{1N,cs}$ = representative cone-tip resistance, normalized for overburden pressure and adjusted for fines content; MSF = magnitude scaling factor to adjust for the duration of shaking; M_w = moment magnitude; K_σ = dimensionless factor incorporating the effect of overburden pressure on liquefaction resistance; g = acceleration of gravity; σ'_{vo} = initial effective stress; σ_{vo} = initial total stress; r_d = dimensionless stress reduction factor accounting for flexibility of the soil column. Olson et al. (2005a) and Green et al. (2005; 2013a) provide guidelines for selection of critical layers and the representative in-situ parameters required in Eq. (2).

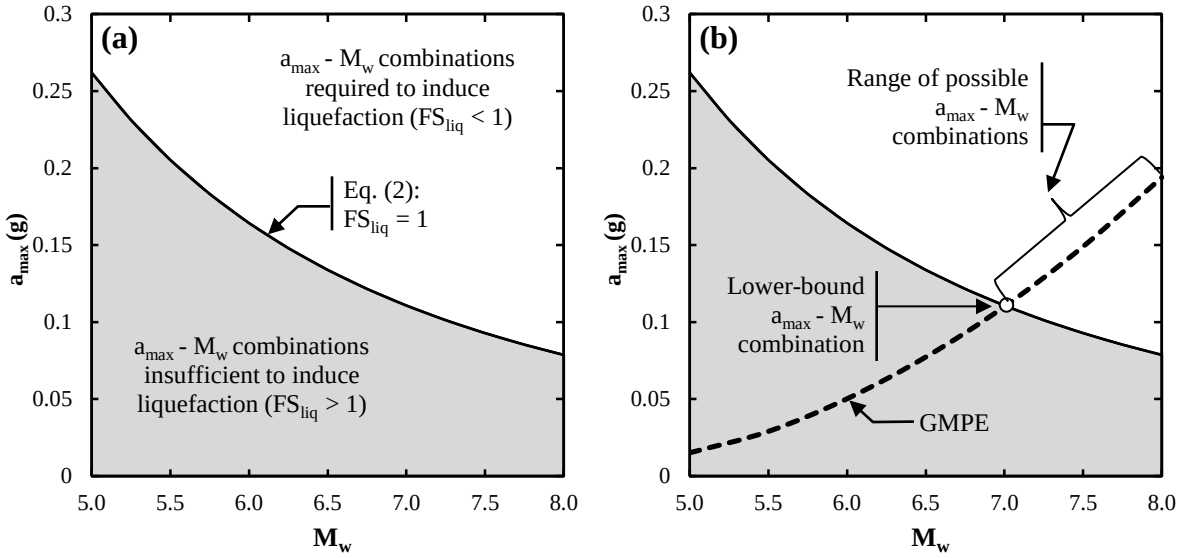

Figure 1. (a) a_{max} – M_w combinations required to induce liquefaction for a hypothetical site; (b) Determination of lower-bound a_{max}-M_w combination for the same hypothetical site (adapted from Green et al., 2005).

As shown in Fig. 1a, the boundary defined by Eq. (2) separates combinations of a_{max} - M_w that are sufficient to induce liquefaction from combinations that are insufficient. As there are infinitely many combinations sufficient to induce liquefaction, a regionally appropriate GMPE is used to determine credible a_{max} - M_w combinations for a given site, where the GMPE defines a_{max} as a function of earthquake magnitude (M_w) and site-to-source distance (R). A GMPE is plotted in Fig. 1b (dashed line) with variable M_w, and R equal to the distance from the liquefaction site to the provisional earthquake source location. Thus, this line represents the expected accelerations at the liquefaction site corresponding to various causative earthquake magnitudes. As indicated in Fig. 1b, the portion of this line plotting above the boundary defined by Eq. (2) corresponds to a_{max} - M_w combinations that could have induced liquefaction at the site. The intersection of the GMPE with the boundary-line (i.e., FS_{liq} = 1) defines the lower-bound a_{max} - M_w combination for the given site. In other words, this gives the minimum magnitude earthquake that could have induced liquefaction. To cap the estimate of earthquake magnitude, upper-bound a_{max} - M_w combinations are computed by repeating this procedure at sites that did not liquefy. In this case, the resultant is the maximum magnitude earthquake (i.e., if the earthquake magnitude had been any greater, liquefaction would have been induced at the site).

Finally, to obtain a best-estimate of the causative earthquake magnitude, a regional assessment of a_{max} - M_w combinations is performed by incorporating individual back-analyses from sites of liquefaction (i.e., lower-bound values) and non-liquefaction (i.e., upper-bound values). The recommended approach (Green et al., 2005), illustrated in Fig. 2, is to plot the a_{max} value determined for each site as a function of the site-to-source distance, R. In cases where the fault location and direction of fault movement are known, data may be plotted corresponding to, for example, the directions of forward and reverse rupture directivity. Thus, the "+" and "-" symbols seen in Fig. 2 indicate different directions from the earthquake source. While it is not critical to parse data in this manner, this approach may provide clarity in cases where the character of ground motions is direction-dependent. In cases where the fault orientation and direction of fault movement are unknown, data could be plotted corresponding to general opposing directions from the provisional source location.

As shown in Fig. 2, different symbols are used to differentiate a_{max} values from sites with and without liquefaction. The GMPE used to compute a_{max} - M_w combinations at individual sites is then plotted such that it separates the regional liquefaction and non-liquefaction data; the M_w input corresponding to this boundary-line represents a best-estimate of the causative earthquake magnitude. If the provisional earthquake source location is invalid, a distinct boundary between liquefaction and non-liquefaction data may not be apparent (the use of this criterion for determining earthquake source location is demonstrated later in this paper). In general, the locations of data points relative to the separating boundary are a function of FS_{liq}. For example, sites with severe liquefaction manifestations tend to plot further below the boundary as compared to sites with marginal manifestations of liquefaction. This is due to the fact that FS_{liq} was assumed to be 1.0 in the back-analyses, but in reality, was likely much less than 1.0 at sites with severe liquefaction. As a result, the back-calculated a_{max} - M_w combinations for these sites are likely less than the actual causative earthquake. Similarly, for sites that did not liquefy, those having very high resistance to liquefaction (i.e., $FS_{liq} >> 1$) tend to plot further above the boundary. Conversely, at sites of marginal liquefaction, FS_{liq} is likely close to the

assumed value of 1.0, and the back-calculated a_{max} - M_w combinations are thus presumed to be close to actuality. As a result, these sites tend to be most valuable for estimating the causative earthquake magnitude. One exception to the preceding discussion is the case of lateral spreading, a unique form of liquefaction manifestation associated with large lateral ground displacements. The severity of lateral spreading is influenced by additional criteria, including the ground slope, the height of the nearest free-face (e.g., river bank), and the lateral distance between the free-face and spreading crack (e.g., Youd et al., 2002). As such, FS_{liq} may not be significantly less than 1.0 for cases of severe liquefaction manifested as lateral spreading.

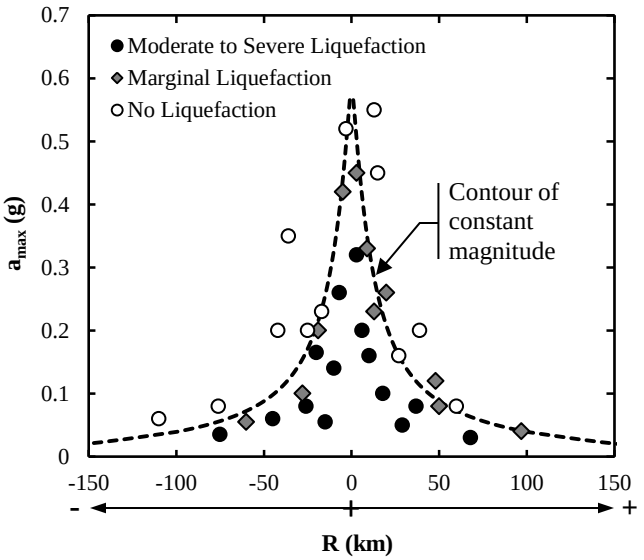

Figure 2. Illustration of proposed regional assessment of liquefaction sites, as described in text.

The advantages of the site-specific approach are that it (1) offers a robust semi-theoretical solution based on the methodologies of liquefaction triggering and ground-motion prediction; (2) incorporates results from multiple sites, thus reducing the influence of anomalous cases; (3) results in a median estimate of earthquake magnitude (as will be subsequently discussed, this is generally not the case with the magnitude-bound approach); and (4) provides a means for corroborating the provisional earthquake source location. The disadvantages of the site-specific approach are as follows: (1) the analyst must be familiar with the use of liquefaction evaluation procedures and GMPEs, and accordingly, the many nuances and uncertainties inherent to each; and (2) in-situ testing is required at numerous investigation sites, increasing the cost and complexity of analysis.

In summary, the site-specific approach is rooted in more than four decades of soil-liquefaction research and provides an intensive back-analysis of multiple sites across an affected region to estimate the causative earthquake magnitude. An understanding of the procedures comprising this approach and the complexities of their application is critical.

2.1.2 Magnitude-bound approach

Relations between earthquake magnitude and the most distal observation of liquefaction from the earthquake source are widely used to estimate the magnitudes of prehistoric/preinstrumental earthquakes from paleoliquefaction evidence. Derived from observations of liquefaction induced by modern earthquakes, these relations are commonly referred to as "magnitude-bound" curves. Kuribayashi and Tatsuoka (1975) first collected data from 32 Japanese earthquakes to develop a relation between earthquake magnitude and the maximum site-to-source distance of liquefaction. Building upon the work of Kuribayashi and Tatsuoka (1975) and others, Ambraseys (1988) proposed a magnitude-bound relation using worldwide data from 137 shallow earthquakes. Since then, numerous magnitude-bound correlations have been proposed using both worldwide and region-specific data. Fig. 3 presents several such correlations for a variety of geographic and tectonic settings, where site-to-source distance is quantified in terms of epicentral distance (Fig. 3a) and the closest distance to fault rupture (Fig. 3b). The location of these curves, which bound the most distal liquefaction features, are inherently a function of the most optimal combination of earthquake source characteristics (i.e., rupture mechanism), transmission characteristics (i.e., ground-motion attenuation and site effects), and soil liquefaction susceptibility (i.e., soil density and gradation, and ground water depth). Because these factors are regionally dependent, use of region-specific magnitude-bound correlations may yield more accurate estimates of paleomagnitudes than those based on worldwide data (Obermeier et al., 2001; Olson et al., 2005a; 2005b).

In addition, inherent to these curves are differing criteria for data inclusion, including the quality of liquefaction observation and extent of field study, the certainty of earthquake source location and magnitude (e.g., instrumental vs. macroseismic), the style of faulting and depth of focal mechanism, and the overall anomalousness of case-history data. For example, Ambraseys (1988) did not consider data from either (1) deep-focus earthquakes, which have been shown to produce more distal liquefaction than shallow crustal earthquakes; or (2) anomalous cases that would bias the maximum source distance of liquefaction features, including those where local conditions greatly enhanced liquefaction susceptibility, such as artesian pressures, heavy rainfall, irrigation of fields, or sloping ground. Conversely, Castilla and Ardemard (2007) included both deep-focus earthquakes and anomalous cases when constructing their magnitude-bound curve from global data. For example, Castilla and Ardemard include data from the 1977 M_w7.5 Bucharest, Romania earthquake, having an estimated focal depth of 91–110 km (Ambraseys, 1988; Berg et al., 1980). They also include data from aftershocks following the 1989 M_w5.9 Boca del Tocuyo, Venezuala and 1989 M_w6.9 Loma Prieta, USA earthquakes. While further research is needed, we have observed that liquefaction may be possible at greater source distances during aftershocks than in equivalent-magnitude mainshocks, possibly due to prior disturbance, or to the presence of existing liquefaction dikes which act as readily available conduits between the ground surface and liquefied stratum. Due to the inclusion of these data, and as shown in Fig. 3a, the Castilla and Ardemard magnitude-bound relation estimates a significantly lower magnitude as compared to those of other authors, particularly at shorter source distances. This discussion is not intended to criticize the work of Castilla and Ardemard, but rather, is

intended to show that differing criteria for data selection amongst authors result in significant differences to the magnitude-bound curves. Familiarity with the provenience of a magnitude-bound relation can thus provide insight into its appropriateness and utility in specific settings.

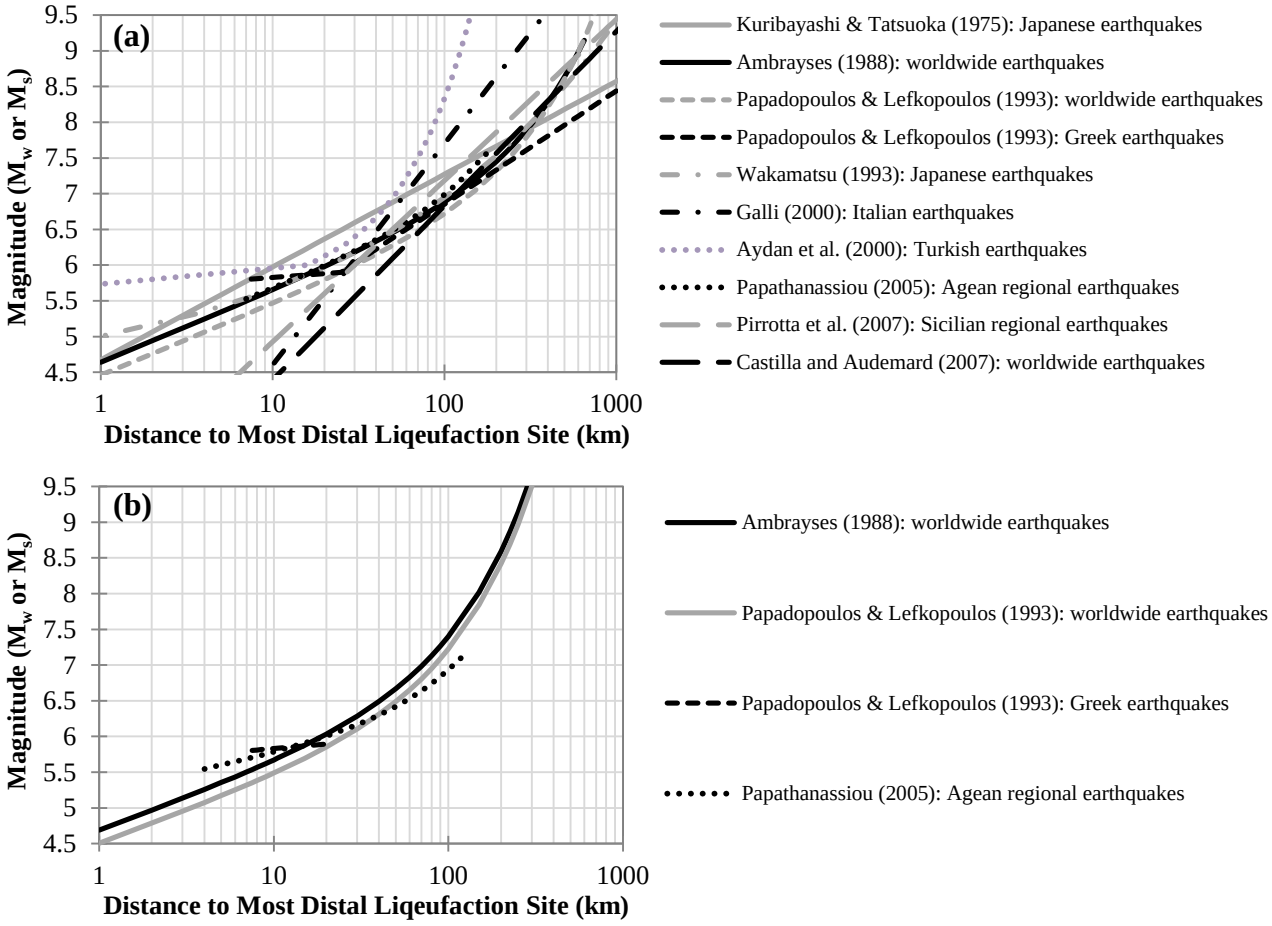

Figure 3. Magnitude-bound curves for varying geographic and tectonic settings, where site-to-source distance is quantified in terms of (a) epicentral distance and (b) closest distance to fault rupture.

The advantages of the magnitude-bound approach are that (1) only a single data point is required (i.e., the site-to-source distance of the most distal liquefaction site); (2) there is no need for costly in-situ testing (e.g., SPT; CPT) at numerous investigation sites; and (3) it is simple to use and does not require an understanding of either liquefaction triggering methodology or GMPEs. The disadvantages of the magnitude-bound approach are as follows: (1) significant time and effort are still required to search for the most distal liquefaction site and it cannot be known with any certainty whether the most distal feature has actually been located; (2) as a single-point approach, the advantage of averaging regional data from multiple sites is absent, and consequently, anomalous cases may influence results; (3) the validity of the provisional earthquake source location is difficult to assess; and (4) nearly all magnitude-bound curves in the literature are constructed such that they bound the

liquefaction data, rather than pass through it. As a result, magnitude-bound curves almost always give a lower-bound estimate of magnitude, rather than a median estimate; two known exceptions are the relations proposed by Obermeier et al. (1993) for the central U.S. and Olson et al. (2005b) for the WVSC.

In summary, magnitude-bound relations are widely employed and relatively simple to use. Because these relations are functions of regional factors, region-specific correlations will provide more accurate estimates of earthquake magnitude than those based on global data. In addition, knowledge of a magnitude-bound relation's source data and manner of derivation are critical to understanding the context of results.

2.1.3 Determination of earthquake source region

As evident from the preceding outlines, knowing or accurately estimating the earthquake source location is critical; for either back-analysis approach, the back-calculated earthquake magnitude is a function of the distance between the earthquake source location and sites of liquefaction. It is obviously impossible to determine an instrumental epicenter for a paleoearthquake, and in many cases, paleoliquefaction studies are performed because there are no surface faults available for a paleoseismic assessment. The earthquake source region must often therefore be located by other means. In many cases, only the "energy center," or centroid of strongest shaking, can be estimated (e.g., Obermeier, 1996; Obermeier et al., 2001; 2005). Obermeier (1996) observed that a provisional energy center can be effectively interpreted from a regional assessment of the distribution and size of liquefaction features. As such, an energy center derived from liquefaction evidence is similar to an epicenter inferred from macroseismic data. From an analysis of modern instrumental epicenters and historic intensity reports in the WVSC (Rhea and Wheeler, 1996), Obermeier et al. (2001) suggested that using liquefaction features for locating an earthquake source region is "generally accurate to within a few tens of kilometers, at least for earthquakes of moderate size."

In addition to the uncertainty of source location, the use of energy center as a proxy for various seismotechnic parameters (epicenter, hypocenter, fault rupture, etc.) introduces additional ambivalence to the back-analyses. As seen in the magnitude-bound relations plotted in Fig. 3, the definition of site-to-source distance significantly influences the position of the curve (i.e., epicentral vs. fault distance), particularly for larger magnitude earthquakes (e.g., see Ambraseys, 1988). Likewise, the GMPEs requisite for the site-specific approach employ various distance metrics (epicentral distance, hypocentral distance, rupture distance, etc.) that will invariably predict different PGAs, with the discrepancy increasing for larger magnitude earthquakes. Thus, once the earthquake source location is provisionally located, the distance metric chosen for back-analysis could affect the magnitude estimate. As mentioned previously, the validity of a provisional source location can be assessed using the site-specific approach, where lack of a discernible boundary between liquefaction and non-liquefaction data may indicate an invalid source location (conversely, there is no way to corroborate a provisional source region using magnitude-bound relations). Green et al. (2005) used this approach in their back-analysis of the Vincennes earthquake (~6100 years BP) in the WVSC, and concluded that

the distribution of back-calculated PGAs was consistent with the provisional energy center (i.e., the provisional source location inferred from liquefaction features appeared accurate). In addition, by comparing results from GMPEs based on various distance metrics, Green et al. found that variability due to inconsistency in the measure of site-to-source distance was relatively small for their back-calculated estimate of M_w7.5. Thus, despite the uncertainties, accurate estimates of earthquake magnitude may be possible. The significance of source location and distance metric for the back-analyses of the Darfield and Christchurch earthquakes is discussed later in this report.

2.2 Overview of 2010-2011 Canterbury (New Zealand) earthquake sequence (CES)

The 2010-2011 CES caused severe and recurring damage throughout the Christchurch urban area, located on the eastern margin of the South Island's Canterbury Plains. The CES includes the M_w7.1 Darfield and M_w6.2 Christchurch earthquakes, as well as eleven other $M_w \geq 5.0$ earthquakes epicentrally located within 20 km of central Christchurch (GeoNet, 2012). An overview of the Canterbury Plains region and Canterbury earthquake sequence is shown in Fig. 4. On 4 September 2010, the previously unmapped Greendale fault ruptured, producing the M_w7.1 Darfield earthquake. The Darfield event was the result of a complex rupture mechanism consisting of several sub-events, the largest being a right-lateral strike-slip rupture on the Greendale fault (Barnhart, 2011). While the epicenter for this event was approximately 40 km west of central Christchurch, the distances from the eastern edge of the rupture plane to the western suburbs of Christchurch, and to the CBD, were less than 10 km and 20 km, respectively (e.g., Cubrinovski and Green, 2010). Recorded geometric-mean horizontal peak ground accelerations (PGAs) were approximately 0.2 g throughout much of the Christchurch urban area, 0.25 g in the western suburbs, and 0.3 g in the towns of Kaiapoi and Lyttelton, north and south of Christchurch, respectively (e.g., Bradley, 2012a; Bradley, 2012b). As with the Darfield earthquake, the 22 February 2011 M_w6.2 Christchurch earthquake ruptured on a previously unmapped fault, the Port Hills fault. The Christchurch earthquake resulted from a mixture of reverse and right-lateral slip and was epicentrally located about 6 km south of central Christchurch in the Port Hills, with the rupture plane located directly beneath the southernmost environs of Christchurch (Beavan et al., 2011). Recorded geometric-mean horizontal PGAs were approximately 1.3 g in the near-fault region, 0.3 – 0.6 g throughout much of the Christchurch urban area, 0.2 g in Kaiapoi (north of Christchurch), and 0.1 g in the western suburbs (e.g., Bradley and Cubinovski, 2011; Bradley, 2012b).

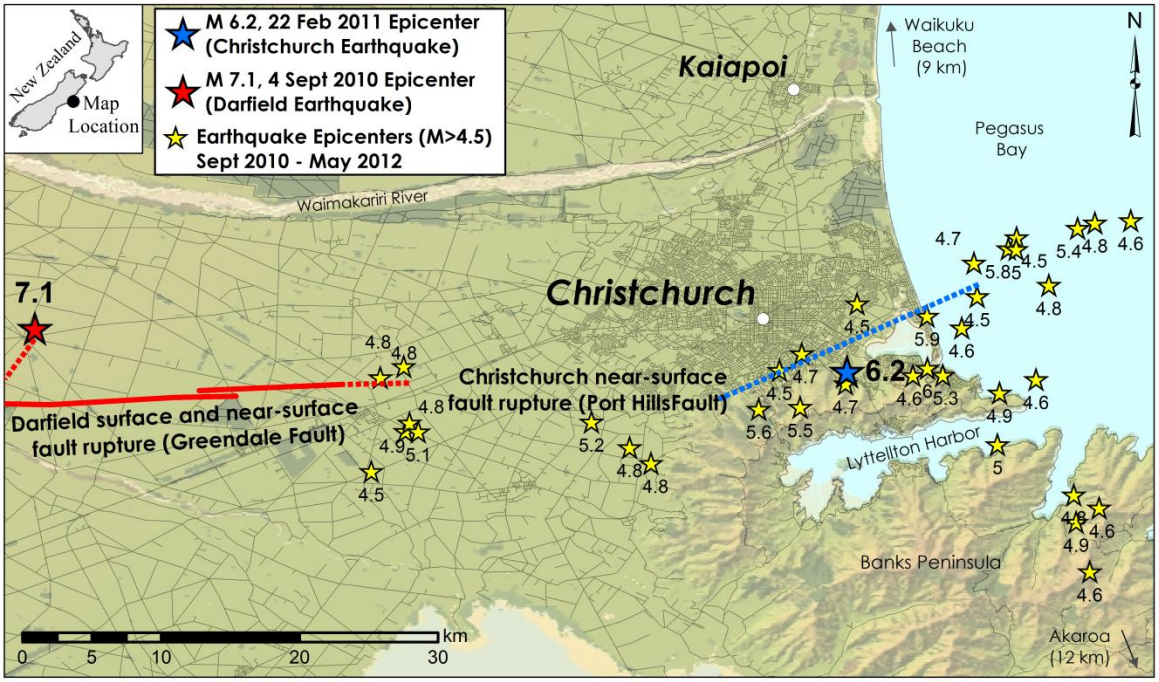

Figure 4. Regional overview of the Canterbury metropolitan area and 2010 – 2011 Canterbury earthquake sequence (CES).

Owing to its location amongst the Avon, Heathcote, and Waimakariri Rivers, and to a history of lagoon, estuarine, and alluvial sediment deposition resulting from coastline transgression and progradation, much of Christchurch has a shallow water table and near-surface soil stratigraphy characterized by loose Holocene sands and silts (Brown et al., 1995), resulting in very high liquefaction susceptibilities (e.g., Maurer et al., 2013). Liquefaction induced during the Darfield and Christchurch earthquakes was widespread and severe, occurring throughout Christchurch and the town of Kaiapoi. Manifestations of soil liquefaction observed during the CES include sand blows and lateral spreading, settlement and tilting of structures, cracking of pavements, and failure of buried lifelines due to flotation or differential settlements. To characterize the distribution of liquefaction, the authors classified liquefaction manifestation severity (sand blows and lateral spreading only) at approximately 1500 reconnaissance sites following both the Darfield and Christchurch earthquakes. This was accomplished using ground reconnaissance and high-resolution satellite imagery (CGD, 2012a) performed in the days immediately following each of the earthquakes. In addition, lateral spreading observations and measurements from the Canterbury Geotechnical Database (CGD, 2012b) were utilized.

The distributions of liquefaction severity observations following the Darfield and Christchurch earthquakes are shown in Figure 5a and Figure 5b, respectively. The distributions of liquefied areas reflect the combined effects of liquefaction susceptibility and seismic loading. The areas most severely affected by liquefaction during both events were along the Avon River northeast of the CBD. The more extensive liquefaction observed in these areas during the Christchurch earthquake is consistent with the greater seismic loading relative to the Darfield earthquake (e.g., Bradley, 2012b). Conversely,

along the southwestern margins of the city and in Kaiapoi, liquefaction was more extensive during the Darfield earthquake due to greater seismic loading in these areas during this event. In addition to the sand blow and lateral spread manifestations mapped herein, liquefaction caused extensive damage to residential and commercial structures, high-rise buildings, utility networks, bridges, and roads. A large body of literature exists pertaining to liquefaction and its effects during the Darfield and Christchurch earthquakes, including overviews by Cubrinovski and Green (2010), Cubrinovski et al. (2011a; 2011b), Green et al. (2011) and Orense et al. (2011), among others.

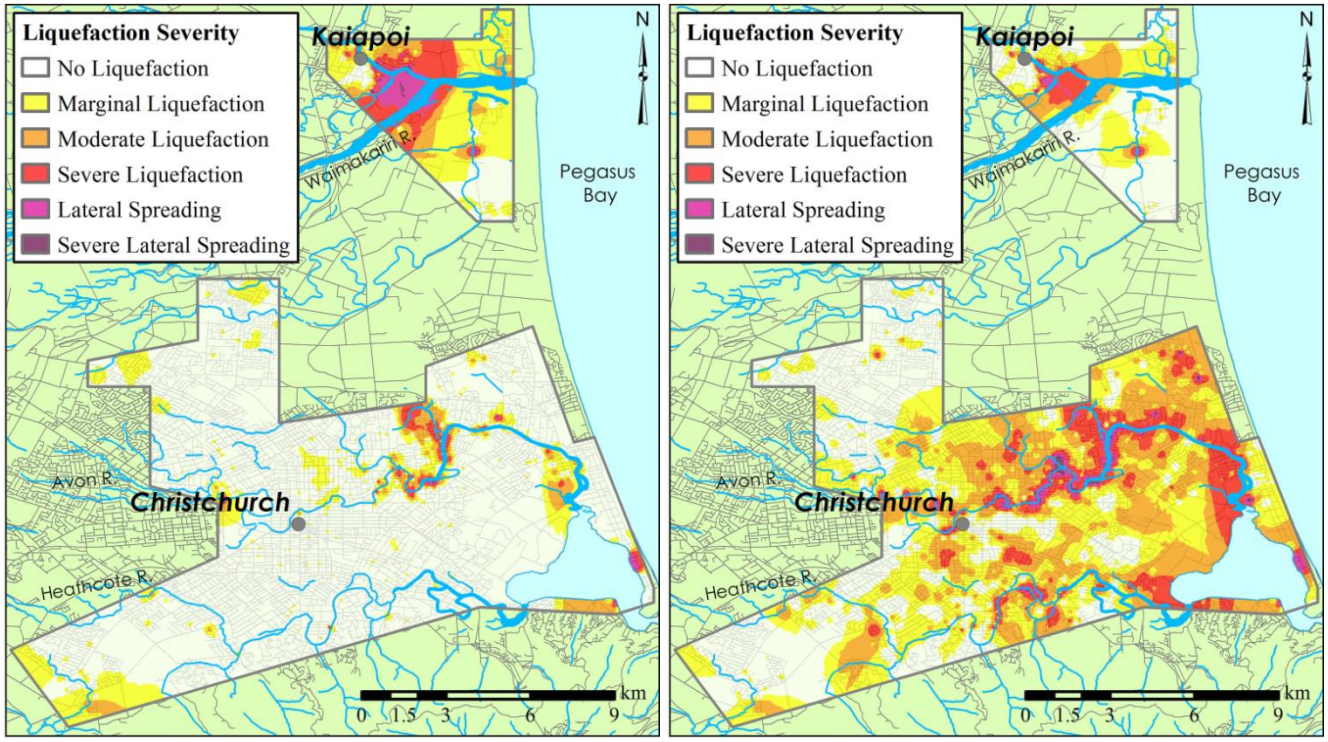

Figure 5. Liquefaction severity observations following the (a) Darfield and (b) Christchurch earthquakes. The criteria used to classify liquefaction severity are as described by Maurer et al. (2013).

3. Analysis

3.1 Site-specific approach

A two-step approach will be taken to assess the efficacy of the site-specific approach for estimating earthquake magnitudes. First, it is assumed that the earthquake source locations are known, and second, assuming these locations are unknown, techniques for their determination are demonstrated and the associated magnitude estimates are assessed. In each case, liquefaction observations and in-situ soil characterization data from 75 investigation sites are utilized. This hypothetical scenario is intended to resemble that of a thoroughly investigated paleoseismic region such as the NMSZ, where the seismic hazard remains an enigma. Assembling a database of this size for a paleoearthquake could

require years or even decades of field investigation and in-situ testing. As such, this dataset represents a best-case scenario of what could be potentially obtained from a paleoliquefaction investigation in the Christchurch region over many years. Following these analyses, the sensitivity of magnitude estimates to the number of investigation sites is also investigated.

3.1.1 Investigation sites, CPT Data, and liquefaction evaluation

Of the nearly 1500 investigation sites where the authors characterized the severity of surficial liquefaction manifestation during the Darfield and Christchurch earthquakes (Fig. 5), 75 are randomly selected for the hypothetical paleoliquefaction scenario. For this study, it is assumed that the occurrence or non-occurrence of liquefaction would be accurately interpreted in a paleoliquefaction investigation, and moreover, that liquefaction effects would be properly attributed to their respective causative earthquakes. These assumptions are not intended to diminish the importance or trivialize the difficulty of field interpretation; the objective herein is to evaluate the accuracy of quantitative back-analysis methods, rather than to discuss the field investigation methods prerequisite for such analyses. The reader is referred to the overviews of field interpretation given by Obermeier et al. (2001; 2005), and to the paleoliquefaction investigations of Obermeier and Dickenson (2000), Tuttle (2001), Talwani and Schaeffer (2001), Cox et al. (2004), and Tuttle et al. (2002a; 2002b; 2005), among others, for specific case studies. In addition, Sims and Garvin (1995), Quigley et al. (2013), and Part B of this report discuss field interpretation specific to recurrent liquefaction events closely spaced in time, such as the CES.

CPTs were performed at each of the 75 investigation sites shortly after the start of the CES. A summary of the CPT database used in the magnitude back-calculations, including critical layers and representative in-situ soil characteristics, is given in Table A1 (Appendix); the criteria used to classify the severity of liquefaction is given in Table A2. The selection of critical layers and in-situ parameters was aided by the guidelines of Olson et al. (2005a) and Green et al. (2005; 2013a). Back-calculations (see Eq. 2) were performed using the CPT-based liquefaction evaluation procedure proposed by Robertson and Wride (1998) (see also Youd et al., 2001). To compute the total and effective vertical stresses as a function of depth, soil unit weights were estimated from CPT data using the method proposed by Robertson and Cabal (2010). Ground water table (GWT) depths were inferred from CPT pore pressure (u) measurements and corroborated by nearby well logs and borings. The soil behavior type index, I_c, was used to identify non-liquefiable soils, where soils with $I_c > 2.6$ were considered to be too plastic to liquefy.

3.1.2 Ground motion predictive equations (GMPEs)

As discussed previously, a GMPE is used to bound possible a_{max} - M_w combinations for each investigation site (Fig. 1a) and to estimate the causative earthquake magnitude from regional data (Fig. 2). Because the accuracy of the GMPE (i.e., agreement between actual and predicted ground motion) directly affects the accuracy of the magnitude estimate, the most recent and regionally applicable GMPE should be used. Further, since different GMPEs will invariably predict different ground

motions, it is prudent to perform back-calculations using multiple GMPEs and then compute a final estimate of magnitude applying weighting factors to each GMPE. For the study presented herein, the selected GMPEs include the McVerry et al. (2006), Boore and Atkinson (2008), Chiou and Youngs (2008), Ambrahamson and Silva (2008), and Bradley (2010; 2013) models, abbreviated respectively as McV06, BA08, CY08, AS08, and B10. The McV06 model is the current design basis for hazard analysis and seismic practice in New Zealand. The BA08, CY08, and AS08 predictive equations are Next Generation Attenuation (NGA) models developed from the most extensive collection of active shallow crustal recordings presently available. Adjustments to small-to-moderate magnitude predictions for the CY08 and BA08 models were given by Chiou et al. (2010) and Atkinson and Boore (2011), respectively. Lastly, the B10 model is a NZ-specific modification of CY08, developed prior to the CES, which corrects empirically identified discrepancies for New Zealand recordings.

From the distribution of Christchurch strong motion station (SMS) site classifications, based on generalized soil profiles (GeoNet, 2013), it is assumed that New Zealand (NZ) Site Class D profiles are predominant throughout the study area. To refine the site classifications of 13 SMS sites, Wood et al. (2011) performed active- and passive-source surface wave testing and found that many of the sites in the region of liquefaction were at the lower end of Site Class D (i.e., bordering Site Class E). While it might be argued that a hybrid Site Class D/E should therefore be used in the back-analyses, such precision is not typically available in paleoliquefaction studies; in the absence of dynamic site characterization, it is reasonable to assume Site Class D conditions for profiles with liquefiable soils. As such, the GMPEs are used to compute a_{max} at the ground surface assuming NZ Site Class D soil profiles for all investigation sites. Because the New Zealand Loadings Standard (NZS1170.5) uses a slightly different site classification system than other international standards such as the International Building Code (IBC), the NZ site classes must be converted into the predictor variables required by NGA models. The compatibility matrix of Bradley (2010) is adopted herein for this purpose and is shown in Table 1; an average shear wave velocity over the top 30 m of the subsurface (V_{s30}) of 250 m/s is adopted for compatibility with McV06 / NZS1170.5 Site Class D. In addition to $V_{S30,}$ the CY08, AS08, and B10 models require the basin depth to the 1 km/s shear wave velocity horizon, $Z_{1.0}$. Since site-specific basin depths are not yet available for the study area, the relationship proposed by CY08, given by Eq. (3), is adopted.

$$Z_{1.0} = \exp\left[28.5 - 0.4775 \ln\left(V_{s,30}^{8} + 378.7^{8}\right)\right] \quad (3)$$

For comparison to a hybrid D/E Site Class, a V_{s30} of 225 m/s would typically increase the expected a_{max} by ~ 0.03 g in the near-fault region and < 0.01g at site-to-source distances beyond 10 km, as predicted by the GMPEs used herein considering a range of possible earthquake magnitudes and source mechanisms. Thus, while the D/E Site Class refinement could change some spectral accelerations more significantly, it is relatively insignificant for earthquake magnitudes back-calculated from a_{max}.

Table 1. Compatibility matrix for the considered active crustal GMPEs (adapted from Bradley, 2010)

McV06 / NZS 1170.5		**BA08, CY08, AS08, B10**
Site Class	***Description***	***V_{s30} (m/s)***
C	Shallow Soil	450
D	Deep or Soft Soil	250
E	Very Soft Soil	200

A comparison of GMPE inputs, including site-to-source distance metrics, site conditions, and source mechanisms, is shown in Table 2. For the scenario assuming known earthquake source locations, the known source mechanisms (Barnhart et al., 2011; Beavan et al., 2011; Quigley et al., 2012), shown in Table 2, are used in the analyses. For the scenario of unknown source locations, the analyses of both the Darfield and Christchurch earthquakes assume a shallow strike-slip event. For this case, the depth to the top of the fault rupture plane, Z_{TOR}, a predictor variable in the CY08, AS08, and B10 models, is assumed to be 1 km. In the absence of further information, these inputs represent reasonable assumptions for a paleoliquefaction study in the Christchurch region. It can also be seen in Table 2 that the selected GMPEs employ differing site-to-source distance metrics. For the scenario assuming known source locations, the respective distances to the known rupture planes are used. For the case of unknown source locations, the source is modeled as a point with 1 km depth, and the respective site-to-source distances are measured accordingly.

Table 2. Comparison of inputs for the considered active crustal GMPEs

GMPE	**Site-to-Source Distance Metric(s)**	**Site Condition**	**Darfield (M_w7.1) Source Mechanism**	**Christchurch (M_w6.2) Source Mechanism**
McV06	R_{rup}	NZ Site Class D	Other	Reverse-Oblique
BA08	R_{jb}	$V_{s,30}$ = 250 m/s	Strike-Slip	Reverse
CY08, AS08, B10	R_{rup}, R_{jb}, R_x	$V_{s,30}$ = 250 m/s	$\delta = 90°$, $\lambda = 0°$	$\delta = 69°$, $\lambda = 146°$

Site-to-source distance: R_{rup} - the closest distance to the rupture surface; R_{jb} - Joyner-Boore distance to the rupture surface; R_x – distance from the surface projection of the updip edge of the fault plane, measured perpendicular to the fault strike (positive in the downdip direction).

In Fig. A1 (Appendix), the median a_{max} predictions from each GMPE for Site Class D conditions, using the input parameters given in Table 2, are compared to the values recorded at local SMS sites during the Darfield earthquake; this is repeated for the Christchurch earthquake in Fig. A2. This is done to elucidate sources of error in the analyses and assess the sensitivity of back-calculated earthquake magnitudes to differences in GMPEs. For example, using average total residual [i.e., $\ln(PGA_{recorded}/PGA_{predicted})$] as a metric for GMPE performance, it can be seen that in the Christchurch earthquake (Fig. A2), CY08 and B10 were most accurate over relevant site-to-source distances (1-20 km). Thus, should the earthquake magnitudes back-calculated using these models deviate from the actual magnitude, GMPE performance might be eliminated as the source of error since a_{max} was well

predicted. Conversely, it can be seen in Fig. A2 that BA08 had the greatest average residual over relevant distances, indicating consistent under-predictions of a_{max}. As such, the earthquake magnitude back-calculated using BA08 will be greatest, and by comparing GMPE residuals with the distribution of back-calculated magnitudes, a general assessment of the sensitivity of magnitude estimates to GMPEs will be made. In the Darfield earthquake (Fig. A1), BA08 and AS08 had the least and greatest average residuals over relevant site-to-source distances (10-40 km), respectively, while CY08 and B10 were most accurate. Accordingly, BA08 and AS08 are expected to give the lowest and highest estimates of earthquake magnitude.

3.2 Site-specific results and discussion

3.2.1 Known earthquake source locations

Using existing source models and fault slip distribution maps for the Darfield and Christchurch earthquakes (i.e., known earthquake source locations and fault mechanisms) (Barnhart et al., 2011; Beavan et al., 2011; Quigley et al., 2012), lower-bound (liquefaction) and upper-bound (non-liquefaction) a_{max} values were back-calculated at each investigation site with each of the 5 GMPEs; regional results using the B10 GMPE are shown in Figs. 6a and 6b for the Darfield and Christchurch earthquakes, respectively. While the causative earthquake magnitude may be subjectively estimated from this regional data, an objective approach is taken herein, utilizing the "error-of-fit", E_f, computed as:

$$E_f = \sum_{i=1}^{n} S_i \qquad (4)$$

where $S_i = \left|\ln(a_{max,LIQ,i}) - \ln(a_{max,GMPE,i})\right|$ if $\begin{Bmatrix} a_{max,LIQ,i} > a_{max,GMPE,i} \text{ at liquefaction sites} \\ a_{max,LIQ,i} < a_{max,GMPE,i} \text{ at non-liquefaction sites} \end{Bmatrix}$

else $S_i = 0$

In this equation, $a_{max,LIQ,i}$ = the a_{max} back-calculated from in-situ test data at an investigation site with given site-to-source distance using the procedure outlined in *2.1.1*; $a_{max,GMPE,i}$ = the expected a_{max} at an investigation site with given site-to-source distance, as predicted by a GMPE with variable M_w; and n = the total number of investigation sites. The best-estimate of the causative earthquake magnitude, M_w, is that which minimizes E_f. In other words, and referring to Fig. 6, the magnitude solution is that which best segregates points of liquefaction and non-liquefaction in accordance with Eq. (4). As discussed previously, it is possible for FS_{liq} at sites of lateral spreading to be near unity, and thus, some moderate-to-severe liquefaction points may plot near the liquefaction/non-liquefaction boundary. Data points from sites of marginal liquefaction and moderate-to-severe liquefaction are therefore weighted equally in the computation of E_f. As shown in Fig. 6 using the B10 GMPE, the best-estimate magnitudes of the Darfield and Christchurch events (which minimize E_f) are 7.1 and 6.2,

respectively, which match the actual earthquake magnitudes. Regional results and magnitude estimates using each of the 5 GMPEs are shown in Figs. A3 and A4 for the Darfield and Christchurch earthquakes, respectively; a summary of these findings is given in Table 3. It can be seen that the site-specific approach performs well when earthquake source locations and mechanisms are known, with the accuracy of magnitude estimates improving with the accuracy of the GMPEs (i.e., agreement between GMPE predictions and actual ground motions). As expected from the performance of GMPEs, CY08 and B10 give the most accurate estimates of earthquake magnitude for both events. Also as expected, BA08 and AS08 produced the lowest (M_w6.90) and highest (M_w7.21) respective estimates for the Darfield earthquake. Over relevant site-to-source distances (10-40 km), BA08 and AS08 had average residuals (see Figs A1-A2) of -0.06 and 0.16, respectively. For the Christchurch earthquake, BA08 produced the highest estimate (M_w6.45) and had an average residual of 0.10 over relevant site-to-source distances (1-20 km). Given that a residual of 0.10 corresponds to a relatively minor a_{max} prediction error (e.g., 0.22 g recorded vs. 0.20 g predicted), the back-calculated magnitudes are relatively sensitive to GMPE performance for these cases (the sensitivity of estimates to the number of investigation sites will be evaluated later in this paper). In summary, if all GMPEs are weighted equally in the final assessment, the average estimates for the Darfield and Christchurch earthquakes are M_w7.1 and M_w6.3, respectively.

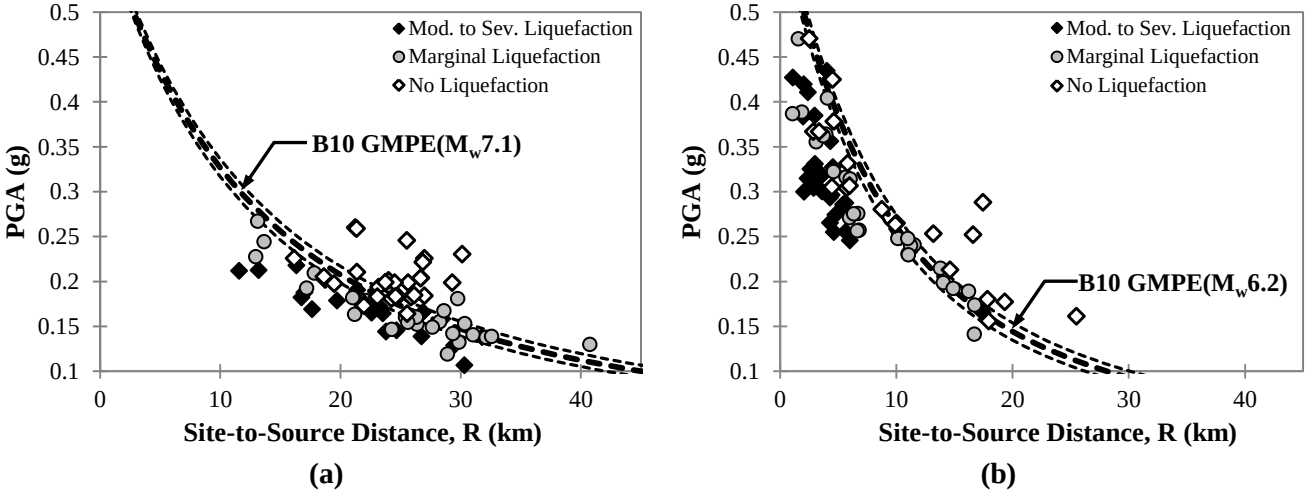

Figure 6 Regional assessment of the strength of shaking using the B10 GMPE for the (a) 4 Sept 2010 Darfield earthquake and (b) 22 Feb 2011 Christchurch earthquake. The back-calculated best-fit magnitude solutions are shown in addition to ± 0.1M_w solutions.

3.2.2 Unknown earthquake source locations

While the site-specific approach performed very well with known earthquake source locations/models, these are often unknown in paleoseismic investigations. As discussed previously, an energy center is commonly located using a regional assessment of the size of liquefaction features; the severity of liquefaction, which correlates to the strength of shaking, could thus be used to estimate the source

location from which magnitude back-calculations are computed. While this approach must be relied upon for the magnitude-bound approach, use of the objective parameter E_f for estimating earthquake magnitudes allows for the automated processing of infinitely many source locations. Thus, in cases where the source location is unknown (e.g., regions where the liquefaction susceptibility of deposits is not spatially uniform), an analyst can geospatially assess the likelihood of any source location considering E_f and the corresponding magnitude estimate. For example, if assessing paleoliquefaction in Christchurch, earthquake scenarios on the alpine fault and in the foothills of the Southern Alps would be considered likely sources, as these scenarios strongly influence the seismic hazard of the region and have the potential to induce liquefaction. In Fig. 7, these scenarios are considered as possible sources of the liquefaction field induced by the Feb 2011 Christchurch earthquake. The foothills earthquake (assumed source: -42.70, 172.44), with possible ruptures on the Ashley or Cust faults, is believed to be capable of producing an M_w6.9 – M_w7.4 (Stirling et al., 2007); historical analogs include the 1888 ~M_w7.1 North Canterbury and 1901 ~M_w6.9 Cheviot earthquakes. The alpine earthquake (assumed source: -42.82, 171.48) is believed to be capable of an ~M_w8.0 rupture (Stirling et al., 2007). It can be seen that the accelerations back-calculated from investigation sites fit very poorly with the rates of attenuation predicted by B10 for source locations considered in both the foothills (Fig. 7a) and on the alpine fault (Fig. 7b). Moreover, it can be seen that in both cases, the disagreement between the GMPE and back-calculated a_{max} values seems to indicate that the true source location is on the opposite side of the liquefaction field from the provisional source location (i.e., source locations south or southeast of Christchurch would fit the data better). In addition, the best-estimate earthquake magnitudes corresponding to the foothills and alpine fault scenarios are M_w8.5 and M_w8.8, respectively, which exceed the characteristic ruptures for these locations. Considering the unreasonable estimates of magnitude and poor fit of the data by the GMPE (i.e., high E_f), the foothills and alpine fault are unlikely sources of the earthquake which produced the observed liquefaction field in Christchurch.

Table 3. Estimates of the Darfield and Christchurch earthquake magnitudes obtained using the site-specific approach with known source locations and mechanisms.

	Darfield (M_w7.1)		**Christchurch (M_w7.1)**	
GMPE	**Estimated M_w**	**Estimate Error (%)**	**Estimated M_w**	**Estimate Error (%)**
BA08	6.90	-2.8	6.45	3.5
McV06	7.16	0.8	6.30	1.4
CY08	7.15	0.7	6.22	0.3
AS08	7.21	1.5	6.41	3.0
B10	7.12	0.3	6.20	0.0

Next, this approach is used to evaluate a grid of potential source locations for the Christchurch earthquake spaced ~4.5 km apart and covering an area roughly 30,000 km^2. The E_f at each grid location is then normalized with respect to the largest E_f computed in the grid to identify the most and least likely source locations, as based on agreement between regional back-calculated a_{max} values and the B10 GMPE. The distributions of normalized E_f values and best-estimate magnitudes for the Christchurch earthquake are shown in Figs. 8a and 8b, respectively. It can be seen that, based on E_f, the most likely source locations are in the Port Hills and northern margin of Banks Peninsula, while the least likely locations are found on the plains north of Christchurch and throughout the Southern Alps. In addition to many locations having high E_f values, the corresponding best-estimate magnitudes are often unreasonable. For example, aside from the foothills and easternmost mountain areas, the back-calculated magnitudes throughout most of the Southern Alps are unreasonably high. Thus, considering both E_f and magnitude estimates, the inferred most-likely source of the Christchurch earthquake is close to its actual location. It should be noted that the earthquake magnitudes are slightly higher (~0.2M_w) here as compared to the scenario with known source location/model because a strike-slip rupture is assumed rather than the actual reverse mechanism (see *3.1.2*). Corresponding to the source location with minimum E_f, the best-estimate magnitude of the causative earthquake is M_W6.8. The discrepancy between this estimate and the actual causative magnitude (i.e., M_w6.2) can be attributed to the aforementioned difference in assumed rupture mechanisms, and to the best-estimate source location being several km further from the liquefaction field as compared to the actual fault rupture.

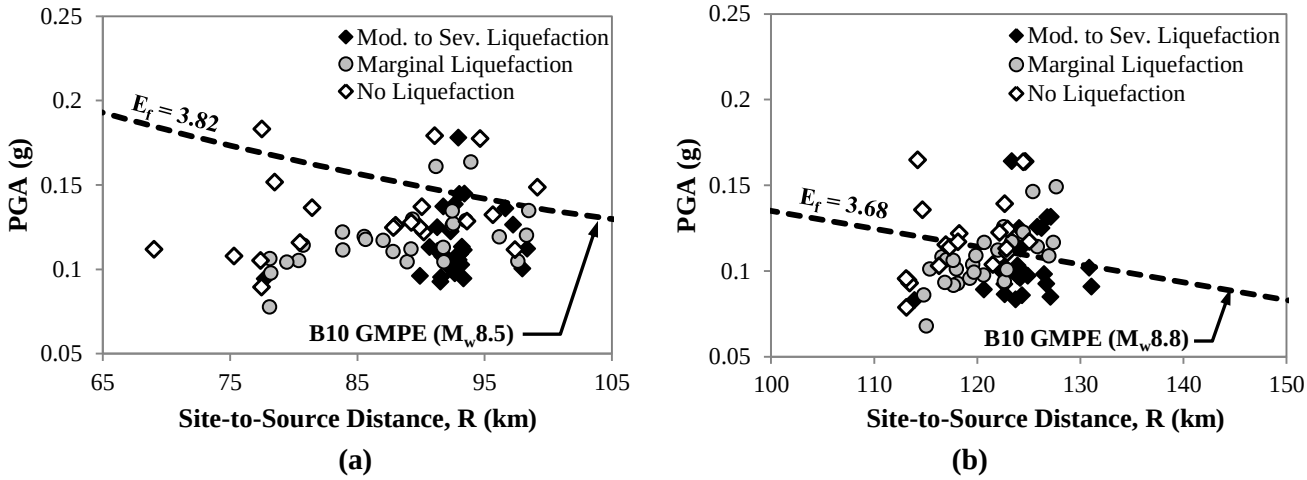

Figure 7 Regional assessment of the strength of shaking using the B10 GMPE for the 22 Feb 2011 Christchurch earthquake, considering source locations in the (a) foothills of the Southern Alps; and (b) on the alpine fault.

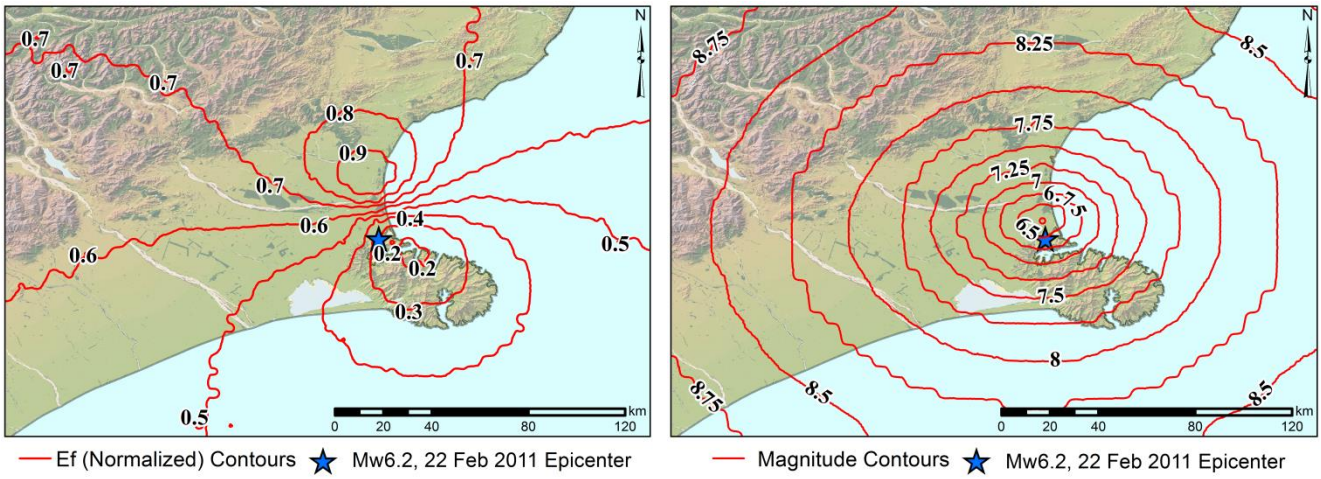

(a) **(b)**

Figure 8. Spatial distribution of (a) normalized E_f and (b) best-estimate magnitudes for the Christchurch earthquake. Together, E_f and the magnitude estimates can be used to identify likely source locations of a liquefaction-inducing earthquake.

Next, the grid-search technique is applied to the dataset from the Darfield earthquake; the spatial distributions of normalized E_f and earthquake magnitude are shown in Figs. 9a and 9b, respectively. It can be seen that, based on E_f, the least likely source locations for the Darfield earthquake are located in central Christchurch and extend throughout the metropolitan area. Unlike the Christchurch earthquake, the source location cannot be identified with any certainty. Although the minimum E_f is found in the general region of the actual rupture, its location is not well-bounded; it can be seen that potential source locations throughout a large area west, south, and north of Christchurch are nearly equally-likely. Using the $E_f = 0.2$ contour as the maximum threshold for consideration, and overlaying Fig. 9b, the causative earthquake is estimated to be $\geq M_w7.0$, but this estimate cannot be capped. It is hypothesized that lack of a precise source location for the Darfield earthquake is a consequence of lower GMPE attenuation rates at increasing site-to-source distances. Referring to Fig. 6, it can be seen that a_{max} attenuates more rapidly at shorter site-so-source distances than it does in the far-field. Therefore, when the earthquake source and liquefaction sites are close together (see Figure 6b), a_{max} is attenuating relatively quickly across the liquefaction field, resulting in a "steeper" dataset of back-calculated a_{max} values. Conversely, when the liquefaction field and earthquake source location are far apart (see Fig. 6a), the back-calculated a_{max} values fall on the "flatter" portion of the GMPE curve. As a result, for more distal earthquake sources, differences in E_f between the actual source location and other equally distal locations are likely to be subtle, even if these locations are in opposite directions from the liquefaction field. Nonetheless, this analysis suggests that a local earthquake is unlikely to be the cause of liquefaction observed in the Darfield earthquake and that the causative earthquake was likely $\geq M_w7.0$. Had the analysis been based on a single source location placed in central Christchurch in accordance with the centroid of liquefaction severity (as is generally done in paleoliquefaction studies), the best-estimate magnitude would be ~$M_w6.25$ with an E_f up to ten times higher than locations more distal from Christchurch.

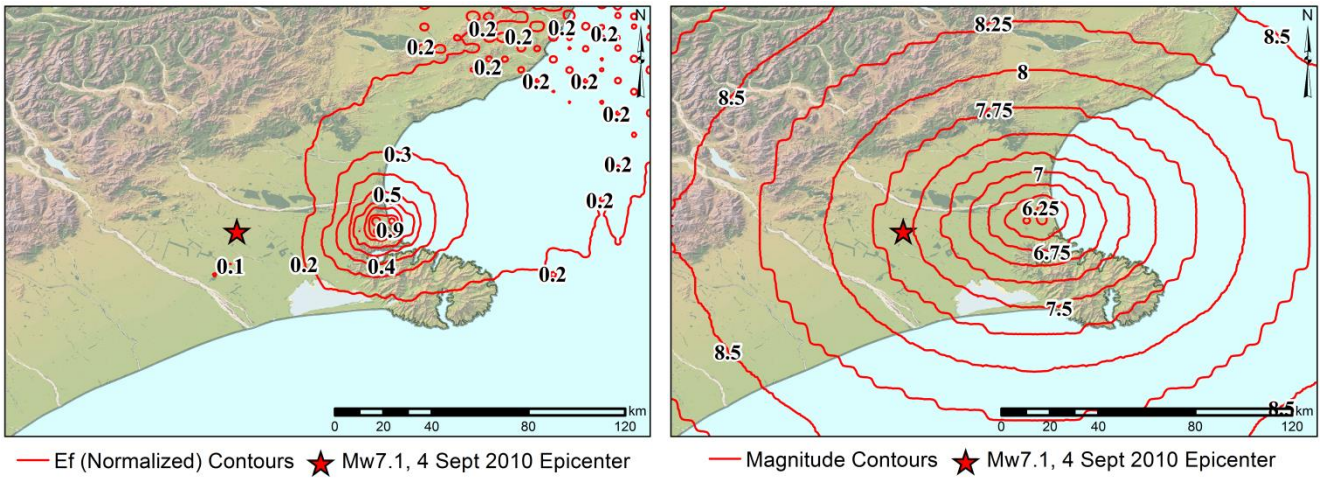

Figure 9. Spatial distribution of (a) normalized E_f and (b) best-estimate magnitudes for the Darfield earthquake. Together, E_f and the magnitude estimates can be used to identify likely source locations of a liquefaction-inducing earthquake.

3.2.3 Evaluating the sensitivity of the site-specific approach to the number of investigation sites

While it has been shown that seismic parameters can be accurately derived from the hypothetical scenario involving 75 investigation sites, the sensitivity of the site-specific approach to the number of data points (i.e. investigation sites) is unknown. Because field investigations can require years or decades of ongoing work, even the most thoroughly studied paleoseismic regions rely on fewer data points in their infancy, and many investigations would likely never attain 75 sites. As the analyses presented thus far represent reasonable best-case scenarios for a paleoliquefaction investigation in Christchurch, an assessment of scenarios utilizing fewer data points will complete the evaluation of the site-specific approach. To investigate the sensitivity of site-specific results to the number of data points, a uniformly-distributed random number generator is used to select datasets of varying size (5-75 points) from the database of 75 investigation sites. The relationship between the best-estimate magnitude and the number of data points is shown in Fig. 10 for the Darfield and Christchurch earthquakes, assuming both known and unknown source locations. It can be seen that when the source locations are known, the resulting best-estimate magnitudes are relatively insensitive to the number of investigation sites. For either earthquake, only 10 investigation sites are required to accurately estimate the actual magnitude with acceptable uncertainty ($\pm 0.1 M_w$); as the number of sites used in the analyses increases beyond 10, the back-calculated magnitudes remain stable, with uncertainty attenuating to zero. For the case of unknown source locations, significantly more investigation sites are required to reach a stable best-estimate magnitude. For either earthquake, approximately 35 investigation sites are required to compute a stable solution, with uncertainties differing between the two earthquakes. The variability of back-calculated magnitudes is insignificant beyond 30 investigation sites for the Darfield earthquake, but remains greater than $\pm$ 0.1M_w for the Christchurch earthquake until 60 investigation sites are used. This discrepancy is due, in part, to the diminishing rate of ground motion attenuation

with increasing site-to-source distance, as demonstrated by the magnitude-contours shown in Figs. 8 and 9. As such, it is likely that back-calculations will reach stability with fewer data points for more distal earthquake sources. In addition to requiring more investigation sites for a stable solution, it can be also be seen that the best-estimate magnitudes differ from the actual causative magnitudes, as discussed in section *3.3.2*.

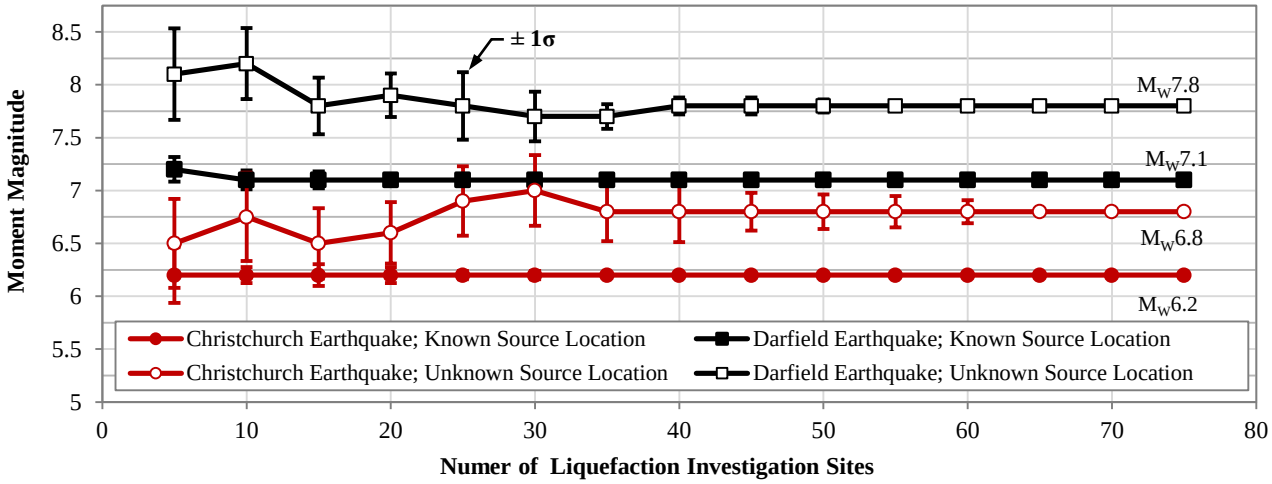

Figure 10. Sensitivity of the site-specific approach to the number of investigation sites.

3.3 Magnitude-bound approach

As discussed previously, one limitation of the magnitude-bound approach is that is yields a lower-bound estimate of magnitude rather than a median, or best-estimate magnitude. Because regional or site-specific factors (e.g., tectonic setting, liquefaction susceptibility) influence the maximum site-to-source distance at which liquefaction features are likely to occur, the magnitude-bound approach may significantly underestimate paleomagnitude in some cases. Thus, as discussed by Obermeier et al. (2001) and Olson et al. (2005a; 2005b), a regional or site-specific magnitude-bound correlation could yield a more accurate estimate. Accordingly, four different magnitude-bound relations, corresponding to differing degrees of site-specificity, are used herein to estimate the magnitudes of the Darfield and Christchurch earthquakes. The first is the Ambraseys (1988) magnitude-bound correlation, based on global liquefaction observations and used in numerous paleoliquefaction studies (e.g., Talwani and Schaeffer, 2001; Tuttle, 2001; Cox et al., 2004; González de Vallejo et al., 2005). The Ambraseys (1988) magnitude-bound relations for epicentral distance and fault distance are shown in Fig. 11a along with the global database of liquefaction observations used to develop the relations. The three remaining magnitude-bound relations utilized herein are developed specifically for this study.

The second approach is an empirical, New Zealand specific magnitude-bound relation developed in the style of Ambraseys (1988), but based on data from earthquakes in New Zealand only. In Table 4, historic New Zealand earthquakes with documented liquefaction observations are summarized. While some of these historic earthquakes are also found in the Ambraseys (1988) database, the estimated magnitude and/or site-to-source distance of liquefaction are in most cases

updated using recent refinements from the literature. For example, the 1848 Marlborough, New Zealand earthquake is listed in the Ambraseys (1988) database as having a surface wave magnitude of M_s7.1, derived from macroseismic data. More recently, Mason and Little (2006) reinvestigated the rupture length and displacement of the Awatere Fault during the Marlborough earthquake and proposed a refined moment magnitude estimate of M_w7.4 - M_w7.7. Since this event strongly influences the location of the magnitude-bound curve, refinement of the estimated magnitude is significant. The resulting empirical magnitude-bound relations for epicentral distance and fault distance are shown in Fig. 11b along with the database of New Zealand liquefaction observations used to develop the relations; to avoid bias in estimating the magnitudes of the Darfield and Christchurch earthquakes, data from the CES were omitted when curve-fitting the magnitude-bound relations. Although the relation based on fault distance is poorly constrained at short distances (<10 km) due to due limited case-history data, it is known that epicentral distance and fault distance must converge with diminishing earthquake magnitude. Accordingly, the trends identified where data is most dense (i.e., separation between epicentral- and fault-distance) were extrapolated to the near-field in a manner accounting for this requisite convergence.

The third and fourth approaches used herein are "theoretical" magnitude-bound relations. Using a similar approach to that of the site-specific geotechnical method (*see 3.1*), representative in-situ soil parameters may be used in conjunction with a liquefaction evaluation procedure (e.g., Robertson and Wride, 1998) to compute the minimum PGA required to induce liquefaction (i.e. FS_{liq} = 1). A regionally-appropriate GMPE is then used to compute the causative minimum magnitude earthquake required to induce liquefaction at any source distance (i.e., a magnitude-bound relation). Since the liquefaction evaluation procedure also depends on magnitude (via the MSF), the back-calculated magnitude is an iterative solution. In addition, the threshold strain concept (Dobry et al., 1980) affects the shape of the magnitude-bound correlation at far-field distances, where the exact influence and relevant source-distance depend on dynamic soil properties. Accordingly, the iterative solutions to develop magnitude-bound relations should also account for the threshold-strain PGA where applicable.

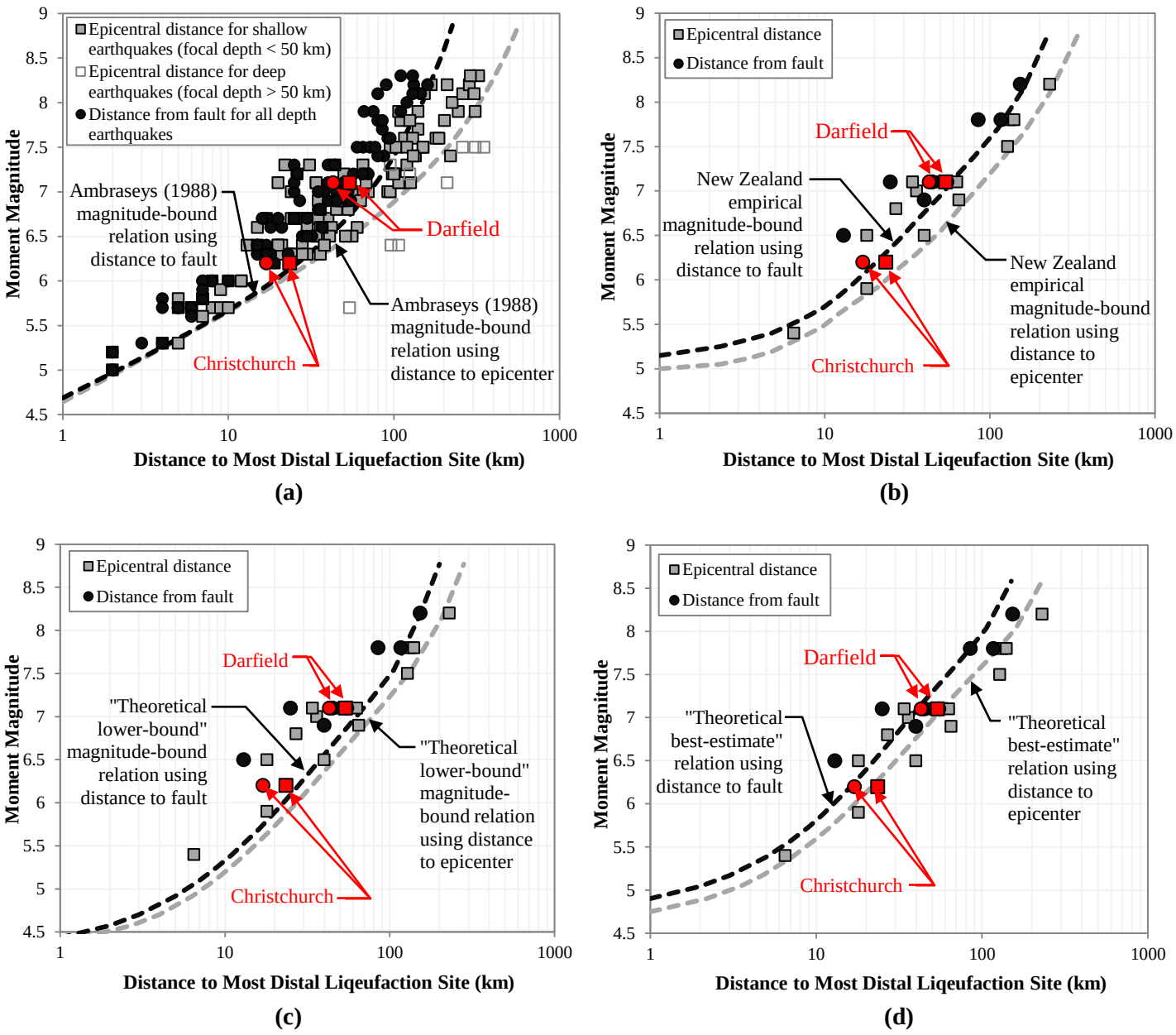

Figure 11. Magnitude-bound relations for epicentral distance to most distal liquefaction site and distance from fault to most distal liquefaction site, using: (a) worldwide data (Ambraseys, 1988); (b) New Zealand data (empirical approach, a la Ambraseys, 1988); (c) theoretical lower-bound approach, as described in text; and (d) theoretical best-estimate approach, as described in text. Worldwide data from earthquakes with liquefaction observations, as given by Ambraseys (1988), are shown in (a). Data from historic earthquakes in New Zealand with liquefaction observations, as given by Table 4, are shown in (b), (c), and (d).

Table 4. Historic earthquakes in New Zealand with liquefaction observations

Date	Earthquake	Estimated M[(a)]	Reference	Plotted M	Estimated R_e (km)[(d)]	Estimated R_f (km)[(e)]	Reference	Plotted R_e (km)	Plotted R_f (km)
16 Oct 1848	Marlborough	7.1[(b)]	Fairless & Berrill (1984); Ambraseys (1988)	7.5	128	-	Fairless & Berrill (1984)	128	-
		7.4 - 7.7	Mason & Little (2006)		126	-	Ambraseys (1988)		
23 Jan 1855	Wairarapa	7.6	Ambraseys (1988)	8.2	175	-	Fairless & Berrill (1984)	230	153
		8.2	Hancox (2005)		168	132	Ambraseys (1988)		
		8.2 - 8.3	GeoNet (2013)		230	153	Hancox (2005)		
31 Aug 1888	N. Canterbury	7.0[(c)]	Fairless & Berrill (1984)	7.1	50	45	Ambraseys (1988)	50	45
		6.9	Ambraseys (1988)		50	-	Fairless & Berrill (1984)		
		7.0 - 7.3	GeoNet (2013)						
15 Nov 1901	Cheviot	7.0	Fairless & Berrill (1984)	6.9	69	-	Fairless & Berrill (1984)	65	40
		7.3[(b)]	Ambraseys (1988)		65	40	Ambraseys (1988)		
		6.9 ± 0.2[(b)]	Dowrick & Smith (1990)						
		7.1 - 7.5	Berrill et al. (1994)						
		6.8[(c)]	GNS Science (2012)						
22 Feb 1913	Westport	6.8[(c)]	De Lange & Healy (1986)	6.8	27	-	Fairless & Berrill (1984)	27	-
25 Dec 1922	Motunau	6.5	Doser & Robinson (2002)	6.5	40	-	Christensen (2001), after Stirling et al. (1999)	40	-
		6.4[(c)]	GNS Science (2012)						
9 Mar 1929	Arthur's Pass	6.9[(b)]	Fairless & Berrill (1984)	7.0	36	-	Fairless & Berrill (1984)	36	-
		6.9[(b)]	Ambraseys (1988)		35	-	Ambraseys (1988)		
		7.0	GeoNet (2013)						
17 Jun 1929	Murchison	7.8[(b)]	Fairless & Berrill (1984); Carr & Berrill (2004)	7.8	132	117	Carr & Berrill (2004), after Benn (1992)	132	117

(a) Moment magnitude (M_w), except where noted
(b) Surface-wave magnitude (M_s)
(c) Unknown magnitude scale
(d) Site-to-source distance from epicenter to most distal liquefaction feature
(e) Site-to-source distance from fault to most distal liquefaction feature

Table 4 (Continued). Historic earthquakes in New Zealand with liquefaction observations

Date	Earthquake	Estimated M[(a)]	Reference	Plotted M	Estimated R_e (km)[(d)]	Estimated R_f (km)[(e)]	Reference	Plotted R_e (km)	Plotted R_f (km)
3 Feb 1931	Hawke's Bay	7.9[(c)]	Fairless & Berrill (1984)	7.8	140	-	Fairless & Berrill (1984)	140	85
		7.7	Ambraseys (1988)		140	85	Ambraseys (1988)		
		7.8[(b)]	GeoNet (2013)						
24 Jun 1942	Wairarapa	7.0[(c)]	Fairless & Berrill (1984)	7.1	63	-	Fairless & Berrill (1984)	63	55
		6.9	Ambraseys (1988)		63	55	Ambraseys (1988)		
		6.9 - 7.2	GeoNet (2013)						
24 May 1968	Inangahua	7.0[(c)]	Fairless & Berrill (1984)	7.1	29	-	Fairless & Berrill (1984)	34	25
		7.1	Ambraseys (1988)		34	25	Ambraseys (1988)		
		7.1	GeoNet (2013)		29		Carr & Berrill (2004)		
2 Mar 1987	Edgecomb	6.5	GeoNet (2013)	6.5	18	13	Franks (1988)	18	13
28 Jan 1991	Hawks Craig	6.2[(c)]	Carr & Berrill (2004)	5.9	18	-	Carr & Berrill (2004)	18	-
		5.9	COSMOS (2013)						
18 July 2004	Lake Rotoehu	5.4	GeoNet (2013)	5.4	6.5	-	Hancox et al. (2004)	6.5	-
4 Sept 2010	Darfield	7.1	GeoNet (2013)	7.1	64	54	Green & Cubrinovski (2010)	54	44
22 Feb 2011	Christchurch	6.2	GeoNet (2013)	6.2	23.5	17	CGD (2012)	23.5	17
13 June 2011	Christchurch	6.0	GeoNet (2013)	6.0	23	17	CGD (2012)	23	17

(a) Moment magnitude (M_w), except where noted
(b) Surface-wave magnitude (M_s)
(c) Unknown magnitude scale
(d) Site-to-source distance from epicenter to most distal liquefaction feature
(e) Site-to-source distance from fault to most distal liquefaction feature

To analytically generate a magnitude-bound relation which bounds all of the data points (i.e., a lower-bound curve), it must be recognized that the data points controlling the location of the curve correspond to the greatest liquefaction susceptibility, the greatest seismic loading, or some combination of the two scenarios. In other words, the source-distance at which liquefaction is likely to occur increases with the presence of highly liquefiable soils and/or greater than expected seismic loading for the respective earthquake magnitude and source distance. Thus, as seen in Figs. 11a and 11b, data points plotting significantly "left" of the bounding curve (i.e., at lesser site-to-source distances) correspond to cases where either (1) the tectonic setting, transmission characteristics, or stochastic variability produce lesser ground motions; or (2) the combination of ground water depth and cyclic resistance ratio result in lesser liquefaction susceptibility. In light of this, a magnitude-bound relation is theoretically computed herein using input parameters corresponding to elevated liquefaction susceptibility and greater than expected seismic loading. For this study, a lower bound curve is generated using the Bradley (2010, 2013) GMPE for Site Class D (soil) conditions with reverse fault-mechanism and + 0.5σ PGA, in conjunction with the Robertson and Wride (1998) liquefaction evaluation procedure and threshold strain concept (Dobry et al., 1980). This theoretical relation is computed using liquefaction evaluation input-parameters (i.e., penetration resistance, σ_v/σ'_v, r_d) corresponding to a "High" to "Very High" liquefaction susceptibility, as given by Olson et al. (2005b) and adapted from Youd and Hoose (1977) and Youd and Perkins (1978). Because the Bradley (2010, 2013) GMPE uses fault-distance as its distance metric, the empirical conversions of site-to-source distance metrics given by Scherbaum et al. (2004) are used to compute the magnitude-bound relation based on epicentral-distance. The resulting theoretical magnitude-bound relations for epicentral distance and fault distance are shown in Fig. 11c along with the database of New Zealand liquefaction observations given in Table 4. As illustrated here, it is thus possible to theoretically compute magnitude-bound relations consonant with empirical data using reasonable assumptions for input-parameters.

As evident from Figs. 11a-11c and prior discussion, the back-calculated magnitudes of some case-history data points are underestimated significantly more than others when they plot far from the magnitude-bound curve. As such, a median or "best-estimate" magnitude could be obtained using a relation which passes *through* the magnitude vs. source-distance data in place of a one that bounds the data. Such a relation can be generated analytically using input-parameters representative of median, rather than extreme, conditions. This method may be further refined by selecting parameters specific to the area of interest, which in effect, is a single-point application of the site-specific method. This approach supplements the three previously discussed magnitude-bound relations to collectively provide both a lower-bound and median estimate of earthquake magnitude. A theoretical best-estimate relation is computed herein using an approach very similar to that of the theoretical lower-bound relation. However, in this case, the Bradley (2010, 2013) GMPE is used to compute the median PGA for a Class D site in a strike-slip tectonic environment. In the absence of further information, these inputs represent reasonable median assumptions for a paleoliquefaction study in the Christchurch region. In addition, this

theoretical relation is computed using liquefaction susceptibility parameters representative of those found throughout much of the Christchurch region. Collectively, these inputs are very similar to those given by Olson et al. (2005b) for a site with "High" liquefaction susceptibility. The resulting best-estimate relations for epicentral distance and fault distance are shown in Fig. 11d along with the database of New Zealand liquefaction observations given in Table 4; as before, the relation based on epicentral distance is computed using the conversions of site-to-source distance metrics given by Scherbaum et al. (2004). As expected, and seen in Fig. 11d, the computed theoretical best-estimate relations pass *through* the data-cloud rather than bound it.

3.4 Magnitude-bound results and discussion

As was done for the site-specific analysis, a two-step approach will be taken to assess the efficacy of the magnitude-bound approach for estimating earthquake magnitudes. First, it is assumed that the earthquake source locations are known, and second, assuming the source locations are unknown, techniques for their determination are demonstrated and the associated magnitude estimates are assessed.

3.4.1 Known earthquake source locations

Using existing source models and fault slip distribution maps for the Darfield and Christchurch earthquakes (Barnhart et al., 2011; Beavan et al., 2011; Quigley et al., 2012), event magnitudes are estimated using the four magnitude-bound relations shown in Fig. 11 based on both epicentral distance and fault distance. The most distal observations of liquefaction in the Darfield event were located near the Ashley River in the coastal town of Waikuku (see Fig. 4); more-distal liquefaction was purported near the village of Akaroa on the Banks Peninsula (Cubrinovski and Green, 2010), but the authors have been unable to validate this report from either field reconnaissance, resident interviews, or a review of literature. In addition, recovering evidence from Akaroa in a paleoliquefaction study seems unlikely due to the fact that: (1) the purported feature(s) may have been located in a tidewater mudflat, reducing the likelihood of preservation in the geologic record (this would also represent an anomalous case, as per Ambraseys, 1988); and (2) Akaroa is geographically isolated, lacks alluvial geomorphology, and has only a small area of possibly liquefiable soil (Tonkin and Taylor, 2008) making it an unlikely location to search for paleoliquefaction evidence. Conversely, Waikuku is in a region of high liquefaction susceptibility (it was the site of documented liquefaction in the 1922 ~M_w6.5 Motunau earthquake: Christensen, 2001) and is situated on a river, where the most distal liquefaction features are often found (Obermeier et al., 2001). Accordingly, the features documented in Waikuku are taken to be most distal for this study, but the possibility exists that more distal liquefaction was induced. The uncertainty of locating the most distal feature immediately following the earthquake emphasizes the difficulty of doing so hundreds to thousands of years later in the absence of surficial manifestations. In the Christchurch earthquake, the most distal

liquefaction was observed in the vicinity of Kaiapoi along the margins of a larger liquefaction field; the authors are not aware of an alternative interpretation.

The site-to-source distances of the most distal features, used to estimate event magnitudes herein, are shown in Table 4. The resulting back-calculated magnitudes are summarized in Table 5; the average estimate errors from the epicenter- and fault-based relations are also given for each event. As expected, all three of the lower-bound magnitude-bound relations (i.e., Ambraseys, 1988; New Zealand empirical; theoretical lower-bound) underestimate the magnitudes of the Darfield and Christchurch earthquakes. Of the three, the New Zealand empirical relation provides the most accurate estimate, underestimating the respective earthquake magnitudes by 5.3% and 2.8%. The theoretical best-estimate approach has the lowest absolute error of the four relations, underestimating the Darfield magnitude by 0.4% and overestimating the Christchurch magnitude by 0.6%. There is no obvious advantage to using relations based on one distance metric over another (i.e., epicentral distance vs. fault distance). Summarily, if the earthquake source locations are known, the magnitude-bound approach performs well, with the accuracy of estimates improving with increasing site-specificity. As evidenced here, use of regional relations will yield more accurate estimates of paleomagnitudes, and their use is recommended, where possible, in lieu of relations based on global data. For this study, using the New Zealand empirical and theoretical best-estimate relations, the Darfield earthquake magnitude is estimated to be at least 6.6 – 6.8, with a median estimate of 7.0 – 7.1; the Christchurch earthquake magnitude is estimated to be at least 6.0, with a median estimate of 6.2 – 6.3.

Table 5. Estimates of the Darfield and Christchurch earthquake magnitudes obtained using the magnitude-bound approach with known source locations.

Magnitude-Bound Relation	Darfield (M_w7.1)			Christchurch (M_w6.2)		
	Estimated M_w using Epicentral Distance	Estimated M_w using Fault Distance	Average Estimate Error (%)	Estimated M_w using Epicentral Distance	Estimated M_w using Fault Distance	Average Estimate Error (%)
Ambraseys (1988)	6.54	6.50	-8.2	6.06	5.94	-3.2
New Zealand Empirical	6.82	6.62	-5.3	6.00	6.05	-2.8
Theoretical "Lower-Bound"	6.63	6.64	-6.5	5.85	5.72	-6.7
Theoretical "Best-Estimate"	7.12	7.03	-0.4	6.25	6.23	0.6

3.4.2 Unknown earthquake source locations

While the magnitude-bound approach performed well with known epicenter and fault location, earthquake source locations are often unknown in paleoseismic investigations. As discussed previously, an energy center is commonly located using a regional assessment of the size of liquefaction features, which correlate to the severity of liquefaction, and thus, to the strength of

shaking. With the severity of liquefaction manifested at the ground surface serving as a proxy for liquefaction feature size, the observations mapped by the authors (see Fig. 5) are used herein to estimate the energy centers of the Darfield and Christchurch earthquakes.

First, the hypothetical paleoliquefaction scenario involving 75 investigation sites (previously studied using the site-specific approach) is evaluated. The observed severity of liquefaction in the Darfield earthquake is mapped for each site in Fig. 12a; the two principal liquefaction fields (shown in Fig. 5) are also outlined. These boundaries generally define the limits of liquefaction observations and the areas of most-intensive geotechnical reconnaissance and in-situ characterization during the CES. It can be seen in Fig. 12a that sites of severe liquefaction are predominately located in central-eastern Christchurch, while several instances of moderate liquefaction are located in Kaiapoi. A provisional energy center (EC-D1), consistent with both the centroid of severe liquefaction and with observations of marginal liquefaction in Waikuku and southwest Christchurch, is mapped in Fig. 12a; the associated liquefaction field (Darfield 1), with maximum site-to-source distance of 20.5 km, is also shown. In the same manner, the observed severity of liquefaction in the Christchurch earthquake is mapped for each investigation site in Fig. 12b. It can be seen that relative to the Darfield event, liquefaction manifestations are more severe and more widespread in central and eastern Christchurch, and slightly less severe in western Christchurch and in Kaiapoi; in addition, liquefaction was not observed in Waikuku. Accordingly, a provisional energy center (EC-C1) is mapped approximately 5 km south of EC-D1, consistent with the centroid of observed liquefaction severity and with the marginal liquefaction observed in southwestern Christchurch; the corresponding liquefaction field (Christchurch 1), with maximum site-to-source distance of 19.5 km, is also mapped. Thus, the provisional energy centers and maximum site-to-source distances are very similar for these two events (i.e., the causative earthquakes have similar inferred magnitudes). However, from a comparison of Figs. 12a and 12b, the stark contrast in liquefaction severity throughout central and eastern Christchurch suggests the causative earthquakes are more dissimilar. In other words, at least one of the provisional energy centers, located using the centroids of liquefaction severity, is not fully compatible with the mapped observations. This is not surprising given that EC-D1 is displaced from the actual Darfield epicenter by more than 40 km.

A critical consideration missing from the magnitude-bound approach is the variability of liquefaction susceptibility within an affected region. The observations mapped in Figs. 12a and 12b are difficult to accurately interpret due to spatial non-uniformity of liquefaction susceptibility in the greater Christchurch region. Coastline transgression and progradation during the late Pleistocene and Holocene resulted in deposition of liquefaction-prone sediments across present-day Christchurch (Brown et al., 1995). The thickness of these deposits is greatest (~40 m) beneath the present-day coastline and attenuates westwardly, terminating 1-2 km west of the present-day CBD (Begg and Jones, 2012). Since the vertical extents of liquefiable soils generally attenuate from east to west, and because the depth to ground water increases from east to west, liquefaction susceptibilities tend to be greatest in the east and gradually diminish heading inland. Moving from the margins of Christchurch west across the Canterbury plains and south onto

Banks Peninsula, liquefaction susceptibility is minimal to none. In cases of such non-uniform susceptibility, the energy center could be located far from the centroid of most severe liquefaction. Therefore, by comparing liquefaction observations with liquefaction susceptibility, an analyst might more accurately locate the earthquake energy center.

Liquefaction potential index (LPI) has been used to develop liquefaction susceptibility maps for numerous locales, including many of paleoseismic interest in the U.S., such as Charleston, South Carolina (Elton and Hadj-Hamou, 1990; Hayati and Andrus, 2008), Memphis, Tennessee (Cramer et al., 2008), Washington State (Palmer et al., 2004), and the St. Louis metropolitan area of Missouri and Illinois (Chung and Rogers, 2011). The use of such maps for our study in Christchurch is thus consistent with many paleoliquefaction investigations. Applying a uniform seismic demand, LPI is computed herein from CPT soundings at ~1200 sites across the principal liquefaction fields using the framework of Iwasaki et al. (1978). The relative susceptibility of each site is classified according to the distribution of computed LPI values, and is mapped in Fig. 13. It can be seen that computed liquefaction susceptibilities are consistent with the known geologic profile, such that areas east of central Christchurch and nearest the coast generally have the greatest liquefaction hazard.

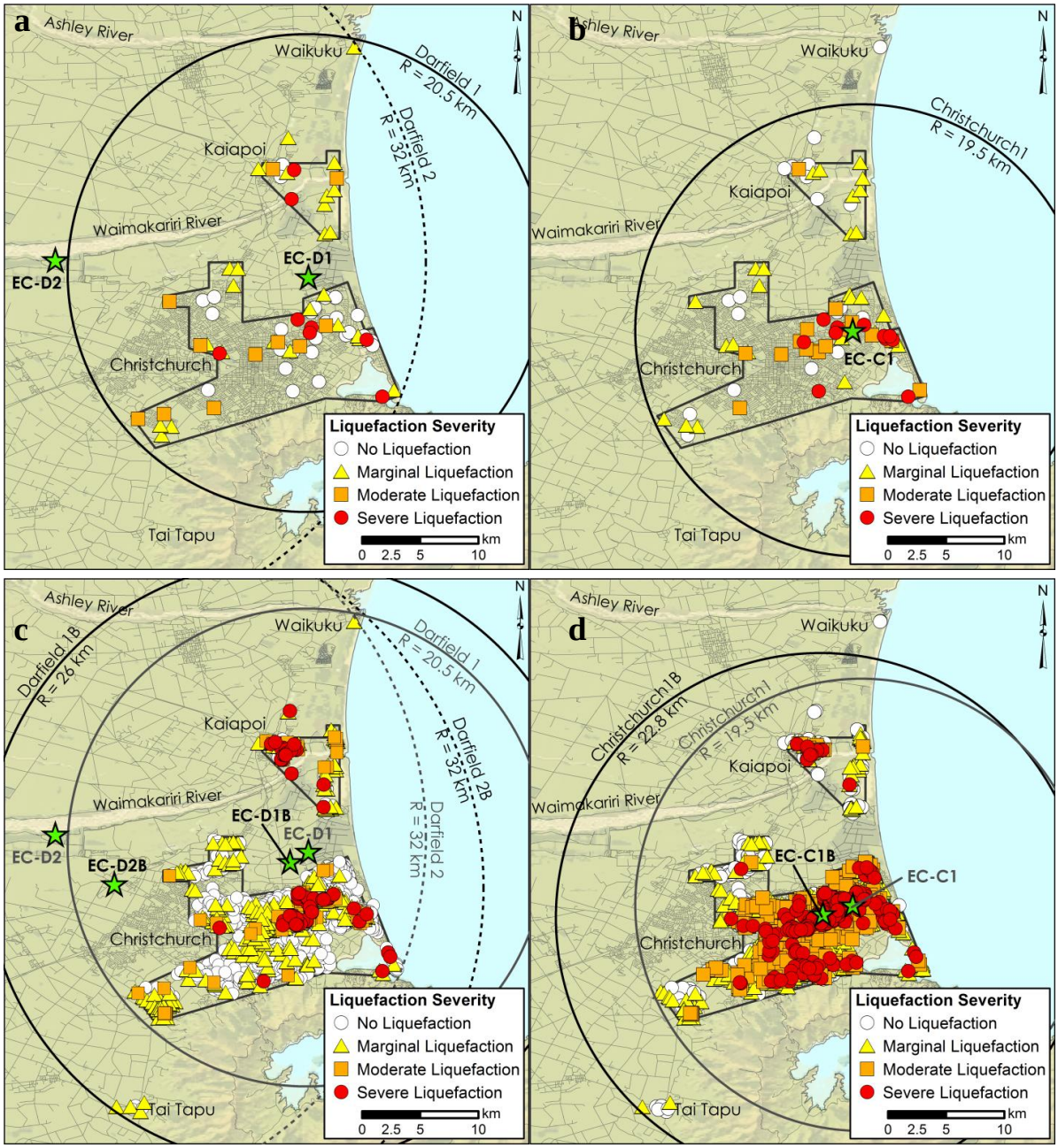

Figure 12. Determination of energy centers and maximum site-to-source distance of liquefaction for the (a) Darfield and (b) Christchurch earthquakes, considering 75 investigation sites; and the (c) Darfield and (d) Christchurch earthquakes, considering all investigation sites (~1500). As discussed in the text, "Darfield 2" is a revision of "Darfield 1" in consideration of the variability of liquefaction susceptibility (Fig. 13).

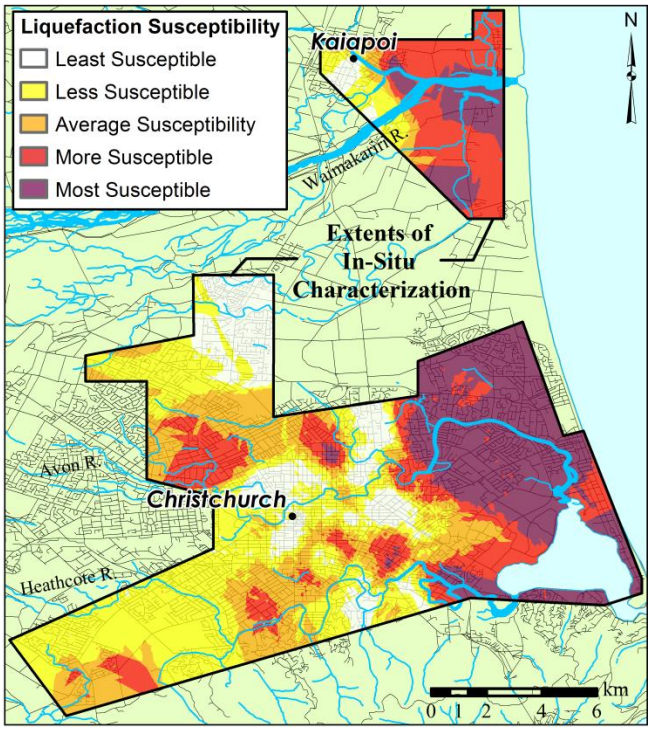

Fig 13. Distribution of relative liquefaction susceptibilities in zones of most intensive geotechnical characterization.

Returning to the Darfield observations mapped in Fig. 12a, and comparing with the susceptibilities mapped in Fig. 13, it can be seen that liquefaction did not manifest at many of the investigation sites located throughout the zone of highest susceptibility in eastern Christchurch. This suggests that the energy center should be relocated west or northwest of its original location. Accordingly, a new energy center (EC-D2) is mapped for the Darfield event in Fig. 12a, agreeable with mapped observations in consideration of the spatial variation of liquefaction susceptibility. In other words, the marginal liquefaction observations in western Christchurch, nearer to EC-D2 than observations of severe liquefaction, are consistent with the west-to-east gradient in susceptibility. The updated liquefaction field (Darfield 2), with maximum site-to-source distance of 32 km, is also shown. While it can be reasonably inferred that the energy center was west of the city, it is difficult to know how far west it might lie without computations to back-calculate the causative shaking at investigation sites. The suggested revised energy center is therefore in only one of many possible locations. Returning to the observations mapped in Fig. 12b for the Christchurch earthquake, observations of severe liquefaction are widespread throughout the region of greatest susceptibility, while observations of marginal liquefaction are dominant throughout the region of least susceptibility. As there are no obvious inconsistencies relating to directional attenuation, there is no compelling reason to relocate the provisional energy center EC-C1.

Next, the entire database of liquefaction observations from ~1500 investigation sites is used to interpret the magnitudes of the Darfield and Christchurch earthquakes. While such a scenario is entirely implausible for a paleoliquefaction investigation, this exercise will determine the limits of the magnitude-bound approach for these events. The observations from all investigation sites are mapped for the Darfield and Christchurch earthquakes in Figs. 12c and 12d, respectively, along with the previously interpreted energy centers and liquefaction field boundaries. For the Darfield event, energy center EC-D1 is adjusted slightly (EC-D1B) to account for the new centroid of liquefaction severity, while the inclusion of liquefaction observations in Tai Tapu, southwest of Christchurch, increases the maximum site to source distance (Darfield 1B) to 26 km. Referring to the liquefaction boundary "Darfield 2", interpreted through consideration of liquefaction susceptibility, it can be seen that observations of severe liquefaction are located near the boundary in southeastern Christchurch. Although these sites are in the region of greatest susceptibility, the presence of severe liquefaction near the boundary of most distal liquefaction is suspect. Accordingly, energy center EC-D2 is relocated approximately 6 km southeast (EC-D2B), with the maximum site-to-source distance remaining 32 km (Darfield 2B). Again, it is difficult to know how far west the energy center might lie without computations to back-calculate the causative shaking at investigation sites. For the Christchurch earthquake, energy center EC-C1 is adjusted slightly (EC-C1B) to account for the new centroid of liquefaction severity, while the liquefaction observations in Tai Tapu increase the maximum site to source distance (Christchurch 1B) to 22.8 km.

Finally, using the maximum site-to-source distances mapped in Figs. 12a-12d, the corresponding earthquake magnitudes are estimated using the empirical New Zealand and theoretical best-estimate magnitude-bound relations. As discussed in section *2.1.3*, an energy center inferred from liquefaction data is similar to an epicenter inferred from macroseismic data. As such, the magnitude-bound relations based on epicentral distance are likely most appropriate and are used herein. The resulting back-calculated magnitudes are summarized in Table 6 for the investigation scenarios discussed above; estimate errors are also given for each case. It can be seen that the Darfield earthquake magnitude is significantly underestimated in all cases, largely due to the inferred energy centers being far from the actual epicenter. The interpretation is improved by consideration of liquefaction susceptibility, with lower-bound and median magnitude estimates of 6.2 and 6.5, respectively, but these results still fall significantly short of the actual M_w7.1. Estimates of the Christchurch event magnitude are considerably more accurate due to the inferred energy centers being relatively closer to the actual epicenter. For the hypothetical investigation using 75 sites, the lower-bound and median magnitude estimates are 5.9 and 6.1, respectively. Using all field observations, the lower-bound and median estimates improve to 6.0 and 6.2, respectively. It should be noted, however, that this apparent accuracy is somewhat coincidental. The interpreted energy centers (EC-C1 and EC-C1b) are each displaced approximately 6.5 km from the actual epicenter, while the liquefaction features taken to be most distal (southeast of Christchurch) are likewise far removed from the actual most distal features located near Kaiapoi.

Table 6. Estimates of the Darfield and Christchurch earthquake magnitudes obtained using the magnitude-bound approach with unknown source locations and four investigation scenarios, as described in text

Investigation Scenario	Magnitude-Bound Relation	Darfield (M_w7.1)		Christchurch (M_w 6.2)	
		Estimated M_w using Epicentral Distance	Estimate Error (%)	Estimated M_w using Epicentral Distance	Estimate Error (%)
A. Hypothetical case using 75 sites	New Zealand Empirical	5.95	-16.2	5.90	-4.8
	Theoretical "Best-Estimate"	6.13	-13.7	6.10	-1.6
B. Hypothetical case using 75 sites, with consideration of liq. susceptibility	New Zealand Empirical	6.22	-12.4	Same as Scenario A	
	Theoretical "Best-Estimate"	6.53	-8.0		
C. Using all field observations	New Zealand Empirical	6.08	-14.4	6.00	-3.2
	Theoretical "Best-Estimate"	6.33	-10.8	6.22	0.3
D. Using all field observations, with consideration of liq. susceptibility	New Zealand Empirical	Same as Scenario B		Same as Scenario C	
	Theoretical "Best-Estimate"				

In summary, the following observations are made regarding the performance of the magnitude-bound approach for estimating the magnitudes of the Darfield and Christchurch earthquakes:

- If the most distal liquefaction features are located, and if the earthquake source locations are known, the magnitude-bound approach performs very well, with the accuracy of estimates improving with increasing site-specificity. Use of both lower-bound and median magnitude-bound relations is recommended.
- In the absence of known earthquake source locations, accurate interpretation is difficult, due in part to the non-uniform liquefaction susceptibility of the region, which allows the most severe liquefaction to be located far from the earthquake source. This is particularly true of the Darfield earthquake, in which case the epicenter and fault rupture are far removed from the liquefaction field. In such cases, consideration of liquefaction susceptibility may enable an analyst to more accurately locate the earthquake energy center. However, once the energy center is moved away from the liquefaction field, it is very difficult to determine the correct location without computations to back-calculate the causative ground motion. Even with

1500 liquefaction observations, the location of the Darfield energy center is still highly uncertain.

- Similarly, if the most distal features are not located, accurate interpretation is difficult. The distal liquefaction observations in Waikuku and Tai Tapu affect the inferred maximum site-to-source distance of liquefaction, and in turn, the back-calculated earthquake magnitudes. This highlights the sensitivity of the magnitude-bound approach to locating the most distal features.
- Finally, while the authors believe the locations of inferred energy centers are based on reasonable assumptions, the process is no doubt highly subjective and speculative. Other analysts might reasonably select different energy centers and/or obtain different magnitude estimates.

4. Summary and Conclusions

In the study presented herein, the accuracies of paleoliquefaction back-analysis methods were assessed using case studies from the 2010-2011 CES. In addition, the challenges, techniques, and uncertainties associated with the application of these methods were explored. It was shown that both the site-specific and magnitude-bound methods are capable of accurately deriving seismic parameters from liquefaction evidence, particularly when the earthquake source location/model is known. Because source location is often unknown in paleoliquefaction investigations, and because accurate interpretation is more difficult in such cases, new analysis techniques were proposed herein. For the site-specific approach, use of the objective parameter E_f enables an analyst to geospatially assess the likelihood of infinitely many provisional source locations, and to more accurately estimate the most likely magnitude of the causative earthquake. For the magnitude-bound approach, consideration of liquefaction susceptibility can likewise enable an analyst to more accurately estimate the location and magnitude of the causative earthquake. Although both approaches have the capacity to produce accurate back-analyses, each has inherent complexities, sensitivities, and sources of uncertainty. As such, a thorough understanding of the source data, derivations, and procedures comprising these approaches is critical.

In addition to assessing the accuracy of back-analysis techniques, this study presents a framework for performing back-analyses in paleoseismic regions worldwide. Even in thoroughly studied regions such as the NMSZ, the computed seismic hazard remains controversial and pervaded by uncertainty, due in large part to the uncertain accuracy of paleoliquefaction analysis techniques. The techniques proposed herein and lessons learned from their application to modern earthquakes could be applied to the NMSZ, where the computed seismic hazard has significant and far-reaching implications. Specific to Christchurch, this study provides a direct framework for analyzing paleoliquefaction evidence discovered in the region. As shown herein, a rupture on the alpine fault producing widespread liquefaction in Christchurch appears unlikely. While this scenario could produce sporadic liquefaction in the most susceptible soils, the liquefaction fields

induced by the Darfield and Christchurch earthquakes would likely require rupture magnitudes unreasonably high for the alpine fault. As the first paleoliquefaction features are discovered in the region, the magnitude-bound relations proposed herein can be used to assess the plausibility of potential source locations; likewise, the site-specific approach can be used at investigation sites to compute lower- or upper-bound earthquake magnitudes corresponding to potential source locations. If and when more paleoliquefaction is discovered, the site-specific approach, in conjunction with E_f, can be used to estimate the most likely location and magnitude of the causative earthquake. Thus, the framework presented herein could ultimately clarify the regions paleoseismic history and lead to a more accurately computed seismic hazard.

Notice

Some figures were created from maps and/or data extracted from the Canterbury Geotechnical Database (https://canterburygeotechnicaldatabase.projectorbit.com), which were prepared and/or compiled for the Earthquake Commission (EQC) to assist in assessing insurance claims made under the Earthquake Commission Act 1993. The source maps and data were not intended for any other purpose. EQC and its engineers, Tonkin & Taylor, have no liability for any use of the maps and data or for the consequences of any person relying on them in any way.

Part A References

Abrahamson, N., and Silva, W., (2008). "Summary of the Abrahamson & Silva NGA ground-motion relations." *Earthquake Spectra,* 24(1): 67–97.

Ambraseys, N.N. (1988). "Engineering seismology." *Earthquake Engineering and Structural Dynamics*, 17: 1-105.

Atkinson, G. M., and Boore, D.M. (2011). "Modifications to existing ground-motion prediction equations in light of new data." *Bulletin of the Seismological Society of America,* 101(3): 1121-1135.

Aydan, O., Ulusay, R., Kumsar, H., and Tuncay, E. (2000). "Site investigation and engineering evaluation of the Duzce-Bolu earthquake of November 12, 1999." Turkish Earthquake Foundation, Istanbul. Report No. TDV/DR 09-51, 307 p.

Barnhart, W. D., M. J. Willis, R. W. Lohman, and A. K. Melkonian (2011). "InSAR and optical constraints on fault slip during the 2010-2011 New Zealand earthquake sequence." *Seismological Research Letters*, 82(6): 815-823.

Bastin, S., Quigley, M. and Bassett, K. (2012). "Characterisation of modern and paleo-liquefaction features in Christchurch following the 2010-2011 Canterbury earthquake sequence." [poster presentation] San Francisco, CA, USA: American Geophysical Union Fall Meeting (AGU), 3-7 Dec 2012.

Beavan, J., Fielding, E., Motagh, M., Samsonov, S., and Donnelly, N. (2011). "Fault location and slip distrivution of the 22 February 2011 M_w6.2 Christchurch, New Zealand, earthquake from geodetic data." *Seismological Research Letters,* 82(6): 789-799.

Begg, J. and Jones, K. (2012). "20,000 years of time in Christchurch." [*presentation*] New Zealand Geotechnical Society, Canterbury Branch, 28 June 2012.

Benn, J. L. (1992.) “A Review of Earthquake Hazards on the West Coast.” The West Coast Regional Council, Greymouth, New Zealand.

Berg, G.V., Bolt, B.A., Sozen, M.A., and Rjahn, C. (1980). “Earthquake in Romania – March 4, 1977: an engineering report.” National Research Council and Earthquake Engineering Research Institute, National Academy Press, Washington D.C., 39 p.

Berrill, J. B., Bienveny, V. C., and Callaghan, M. W. (1988). “Liquefaction in the Buller Region in the 1929 and 1968 Earthquakes.” *Bulletin of the New Zealand National Society for Earthquake Engineering*, 21(3): 174-189.

Berrill, J.B., Mulqueen, P.C., and Ooi, E.T.C. (1994). "Liquefaction at Kaiapoi in the 1901 Cheviot, New Zealand, earthquake." *Bulletin of the New Zealand National Society for Earthquake Engineering*, 27 (3): 178-189.

Boore, D. M., and Atkinson, G.M. (2008). “Ground-motion prediction equations for the average horizontal component of PGA, PGV, and 5%-damped PSA at spectral periods between 0.01 s and 10.0 s.” *Earthquake Spectra*, 24(1): 99–138.

Bradley, B. A. (2010). *NZ-specific Pseudo-spectral Acceleration Ground Motion Prediction Equations Based on Foreign Models*. Department of Civil and Natural Resources Engineering, University of Canterbury, Christchurch, New Zealand, 324 pp.

Bradley, B. A. (2012a). "Strong ground motion characteristics observed in the 4 September 2010 Darfield, New Zealand earthquake." *Soil Dynamics and Earthquake Engineering*, 42: 32-46.

Bradley, B. A. (2012b). "Ground motions observed in the Darfield and Christchurch earthquakes and the importance of local site response effects." *New Zealand Journal of Geology and Geophysics*, 55: 279-286.

Bradley, B. A. (2013). "A New Zealand-specific pseudo-spectral acceleration ground-motion prediction equation for active shallow crustal earthquakes based on foreign models." *Bulletin of the Seismological Society of America* (in press).

Bradley, B. A. and Cubrinovski, M., (2011). "Near-source Strong Ground Motions Observed in the 22 February 2011 Christchurch Earthquake." *Seismological Research Letters*, 82(6): 853-865.

Brown, L.J., Beetham, R.D., Paterson, B.R., and Weeber, J.H. (1995). “Geology of Christchurch, New Zealand.” *Environmental and Engineering Geoscience*, 1: 427–488.

Carr, K. and Berrill, J. (2004). "Liquefaction case histories from the west coast of the south island, New Zealand." *13th World Conference on Earthquake Engineering*, 1-6 Aug 2004, Vancouver Canada, Paper No. 1325.

Canterbury Earthquakes Royal Commission (2012). “Summary and recommendations in volumes 1-3, seismicity, soils, and the seismic design of buildings.” *Final Report: part 1, volume 1*. Canterbury Earthquakes Royal Commission, Wellington, New Zealand.

Castilla, R.A. and Audemard, F.A. (2007). “Sand blows as a potential tool for magnitude estimation of pre-instrumental earthquakes.” *Journal of Seismology*, 11: 473-487.

CDG - Canterbury Geotechnical Database (2012a) "Aerial Photography", Map Layer CGD0100 - 1 June 2012, retrieved [12/12] from https://canterburygeotechnicaldatabase. projectorbit.com

CDG - Canterbury Geotechnical Database (2012b) "Observed Ground Crack Locations", Map Layer CGD0400 - 23 July 2012, retrieved [12/12] from https://canterburygeotechnical database.projectorbit.com

Cetin, K.O., Seed, R.B., Der Kiureghian, A., Tokimatsu, K., Harder, L.F., Kayen, R.E., and Moss, R.E.S. (2004). "Standard Penetration Test-Based Probabilistic and Deterministic Assessment of Seismic Soil Liquefaction Potential." *Journal of Geotechnical and Geoenvironmental Engineering*, ASCE, 130(12): 1314-1340.

Chiou, B. S.-J., and Youngs, R.R (2008). "An NGA model for the average horizontal component of peak ground motion and response spectra." *Earthquake Spectra,* 24(1): 173-215.

Chiou, B., Youngs, R.R., Abrahamson, N., and Addo, K. (2010). "Ground-motion attenuation model for small-to-moderate shallow crustal earthquakes in california and its implications on regionalization of ground-motion prediction models." *Earthquake Spectra*, 26(4): 907-926.

Christensen, S.A. (2001). "Regional liquefaction study for Waimakariri district." *Proceedings of the New Zealand Society of Earthquake Engineering 2001 Technical Conference,* 23-25 Mar 2001, Taupo NZ.

Chung, J.W. and Rogers, D. (2011). "Simplified method for spatial evaluation of liquefaction potential in the St. Louis area." *Journal of Geotechnical and Geoenvironmental Engineering*, 137(5): 505-515.

Cox, R.T. (2004). "Preliminary assessment of sand blows in the southern Mississippi embayment." *Bulletin of the Seismological Society of America*, 94(3): 1125-1142.

Cramer, C.H., Rix, G.J., and Tucker, K. (2008). "Probabilistic liquefaction hazard maps for Memphis, Tennessee." *Seismological Research Letters*, 79(3): 416-423.

Cubrinovski, M. and Green, R.A. (Eds.) (2010). "Geotechnical reconnaissance of the 2010 Darfield (Canterbury) earthquake." *Bulletin of the New Zealand Society for Earthquake Engineering*, 43(4): 243-319.

Cubrinovski, M, Bray, J.D., Taylor, M., Giorgini, S., Bradley, B., Wotherspoon, L., and Zupan J. (2011a). "Soil liquefaction effects in the central business district during the February 2011 Christchurch earthquake." *Seismological Research Letters*, 82(6): 893-904.

Cubrinovski, M., Bradley, B., Wotherspoon, L., Green, R., Bray, J., Woods, C., Pender, M., Allen, J., Bradshaw, A., Rix, G., Taylor, M., Robinson, K., Henderson, D., Giorgini, S., Ma, K., Winkley, A., Zupan, J., O'Rourke, T., DePascale, G., and Wells, D. (2011b). "Geotechnical aspects of the 22 February 2011 Christchurch earthquake." *Bulletin of the New Zealand Society for Earthquake Engineering*, 43(4): 205-226.

De Lange, W.P. and Healy, T.R. (1986). "New Zealand tsunamis 1840-1982." *New Zealand Journal of Geology and Geophysics*, 29: 115-134.

Dobry, R., Powell, D.J., Yokel, F.Y., and Ladd, R.S. (1980). "Liquefaction potential of saturated sand – the stiffness method." *Proceedings of the 7th World Conference on Earthquake Engineering*, Istanbul, *3: 25-32.*

Doser, D.I. and Robinson, R. (2002). "Modeling stress chanfes induced by earthquakes in the southern Marlborough region, south island, New Zealand." *Bulletin of the Seismological Society of America*, 92(8): 3229-3238.

Environment Canterbury (ECan) (2004). "Solid facts on Christchurch liquefaction." Environment Canterbury, Christchurch, New Zealand; http://ecan.govt.nz/publications/General/soid-facts-christchurch-liquefaction.pdf.

Ellis, C. and de Alba, P. (1999). "Acceleration distribution and epicentral location of the 1755 "Cape Ann" earthquake from case histories of ground failure." *Seismological Research Letters,* 70(6): 758-773.

Elnashai, A.S., Cleveland, L.J., Jefferson, T., and Harrald, J. (2009). “Impact of earthquakes on the Central USA.” Mid-America Earthquake Center Report 09-03, University of Illinois at Urbana-Champaign, Urbana, IL.

Elton, D.J. and Hadj-Hamou, T. (1990). “Liquefaction potential map for Charleston, South Carolina.” *Journal of Geotechnical Engineering,* 116(2): 244-265.

Fairless, G., and Berrill, J. (1984). "Liquefaction during historic earthquakes in New Zealand." *Bulletin of the New Zealand Society of Earthquake Engineers,* 17: 280-291.

Franks, C.A. (1988). "Engineering geological aspects of the Edgecomb, New Zealand earthquake of 2 March 1987." *Quarterly Journal of Engineering Geology,* 21: 337-345.

Galli, P. (2000). “New empirical relationships between magnitude and distance for liquefaction.” *Tectonophysics*, 324: 169-187.

González de Vallejo, L.I., Tsigé, M., and Cabrera, L. (2005). “Paleoliquefaction features on Tenerife (Canary Islands) in Holocene sand deposits.” *Engineering Geology,* 76: 179-190.

Green, R.A., Olson, S.M., and Obermeier, S.F. (2005). “Geotechnical analysis of paleoseismic shaking using liquefaction effects: field examples.” *Engineering Geology,* 76: 263-293.

Green, R.A., Allen, A., Wotherspoon, L., Cubrinovski, M., Bradley, B., Bradshaw, A., Cox, B., and Algie, T. (2011). “Performance of levees (stopbanks) during the 4 September M_w7.1 Darfield and 22 February 2011 M_w6.2 Christchurch, New Zealand, earthquakes.” *Seismological Research Letters*, 82(6): 939-949.

Green, R.A., Cubinovski, M., Cox, B., Wood, C., Wotherspoon, L., Bradley, B., and Maurer, B.W. (2013). “Select liquefaction case histories from the 2010-2011 Canterbury earthquake sequence.” *Earthquake Spectra*, *in review*.

Hancox, G.T., Dellow, G., Mc Saveney, B., and Villamor, P. (2004). "Reconnaissance studies of landslides caused by the ML 5.4 Lake Rotoehu earthquake and swarm of July 2004.” Institute of Geological & Nuclear Sciences science report 2004/24. 21p.

Hancox, G.T. (2005). "Landslides and liquefaction effects caused by the 1855 Wairarapa earthquake: then and now.” *The 1855 Wairarapa Earthquake Symposium: 150 Years of thinking about magnitude 8+ earthquakes and seismic hazard in New Zealand (J. Townend, R. Langridge, and A. Jones, eds.).* Greater Wellington Regional Council.

Hayati, H. and Andrus, R.D. (2008). “Liquefaction potential map of Charleston, South Carolina base on the 1886 earthquake.” *Journal of Geotechnical and Geoenvironmental Engineering,* 134(6): 815-828.

Idriss, I.M. and Boulanger, R.W. (2006). “Semi-empirical procedures for evaluating liquefaction potential during earthquakes.” *Soil Dynamics and Earthquake Engineering*, 26: 115-130.

Iwasaki, T., Tatsuoka, F., Tokida, K., and Yasuda, S. (1978). “A practical method for assessing soil liquefaction potential based on case studies at various sites in Japan.” *Proceedings of the 2nd International Conference on Microzonation*, Nov 26-Dec 1, San Francisco, CA, USA.

Kam, W.Y., Akguzel, U., and Pampanin, S. (2011). “4 Weeks on: preliminary reconnaissance report from the Christchurch 22 Feb 2011 6.3M_w earthquake.” Report, New Zealand Society of Earthquake Engineering, Wellington, New Zealand.

Kuhn, G.G. (2005). “Paleoseismic features as indicators of earthquake hazards in North Coastal, San Diego County, California, USA.” *Engineering Geology*, 80: 115-150.

Kuribayahsi, E. and Tatsuoka, F. (1975). “Brief review of liquefaction during earthquakes in Japan.” *Soils and Foundations,* 15(4): 81-92.

Mason, D.P.M. and Little, T.A. (2006). "Refined slip distribution and moment magnitude of the 1848 Marlborough earthquake, Awatere Fault, New Zealand." *New Zealand Journal of Geology and Geophysics,* 49(3): 375-382.

Maurer, B.W., Green, R.A., Cubrinovski, M., and Bradley, B. (2013). "Evaluation of liquefaction potential index (LPI) for assessing liquefaction hazard: a case study in Christchurch, New Zealand." *Journal of Geotechnical and Geoenvironmental Engineering,* ASCE, *in review*.

McVerry, G. H., J. X. Zhao, N. A. Abrahamson, and P. G. Sommerville (2006). "New Zealand acceleration response spectrum attenuation relations for crustal and subduction zone earthquakes." *Bulletin of the New Zealand Society for Earthquake Engineering,* 39(1): 1-58.

Moss, R.E.S, Seed, R.B., Kayen, R.E., Stewart, J.P., Der Kiureghian, A., and Cetin, K.O. (2006). "CPT-based probabilistic and deterministic assessment of in situ seismic soil liquefaction potential." *Journal of Geotechnical and Geoenvironmental Engineering,* ASCE, 132(8):1032-1051.

Obermeier, S.F. (1998). "Liquefaction evidence for strong earthquakes of Holocene and latest Pleistocene ages in the states of Indiana and Illinois, USA." *Engineering Geology,* 50: 227–254.

Obermeier, S.F., Martin, J.R., Frankel, A.D., Youd, T.L., Munson, P.J., Munson, C.A., Pond, E.C. (1993). "Liquefaction evidence for one or more strong Holocene earthquakes in the Wabash Valley of southern Indiana and Illinois." U.S. Geological Survey Professional Paper 1536, 27 p.

Obermeier, S.F. and Dickenson, S.E. (2000). "Liquefaction evidence for the strength of ground motiosn resulting from the late Holocene Cascadia subduction earthquakes, with emphasis on the event of 1700 A.D." *Bulletin of the Seismological Society of America,* 90(4): 876-896.

Obermeier, S.F., Pond, E.C., Olson, S.M. with contributions by Green, R.A., Mitchell, J.K., and Stark, T.D. (2001). "Paleoliquefaction studies in continental settings: geologic and geotechnical factors in interpretations and back-analysis." U.S. Geological Survey Open-File Report 01-029.

Obermeier, S.F., Olson, S.M., and Green, R.A. (2005). "Field occurrences of liquefaction-induced features: a primer for engineering and geologic analysis of paleoseismic shaking." *Engineering Geology,* 76: 209-234.

Olson, S.M., Green, R.A., and Obermeier, S.F. (2005a). "Geotechnical analysis of paleoseismic shaking using liquefaction features: a major updating." *Engineering Geology,* 76: 235-261.

Olson, S.M., Green, R.A., and Obermeier, S.F. (2005b). "Revised magnitude bound relation for the Wabash Valley Seismic Zone of the central United States." *Seismological Research Letters,* 76(6): 756-771.

Orense, R.P., Kiyota, T., Yamada, S., Cubrinovski, M., Hosono, Y., Okamura, M., and Yasuda, S. (2011). "Comparison of liquefaction features observed during the 2010 and 2011 Canterbury earthquakes." *Seismological Research Letters,* 82(6): 905-918.

Palmer, S.P., Magsino, S.L., Bilderback, E.L., Poelstra, J.L., Folger, D.S., Niggemann, R.A. (2004). "Liquefaction susceptibility and site class maps of Washington State, by county." Washington State Department of Natural Resources, Open File Report 2004-20.

Papadopoulos, G.A. and Lefkopoulos (1993). "Magnitude-distance relations for liquefaction in soil from earthquakes." *Bulletin of the Seismological Society of America,* 83(3): 925-938.

Papathanassiou, G., Pavlides, S., Christaras, B., and Pitilakis, K. (2005). "Liquefaction case histories and empirical relations of earthquake magnitude versus distance from the broader Aegean region." *Journal of Geodynamics,* 40: 257-278.

Petersen, M., A., Frankel, S., Harmsen, C., Mueller, K., Haller, R., Wheeler, R., Wesson, Y., Zeng, O., Boyd, D., Perkins, N., Luco, E., Field, C.Wills, and Rukstales, K.(2008). "Documentation for the

2008 update of the United States national seismic hazard maps." U. S. Geological Survey Open-File Report 2008-1128, 61 p.

Pirrotta, C., Barbano, M.S., Guarnieri, P., and Gerardi, F. (2007). "A new dataset and empirical relationships between magnitude/intensity and epicentral distance for liquefaction in central-eastern Sicily." *Annals of Geophysics*, 50(6): 763-774.

Quigley, M., Van Dissen, R., Litchfield, N., Villamor, P., Duffy, B., Barrell, D., Furlong, K., Stahl, T., Bilderback, E. and Noble, D. (2012). "Surface rupture during the 2010 M_w7.1 Darfield (Canterbury) earthquake: Implications for fault rupture dynamics and seismic-hazard analysis." *Geology* 40(1): 55-58.

Quigley, M.C., Bastin, S., and Bradley, B.A. (2013). "Recurrent liquefaction in Christchurch, New Zealand, during the Canterbury earthquake sequence." *Geology, 41(4): 419-422.*

Rhea, S. and Wheeler, R.L. (1996). "Map showing seismicity in the vicinity of the lower Wabash Valley, Illinois, Indiana, and Kentucky." U.S. Geological Survey Miscellaneous Investigation Map I-2583-A, scale 1:250,000.

Robertson, P.K. and Cabal, K.L. (2010). "Estimating soil unit weight from CPT." *2nd International Symposium on Cone Penetration Testing*, Huntington Beach, CA, USA, May 2010, Paper # 2-40.

Robertson, P.K. and Wride, C.E. (1998). "Evaluating cyclic liquefaction potential using cone penetration test." *Canadian Geotechnical Journal* 35(3): 442-459.

Scherbaum, F., Schmedes, J., and Cotton, F. (2004). "On the conversion of source-to-site distance measures for extended earthquake source models." *Bulletin of the Seismological Society of America,* 94(3): 1053-1069.

Seed, H.B. and DeAlba, P. (1986). "Use of the SPT and CPT tests for evaluating the liquefaction resistance of sands," *Use of Iin-situ Tests in Geotechnical Engineering*, ASCE Geotechnical Special Publication, 6: 281-302.

Seed, H.B. and Idriss, I.M. (1971). "Simplified procedure for evaluating soil liquefaction potential." *Journal of the Soil Mechanics and Foundation Division*, ASCE, 97(9): 1249-1273.

Seed, H.B., Tokimatsu, K., Handler, L.F., and Chung, R.M. (1985). "Influence of SPT procedures in soil liquefaction resistance evaluations." *Journal of the Geotechnical Engineering Division*, ASCE, 111(2): 1425-1445.

Sims, J.D., and Garvin, C.D., 1995, Recurrent liquefaction induced by the 1989 Loma Prieta earthquake and 1990 and 1991 aftershocks: implications for paleoseismicity studies: Bulletin of the Seismological Society of America, v. 85, no. 1, p. 51-65.

Smyrou, E., Panagiota, T., Engin Bal, I., and Gazetas, G. (2011). "Ground motions versus geotechnical and structural damage in the February 2011 Christchurch earthquake." *Seismological Research Letters*, 82(6): 882-892.

Stark, T.D. and Olson, S.M. (1995). "Liquefaction Resistance Using CPT and Field Case Histories." *Journal of Geotechnical Engineering*, ASCE, 121(12): 856-869.

Stirling, M., Yetton, M., Pettinga, J., Berryman, K., and Downes, G. (1999). "Probabilistic seismic hazard assessment and earthquake scenarios for the Canterbury region, and historic earthquakes in Christchurch: stage 1 (part b) of Canterbury regional council's earthquake hazard and risk assessment study." *IGNS Report U99/18.*

Stirling, M., Litchfield, N., Smith, W., Barnes, P., Gerstenberger, M., McVerry G., and Pettings, J. (2007). "Updated probabilistic seismic hazard assessment for the Canterbury region." *Environment Canterbury Report No. U06/6.*

Talwani, P. and W.T. Schaeffer (2001). "Recurrence rates of large earthquakes in the South Carolina coastal plain based on paleoliquefaction data." *Journal of Geophysical Research,* 106: 6621-6642.

Tonkin and Taylor (2008). "Slope hazard susceptibility assessment: Akaroa Harbour settlements." Report prepared for Christchurch City council, Job no. 51151, Ver. 1.

Tuttle, M.P. (2001). "The use of liquefaction features in paleoseismology: lessons learned in the New Madrid seismic zone, central United States." *Journal of Seismology,* 5: 361-380.

Tuttle, M.P., Dyer-Williams, K., and Barstow, N.L. (2002a). "Paleoliquefaction study of the Clarendon-Lindon fault system, western New York State." *Tectonophysics,* 353: 263-286.

Tuttle, M.P., Schweig, E.S., Sims, J.D., Lafferty, R.H., Wolf, L.W., and Haynes, M.L. (2002b). "The earthquake potential of the New Madrid Seismic Zone" *Bulletin of the Seismological Society of America,* 92(6): 2080-2089.

Tuttle, M.P. (2012). "Paleoliquefaction lessons learned from the 2010-2011 Canterbury, New Zealand, earthquakes." [abs]. In: Proceedings of the Geological Society of America Annual Meeting; 2012, Nov 4-7; Charlotte NC, USA.

Vidale, J., Atkinson, G., Green, R., Hetland, E., Grant-Ludwig, L., Mazzotti, S., Nishenko, S., and Sykes, L. (2011). "Report of the independent expert panel on New Madrid Seismic Zone earthquake hazards as approved by NEPEC on April 16, 2011." U.S. Geological Survey, 26 p.

Wakamatsu, K. (1993). *History of soil liquefaction in Japan and assessment of liquefaction potential based on geomorphology*. A Thesis in the Department of Architecture Presented in Partial Fulfillment of the Requirements for the Degree of Doctor of Engineering, Waseda University, Tokyo, Japan.

Whitman, R.V. (1971). "Resistance of soil to liquefaction and settlement." *Soils and Foundations*, 11(4): 59-68.

Wood, C.M., Cox, B.R., Wotherspoon, L.M., and Green, R.A. (2011). "Dynamic site characterization of Christchurch strong motion stations." *Bulletin of the New Zealand Society for Earthquake Engineering,* 44(4): 195-204.

Youd, T.L. and Hoose, S.N. (1977). "Liquefaction susceptibility and geologic setting." *Proceedings of the 6th World Conference on Earthquake Engineering,* New Delhi, India, 3: 2189-2194.

Youd, T.L. and Perkins, D.M. (1978). "Mapping liquefaction-induced ground failure potential." *Journal of the Geotechnical Engineering Division* 104: 433-446.

Youd, T.L., Idriss, I.M., Andrus, R.D., Arango, I., Castro, G., Christian, J.T., Dobry, R., Finn, W.D.L., Harder, L.F., Hynes, M.E., Ishihara, K., Koester, J.P., Liao, S.S.C., Marcuson, W.F., Martin, G.R., Mitchell, J.K., Moriwaki, Y., Power, M.S., Robertson, P.K., Seed, R.B., and Stokoe, K.H. (2001). "Liquefaction Resistance of Soils: Summary Report from the 1996 NCEER and 1998 NCEER/NSF Workshops on Evaluation of Liquefaction Resistance of Soils." *Journal of Geotechnical and Geoenvironmental Engineering,* 127(4): 297-313.

Youd, T.L., Hansen, C.M., and Bartlett, S.F. (2002). "Revised multilinear regression equations for prediction of lateral spread displacement." *Journal of Geotechnical and Geoenvironmental Engineering,* ASCE, 128(12): 1007-1017.

Zhao, J. X., J. Zhang, A. Asano, Y. Ohno, T. Oouchi, T. Takahashi, H. Ogawa, K. Irikura, H. K. Thio, P. G. Somerville, Y. Fukushima and Y. Fukushima (2006). "Attenuation relations of strong ground motion in Japan using site classification based on predominant period." *Bulletin of the Seismological Society of America,* 96 (3): 898-913.

Part A Appendix

Table A1. Summary of CPT-based liquefaction triggering database used in magnitude back-calculations

Site ID	Latitude	Longitude	Critical Depth Range (m)	Observed Liq. Severity Darfield Earthquake	Observed Liq. Severity Christchurch Earthquake	Representative In-situ Soil Parameters						
						Depth to GWT(m)	σ_{vo} (kPa)	σ'_{vo} (kPa)	q_c (kPa)	fs (kPa)	Inferred FC (%)	Soil Behavior Type Index, Ic
CPT-01	43.5097	172.7101	1.2-2.1	No Liquefaction	Moderate Liquefaction	1.2	26.0	21.6	4812.9	25.9	8.3	1.8
CPT-02	43.5075	172.7125	2.20-3.20	No Liquefaction	Marginal Liquefaction	1.9	44.6	36.6	4263.8	17.7	7.3	1.9
CPT-03	43.5018	172.7040	3.5-7.0	Marginal Liquefaction	Lateral Spreading	2.0	88.1	56.2	4803.3	31.9	12.1	2.0
CPT-04	43.5038	172.6835	3.10-5.15	Lateral Spreading	Severe Liquefaction	2.1	63.1	43.5	2243.2	10.9	15.9	2.2
CPT-05	43.5023	172.6945	8.00-10.00	Moderate Liquefaction	Moderate Liquefaction	1.3	152.1	76.5	6017.1	37.5	11.1	2.0
CPT-06	43.5052	172.6870	2.20-4.00	No Liquefaction	Moderate Liquefaction	2.2	51.7	42.8	4562.5	30.2	12.8	2.0
CPT-07	43.5217	172.6668	3.10-4.18	Marginal Liquefaction	Moderate Liquefaction	2.8	58.2	50.2	3835.3	17.2	10.3	2.0
CPT-08	43.5229	172.6688	3.00-5.00	No Liquefaction	Moderate Liquefaction	3.0	66.9	57.1	2229.1	21.4	24.5	2.4
CPT-09	43.5229	172.6837	3.00-6.10	No Liquefaction	No Liquefaction	2.2	77.5	54.5	4496.7	35.3	16.9	2.1
CPT-10	43.4836	172.5737	1.60-7.40	Moderate Liquefaction	Marginal Liquefaction	1.5	74.7	45.3	3802.8	28.4	17.1	2.1
CPT-11	43.5124	172.7209	2.0-4.3	Marginal Liquefaction	Severe Liquefaction	1.5	50.2	34.5	3651.7	17.3	8.6	2.0
CPT-12	43.5103	172.7194	1.30-3.90	Marginal Liquefaction	Severe Liquefaction	1.3	41.8	29.0	3975.6	19.9	8.6	1.9
CPT-13	43.5131	172.7260	2.00-7.50	Lateral Spreading	Lateral Spreading	1.5	82.0	50.3	3150.1	23.4	19.2	2.2
CPT-14	43.5140	172.7256	8.00-10.00	No Liquefaction	Moderate Liquefaction	1.5	165.9	92.3	6905.9	77.0	23.5	2.2
CPT-15	43.4580	172.6202	3.50-4.90	Marginal Liquefaction	Marginal Liquefaction	2.0	65.8	44.2	4101.5	35.1	14.2	2.1
CPT-16	43.4582	172.6266	1.50-3.00	Marginal Liquefaction	Marginal Liquefaction	1.5	34.9	27.6	3198.5	19.8	11.8	2.1
CPT-17	43.4087	172.6935	2.50-3.30	Marginal Liquefaction	No Liquefaction	1.5	0.2	0.2	2200.2	41.9	26.6	2.4
CPT-18	43.4018	172.6953	1.30-2.50	Marginal Liquefaction	Marginal Liquefaction	1.3	29.8	24.0	2369.8	15.8	21.3	2.2
CPT-19	43.3973	172.7012	2.00-5.20	Marginal Liquefaction	Marginal Liquefaction	1.0	60.4	34.9	3954.8	24.0	12.0	2.0
CPT-20	43.4899	172.6858	4.90-6.00	No Liquefaction	No Liquefaction	2.5	95.0	66.1	4453.6	48.2	22.4	2.2
CPT-21	43.4892	172.6822	3.50-5.45	Marginal Liquefaction	Moderate Liquefaction	1.4	74.5	44.3	2373.7	25.6	25.8	2.4
CPT-22	43.4918	172.6832	1.20-2.45	No Liquefaction	No Liquefaction	1.2	28.9	22.8	3757.8	22.8	12.4	2.0
CPT-23	43.4975	172.6727	2.10-5.50	Lateral Spreading	Lateral Spreading	2.0	64.4	46.8	3333.7	28.8	18.6	2.2
CPT-24	43.4997	172.6947	5.6-7.3	No Liquefaction	Moderate Liquefaction	2.0	110.4	66.7	7888.9	29.1	5.0	1.7
CPT-25	43.4883	172.6859	3.50-6.00	No Liquefaction	No Liquefaction	2.0	84.0	57.0	4822.7	39.0	16.1	2.1
CPT-26	43.5245	172.6400	2.90-7.90	Moderate Liquefaction	Moderate Liquefaction	2.0	89.0	55.7	2936.8	25.6	28.6	2.4
CPT-27	43.4829	172.5993	2.00-5.50	No Liquefaction	No Liquefaction	2.0	61.0	43.8	4717.0	23.9	10.8	1.9

Table A1 Continued

Site ID	Latitude	Longitude	Critical Depth Range (m)	Observed Liq. Severity Darfield Earthquake	Observed Liq. Severity Christchurch Earthquake	Representative In-situ Soil Parameters						
						Depth to GWT(m)	σ_{vo} (kPa)	σ'_{vo} (kPa)	q_c (kPa)	fs (kPa)	Inferred FC (%)	Soil Behavior Type Index, Ic
CPT-28	43.4802	172.6082	2.00-3.20	No Liquefaction	No Liquefaction	2.0	43.2	37.3	3108.9	21.1	14.0	2.1
CPT-29	43.5183	172.6745	2.80-6.00	Moderate Liquefaction	Moderate Liquefaction	2.8	70.0	54.3	4359.1	16.5	7.3	1.9
CPT-30	43.5078	172.6821	1.90-7.80	Lateral Spreading	Lateral Spreading	1.6	80.9	49.0	4522.4	24.7	14.0	2.0
CPT-31	43.5238	172.6123	3.60-3.90	Lateral Spreading	Moderate Liquefaction	1.8	63.7	44.6	2935.2	20.1	15.4	2.1
CPT-32	43.5176	172.5975	4.50-8.00	Moderate Liquefaction	Marginal Liquefaction	1.3	104.6	56.1	3715.0	41.7	24.8	2.3
CPT-33	43.5167	172.6028	2.30-4.30	Marginal Liquefaction	Marginal Liquefaction	0.8	51.9	27.4	5540.0	17.3	4.6	1.7
CPT-34	43.5743	172.5493	2.00-3.10	Moderate Liquefaction	Marginal Liquefaction	2.0	40.6	35.3	1344.2	12.8	29.0	2.5
CPT-35	43.5869	172.5676	0.80-1.75	Marginal Liquefaction	No Liquefaction	0.8	21.7	17.1	2834.3	24.2	28.4	2.4
CPT-36	43.5802	172.5752	2.00-3.10	Marginal Liquefaction	Marginal Liquefaction	2.0	42.2	36.8	4241.0	28.7	11.7	1.9
CPT-37	43.5792	172.5666	2.00-2.64	Marginal Liquefaction	Marginal Liquefaction	2.0	37.5	34.3	2796.9	21.4	17.0	2.1
CPT-38	43.5707	172.5693	2.00-3.00	Moderate Liquefaction	No Liquefaction	2.0	42.1	37.2	2353.3	17.0	18.3	2.2
CPT-39	43.5660	172.6080	2.30-3.30	Moderate Liquefaction	Moderate Liquefaction	0.9	45.7	27.0	5246.4	36.1	10.0	1.9
CPT-40	43.3840	172.6646	1.00-3.50	Marginal Liquefaction	Marginal Liquefaction	1.0	35.8	23.6	2548.1	14.5	13.6	2.1
CPT-41	43.3780	172.6609	1.40-2.00	No Liquefaction	No Liquefaction	1.4	27.1	24.2	5643.0	26.2	7.1	1.8
CPT-42	43.3820	172.6699	2.50-5.00	Lateral Spreading	Marginal Liquefaction	0.5	60.3	28.4	2144.9	15.6	20.5	2.2
CPT-43	43.3570	172.6654	2.00-3.00	Marginal Liquefaction	No Liquefaction	2.0	38.3	33.4	1412.7	7.3	21.8	2.3
CPT-44	43.3794	172.6484	3.50-5.00	Marginal Liquefaction	No Liquefaction	1.6	66.9	40.9	4652.3	14.9	5.6	1.8
CPT-45	43.3809	172.6424	4.00-6.00	Marginal Liquefaction	No Liquefaction	2.0	82.7	53.3	1700.0	8.4	25.5	2.4
CPT-46	43.3875	172.6597	1.50-3.00	No Liquefaction	No Liquefaction	1.5	37.2	29.9	4622.2	29.1	12.0	1.9
CPT-47	43.3814	172.6536	1.00-2.70	Moderate Liquefaction	Moderate Liquefaction	0.9	28.7	19.4	1114.2	10.4	32.0	2.5
CPT-48	43.4045	172.6679	2.20-3.00	Lateral Spreading	No Liquefaction	2.2	40.8	36.9	1746.7	13.7	24.3	2.4
CPT-49	43.3884	172.7031	1.50-4.00	Moderate Liquefaction	Marginal Liquefaction	1.5	43.1	9.2	3293.7	13.4	7.4	1.9
CPT-50	43.5355	172.6634	5.00-6.00	No Liquefaction	No Liquefaction	3.0	98.7	74.2	9253.0	59.7	7.8	1.8
CPT-51	43.5225	172.6143	6.00-8.00	Marginal Liquefaction	Marginal Liquefaction	1.5	120.7	66.7	4938.1	59.3	21.9	2.2
CPT-52	43.5105	172.7240	2.00-6.00	No Liquefaction	Lateral Spreading	2.0	65.1	45.5	5971.3	32.5	11.2	1.9
CPT-53	43.4964	172.7028	14.00-19.00	No Liquefaction	No Liquefaction	3.4	314.9	186.4	15740.7	121.5	8.4	1.8
CPT-54	43.5142	172.7294	6.00-7.00	No Liquefaction	Marginal Liquefaction	3.5	115.9	86.5	5727.2	34.9	18.2	2.1

Table A1 Continued

Site ID	Latitude	Longitude	Critical Depth Range (m)	Observed Liq. Severity Darfield Earthquake	Observed Liq. Severity Christchurch Earthquake	Representative In-situ Soil Parameters						
						Depth to GWT(m)	σ_{vo} (kPa)	σ'_{vo} (kPa)	q_c (kPa)	fs (kPa)	Inferred FC (%)	Soil Behavior Type Index, Ic
CPT-55	43.5176	172.7305	6.00-7.00	No Liquefaction	Marginal Liquefaction	2.7	118.2	80.9	9563.3	57.2	7.4	1.8
CPT-56	43.4942	172.7191	8.50-12.00	No Liquefaction	Marginal Liquefaction	1.2	187.9	99.1	10921.5	68.1	8.9	1.8
CPT-57	43.4932	172.6067	2.75-4.40	No Liquefaction	No Liquefaction	1.3	56.2	33.9	4657.8	34.1	12.7	2.0
CPT-58	43.3764	172.7011	1.1-4.28	Marginal Liquefaction	Marginal Liquefaction	1.1	44.5	28.9	1918.3	18.0	35.4	2.5
CPT-59	43.4781	172.6930	1.70-2.53	Marginal Liquefaction	Marginal Liquefaction	1.7	32.7	28.6	2937.0	12.3	5.0	2.0
CPT-60	43.4807	172.6941	3.50-5.30	No Liquefaction	Marginal Liquefaction	1.2	74.6	43.2	5201.6	25.9	8.9	1.8
CPT-61	43.5151	172.6575	1.50-2.75	Moderate Liquefaction	Severe Liquefaction	1.5	35.7	29.6	2019.0	29.5	26.7	2.4
CPT-62	43.5145	172.6545	2.00-4.00	Marginal Liquefaction	Moderate Liquefaction	1.5	69.7	42.7	2744.3	33.2	22.5	2.3
CPT-63	43.5205	172.6594	1.50-3.00	No Liquefaction	Moderate Liquefaction	1.5	36.3	28.9	5178.8	48.2	15.3	2.0
CPT-64	43.5572	172.7382	1.60-3.10	Lateral Spreading	Lateral Spreading	1.6	68.6	42.6	5142.0	25.0	9.2	1.9
CPT-65	43.4713	172.6230	1.90-3.70	Marginal Liquefaction	Marginal Liquefaction	1.2	45.3	29.6	3973.3	24.4	10.9	1.9
CPT-66	43.5052	172.6600	3.80-5.75	No Liquefaction	Moderate Liquefaction	1.8	83.1	53.9	5456.7	13.7	4.7	1.7
CPT-67	43.4312	172.6938	1.10-2.50	Marginal Liquefaction	Marginal Liquefaction	1.0	31.6	23.7	2864.2	19.1	18.2	2.1
CPT-68	43.4300	172.6980	2.90-3.90	Marginal Liquefaction	Marginal Liquefaction	1.0	60.8	37.2	4929.8	18.5	7.1	1.8
CPT-69	43.5521	172.6035	5.24-7.24	No Liquefaction	No Liquefaction	2.5	101.8	65.2	6213.7	47.4	13.9	2.0
CPT-70	43.5521	172.7471	2.1-4.2	Marginal Liquefaction	Moderate Liquefaction	2.1	51.2	40.9	3247.6	5.4	5.8	1.9
CPT-71	43.5118	172.6867	2.20-4.00	No Liquefaction	Marginal Liquefaction	2.2	50.9	42.1	4551.9	27.1	11.8	2.0
CPT-72	43.2871	172.7165	0.78-1.18	Marginal Liquefaction	No Liquefaction	0.5	16.6	12.0	2122.8	18.4	30.2	2.4
CPT-73	43.4804	172.7018	3.00-8.30	No Liquefaction	Marginal Liquefaction	2.0	95.9	60.1	6186.7	36.9	12.4	1.9
CPT-74	43.5529	172.6689	3.90-5.30	No Liquefaction	Lateral Spreading	2.9	75.7	59.0	6355.5	35.3	8.7	1.8
CPT-75	43.5456	172.6891	10.00-14.00	No Liquefaction	Marginal Liquefaction	0.6	224.2	112.5	9194.8	58.0	10.0	1.9

Table A2. Liquefaction severity classification criteria

Classification	Criteria
No Liquefaction	No surficial liquefaction manifestation or lateral spread cracking
Marginal Liquefaction	Small, isolated liquefaction features; streets had traces of ejecta or wet patches less than a vehicle width; < 5% of ground surface covered by ejecta
Moderate Liquefaction	Groups of liquefaction features; streets had ejecta patches greater than a vehicle width but were still passable; 5-40% of ground surface covered by ejecta
Severe Liquefaction	Large masses of adjoining liquefaction features, streets impassible due to liquefaction, >40% of ground surface covered by ejecta
Lateral Spreading	Lateral spread cracks were predominant manifestation and damage mechanism, but crack displacements < 200 mm
Severe Lateral Spreading	Extensive lateral spreading and/or large open cracks extending across the ground surface with > 200 mm crack displacement

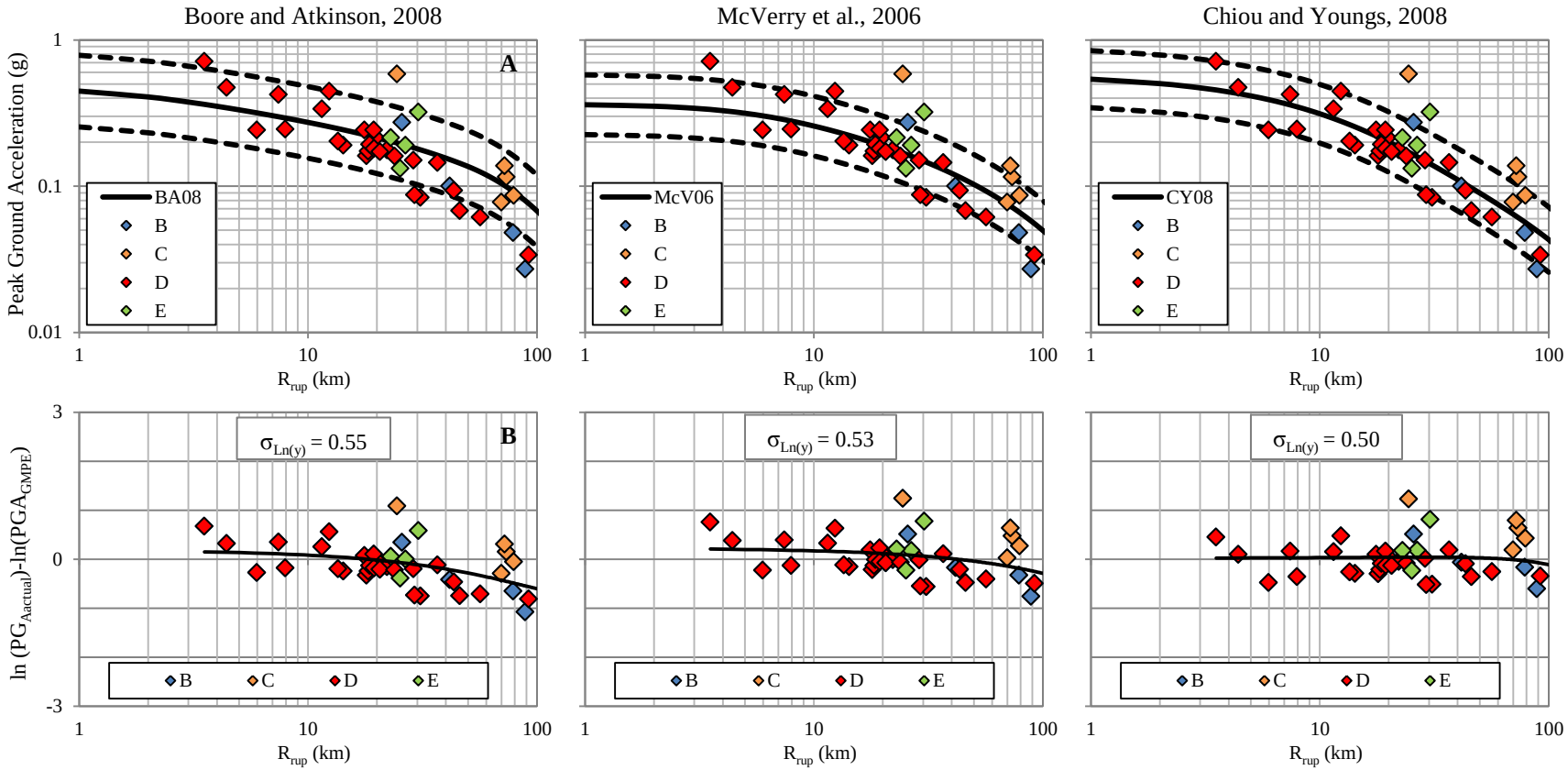

Figure A1. (A) Comparison of PGA values recorded in the Sept. 2010 **M** 7.1 Darfield earthquake and the median and ± 1σ predictions from the five considered active crustal GMPEs for Site Class D; (B) Residuals computed for each GMPE for median Site Class D prediction.

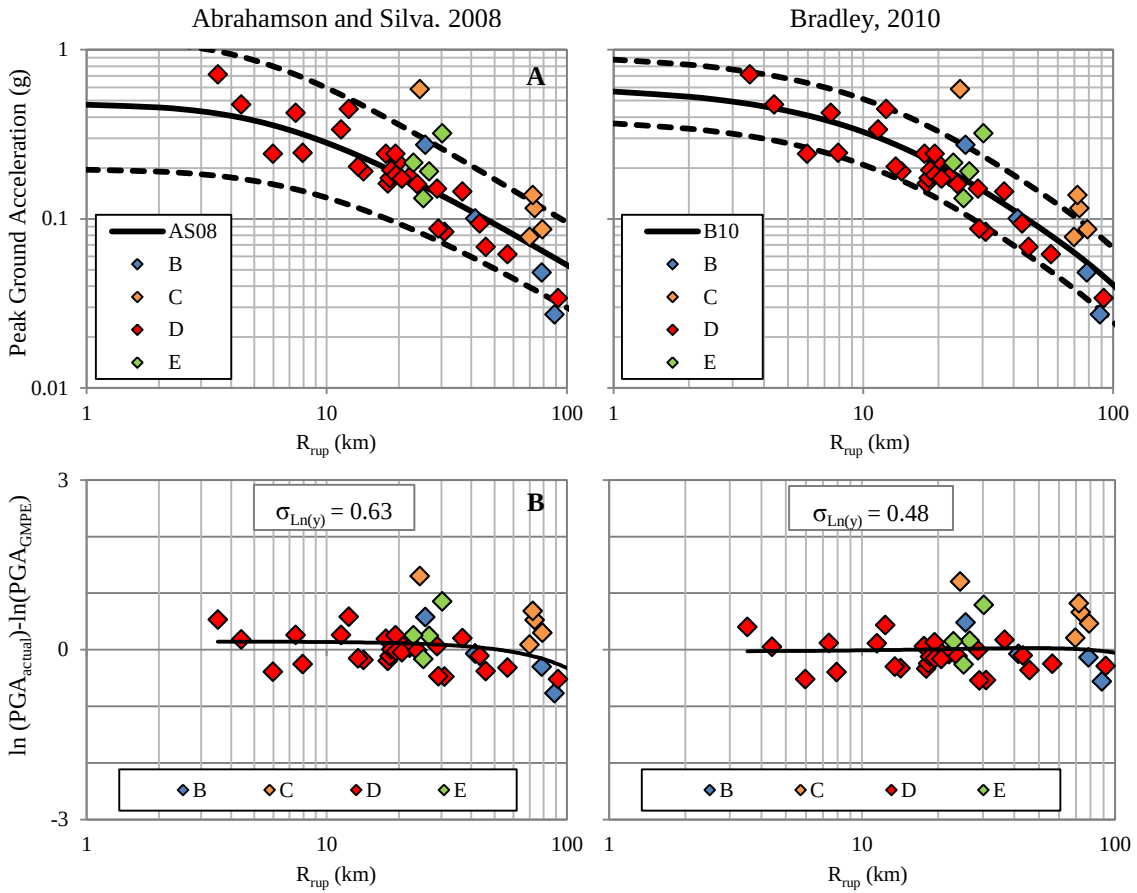

Figure A1 Cont. (A) Comparison of PGA values recorded in the Sept. 2010 **M** 7.1 Darfield earthquake and the median and ± 1σ predictions from the five considered active crustal GMPEs for Site Class D; (B) Residuals computed for each GMPE for median Site Class D prediction.

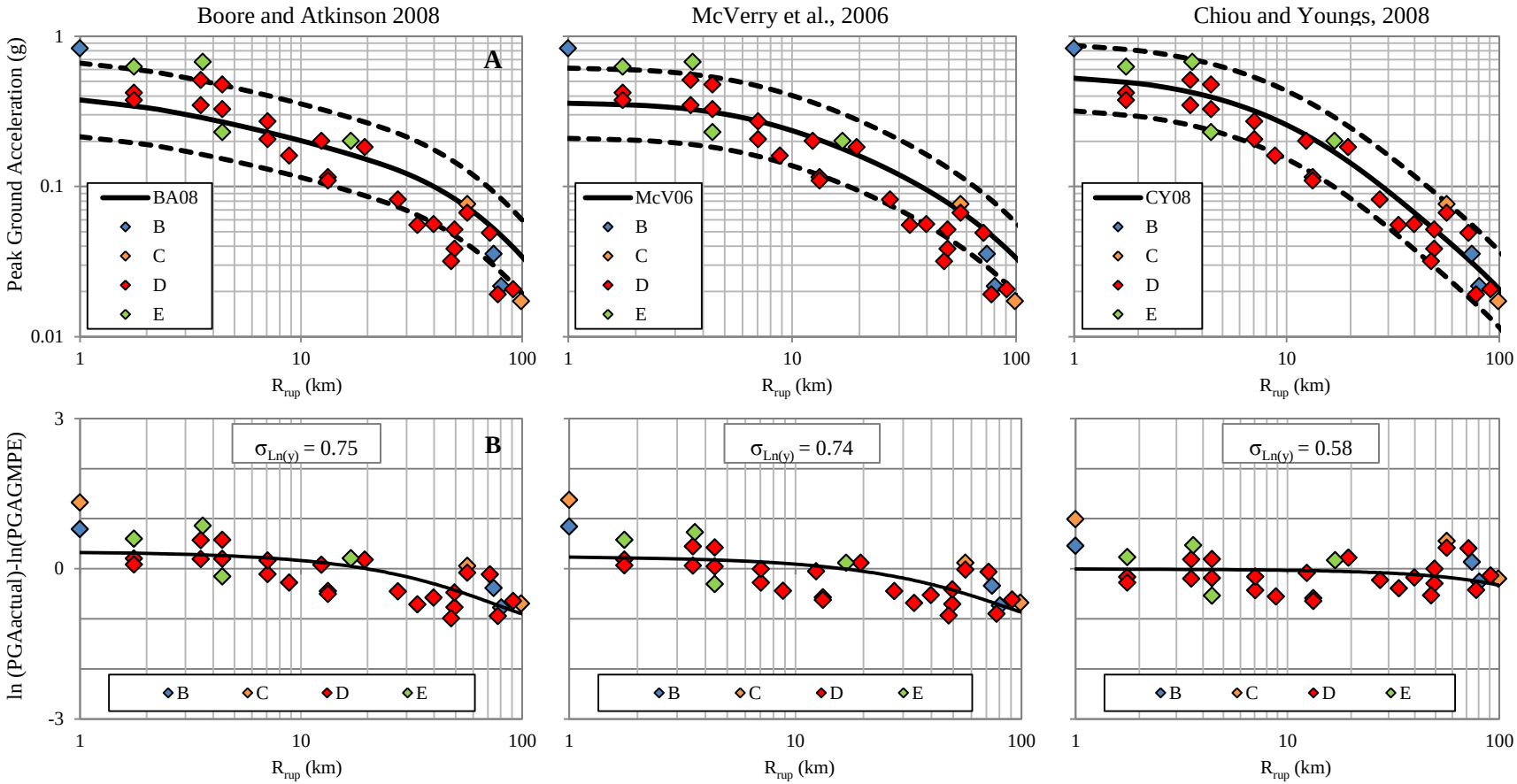

Figure A2. (A) Comparison of PGA values recorded in the Feb. 2011 **M** 6.2 Christchurch earthquake and the median and ± 1σ predictions from the five considered active crustal GMPEs for Site Class D; (B) Residuals computed for each GMPE for median Site Class D prediction.

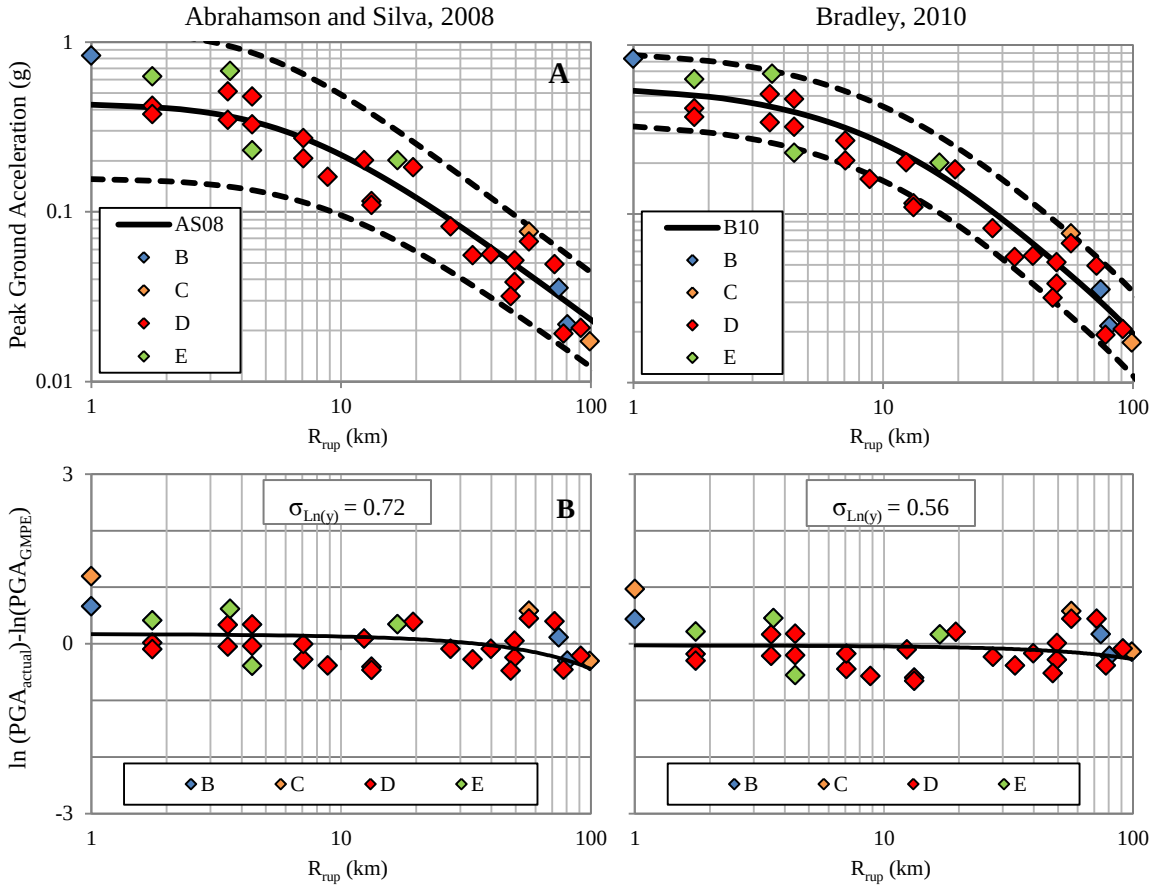

Figure A2 Cont. (A) Comparison of PGA values recorded in the Feb. 2011 **M** 6.2 Christchurch earthquake and the median and ± 1σ predictions from the five considered active crustal GMPEs for Site Class D; (B) Residuals computed for each GMPE for median Site Class D prediction.

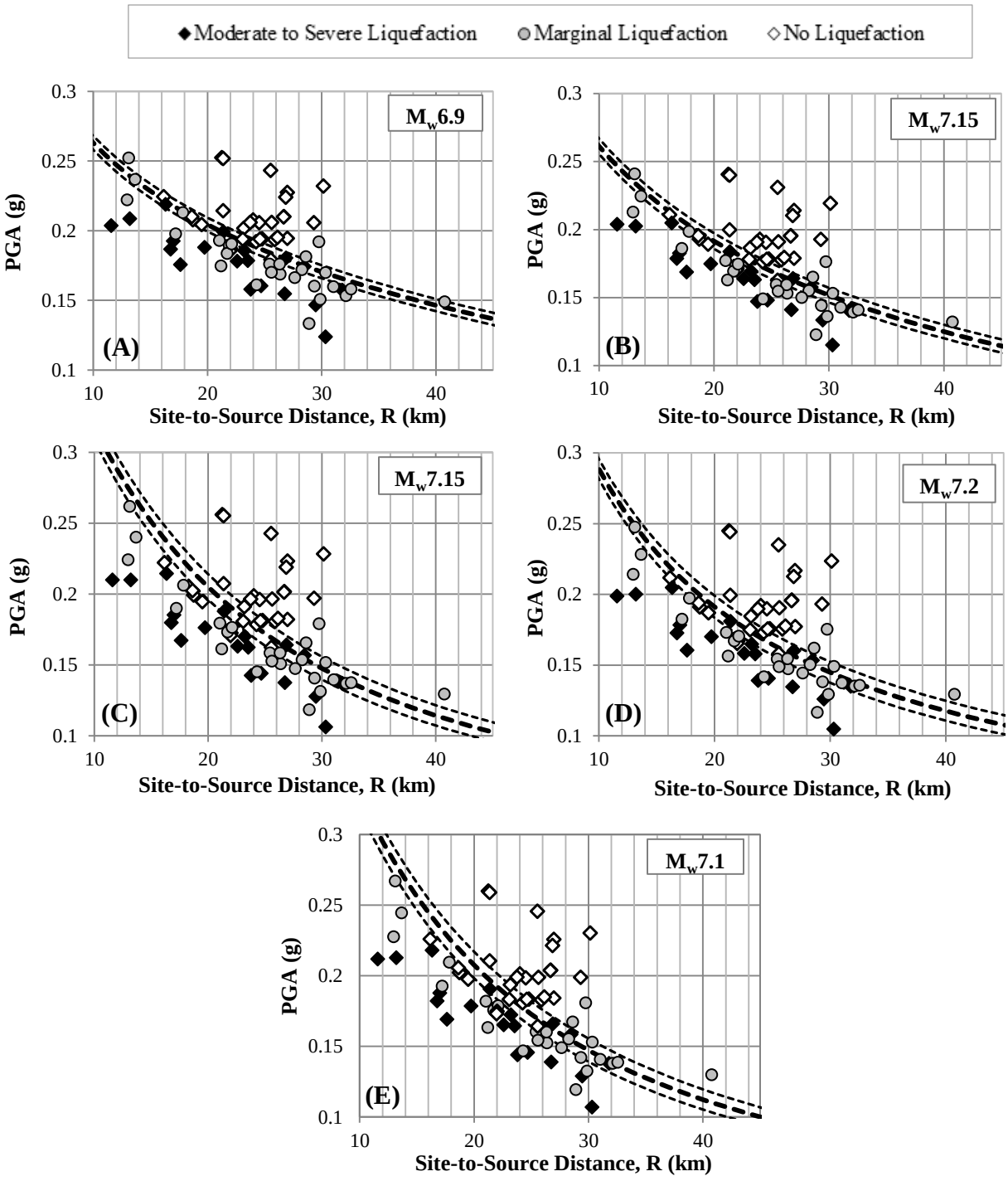

Figure A3. Regional assessment of the strength of shaking of the 4 Sept 2010 Darfield earthquake using the GMPEs given by: (a) BA08; (b) McV06; (c) CY08; (d) AS08; and (e) B10. The back-calculated best-fit magnitude solutions are shown in addition to ± 0.1M_w solutions.

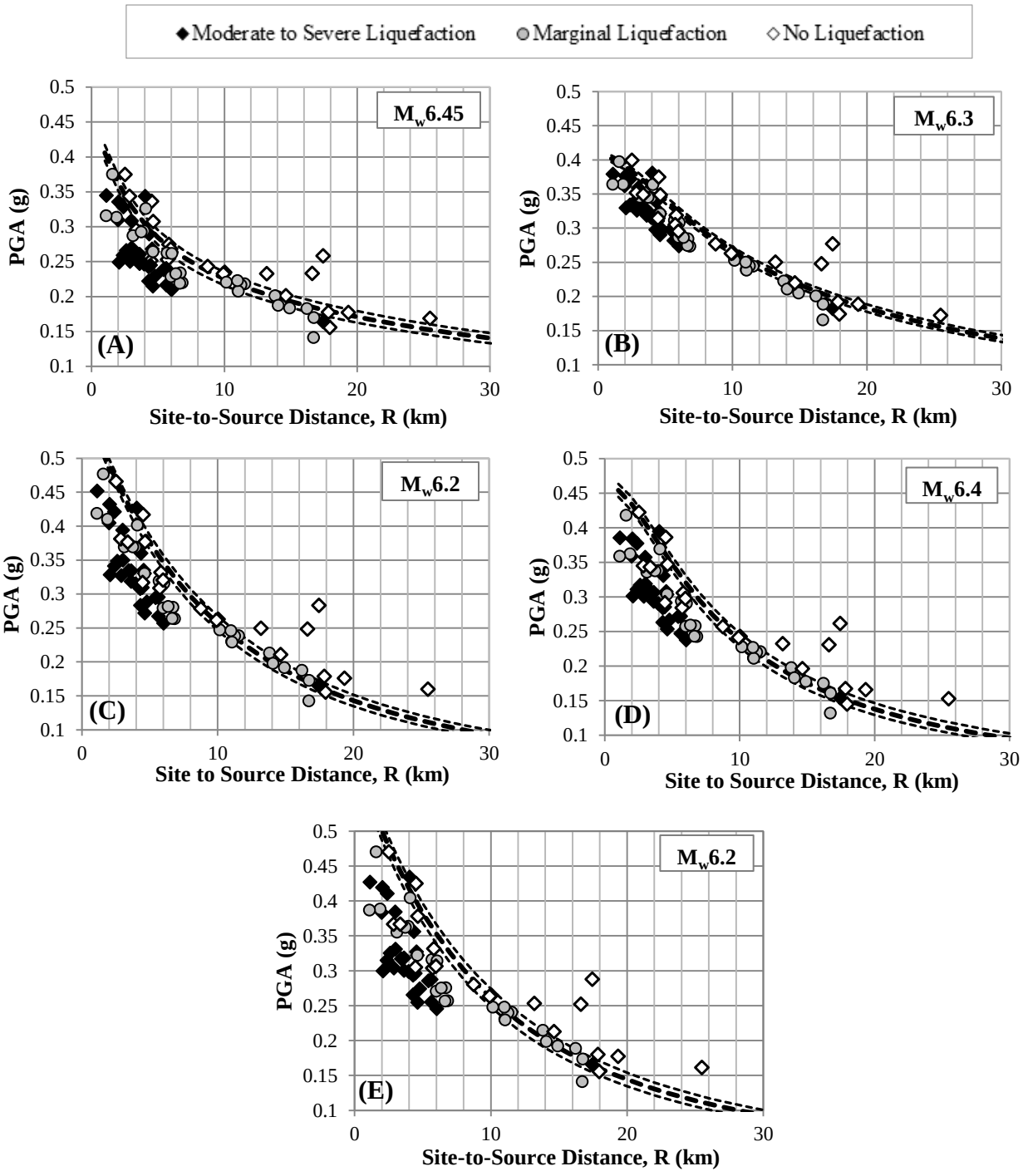

Figure A4. Regional assessment of the strength of shaking of the 22 Feb 2011 Christchurch earthquake using the GMPEs given by: (a) BA08; (b) McV06; (c) CY08; (d) AS08; and (e) B10. The back-calculated best-fit magnitude solutions are shown in addition to ± 0.1M_w solutions.

III. Part B: Field Interpretation of Recurrent Liquefaction: Implications for Paleoseismicity Studies

Summary

Accurate interpretation of paleoseismic records from paleoliquefaction evidence requires detailed characterization of numerous features across a region, with the difficulty of interpretation increasing for sites of repeat liquefaction spaced closely in time. Owing to the uncertainties of paleoliquefaction analyses, computed seismic hazards remain controversial in regions where seismic records are inferred from liquefaction evidence. Accordingly, to better interpret paleoliquefaction evidence, a series of trenches were dug through undisturbed liquefaction features formed during the 2010-2011 Canterbury, New Zealand earthquake sequence at sites of recurrent liquefaction. The structure of blow material was mapped in detail and extensive sampling was performed to analyze spatial trends in particle size gradation. Multiple episodes of liquefaction were clearly evident, separated by silt laminations whose thickness was proportional to the fines content of the liquefied source stratum. However, there were no ubiquitous trends in the spatial sorting of grain sizes in the coarser fraction of the ejecta underlying silt seams, even though these strata were often 10 cm thick and flowed laterally up to several meters. Consequently, recurrent liquefaction cannot be disproven by a lack of trends in the spatial distribution of grain sizes or by lack of inter-event silt seams, if the liquefaction source stratum lacks sufficient fines. Part B provides a modern analog to recurrent paleoliquefaction evidence, and has important implications for interpretation of seismic hazards.

1. Introduction

The objective of Part B is to better interpret paleoliquefaction evidence by studying sites of liquefaction induced by the 2010-2011 Canterbury, New Zealand earthquake sequence, and moreover, to determine whether recurrent liquefaction can be accurately inferred from the structure and grain size distribution of vented sediments. The value of paleoliquefaction evidence for interpreting paleoseismic records is widely recognized in regions of infrequent but potentially damaging seismicity, particularly where prehistoric ruptures and offset features are unavailable. The interpretation of liquefaction induced by a paleoearthquake requires a detailed field-assessment of numerous features across the affected region, followed by a quantitative back-analysis to estimate the causative earthquake's magnitude. The two most widely-used back-analysis methods are the "magnitude-bound" method (e.g., Obermeier and Dickenson, 2000; Tuttle et al., 2002a; Olson et al., 2005a; Green et al., 2005; Papathanassiou et al., 2005; Pirrotta et al., 2007) and the "site-specific geotechnical analysis" (e.g., Obermeier and Dickenson, 2000; Olson et al., 2005b, Green et al., 2005), or for brevity, the "site-specific" approach. For either

back-analysis method, deciphering whether liquefaction features are the result of one earthquake or multiple earthquakes closely spaced in time is critical.

The site-specific approach employs liquefaction triggering methodology (e.g., Robertson and Wride, 1998; Moss et al., 2006; Idriss and Boulanger, 2008) to back-calculate the peak ground acceleration at a site, which, when combined with a ground motion predictive equation (GMPE), yields an estimate of the causative earthquake's magnitude. Difficulties arise when a sequence of large earthquakes closely spaced in time produce adjoining or overlapping liquefaction fields. In this case, if a liquefaction feature were improperly attributed to a more distal source mechanism than actual, the back-calculated earthquake magnitude could be erroneously large. Similarly, if a feature were attributed to a less distal source mechanism than actual, the causative earthquake's magnitude might be underestimated. As such, it is essential that features are properly ascribed to their respective liquefaction field(s). For spatiotemporally neighboring earthquakes, this requires accurate field interpretation of composite features formed by recurrent episodes of liquefaction. For example, CPT sounding data is shown in Fig. 1 for a site in Christchurch, New Zealand, where the "critical layer" is interpreted to be at 3.5 m – 7 m depth (for detailed summaries of the site-specific approach and its application, see: Olson et al., 2005; Green et al., 2005, and Part A of this report). This site is known to have liquefied in both the 2010 M_w7.1 Darfield and 2011 M_w6.2 Christchurch earthquakes, and is respectively located 24 km and 4 km from the Darfield and Christchurch fault ruptures. If the site is interpreted to have liquefied in the Darfield earthquake only, back-analysis of the site data inaccurately suggests the Christchurch earthquake magnitude is $\leq M_w$5.5. Similarly, if the site is interpreted to have only liquefied in the more local Christchurch earthquake, back-analysis suggests the Darfield earthquake magnitude is $\leq M_w$6.7. In similar fashion, it can be shown for other sites where inaccurate field interpretation results in erroneously large magnitude estimates.

The magnitude-bound method, derived from modern liquefaction observations, relates earthquake magnitude to the site-to-source distance of the most distal liquefaction site. Several magnitude-bound curves are shown in Fig. 2 for a variety of geographic and tectonic settings. Since the determination of the areal extent of a liquefaction field is central to estimating the causative earthquake's magnitude, the magnitude-bound method is likewise sensitive to accurate field interpretation. For example, it is known that three pre-instrumental mainshocks collectively induced widespread liquefaction in the NMSZ between Dec. 1811 and Feb. 1812 (e.g., Obermeier, 1989). From the spatial distribution and stratigraphy of sand blows, Tuttle et al. (2002a) interpreted three liquefaction fields, mapped in Fig. 3. However, if the liquefaction fields are reinterpreted as being caused by a single earthquake (Fig. 3), or reinterpreted as being augmented by additional spatially-distributed large aftershocks, the maximum site-to-source distance of liquefaction changes, and consequently, the back-calculated magnitude(s) will be decidedly different.

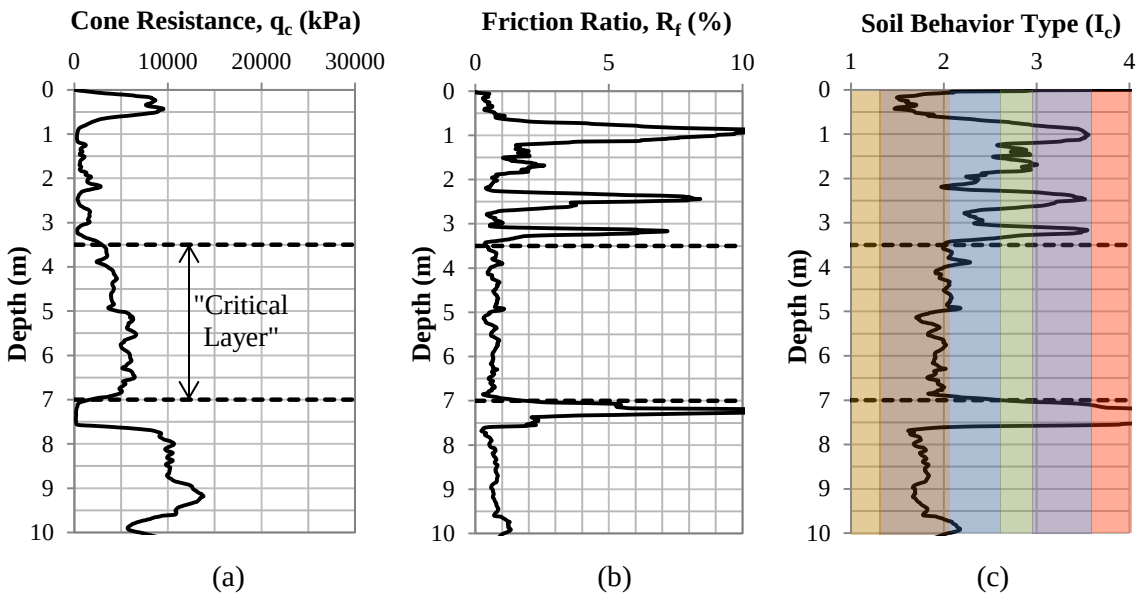

Figure 1. CPT-AVD-13 sounding data from liquefaction investigation site in Christchurch, New Zealand. (a) Cone tip resistance, q_c; (b) Friction ratio, R_f; and (c) Soil behavior type index, I_c.

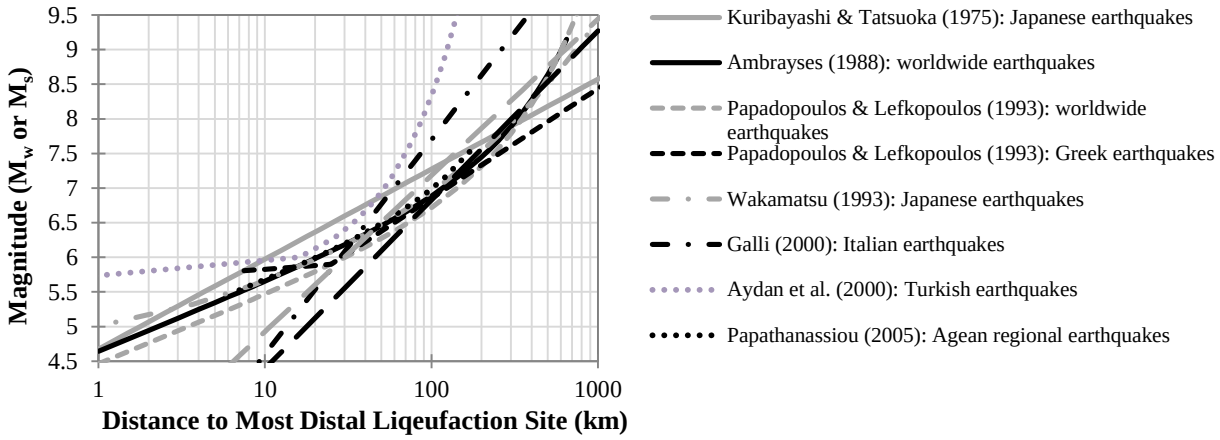

Figure 2. Magnitude-bound curves for varying geographic and tectonic settings, where site-to-source distance is quantified in terms of epicentral distance.

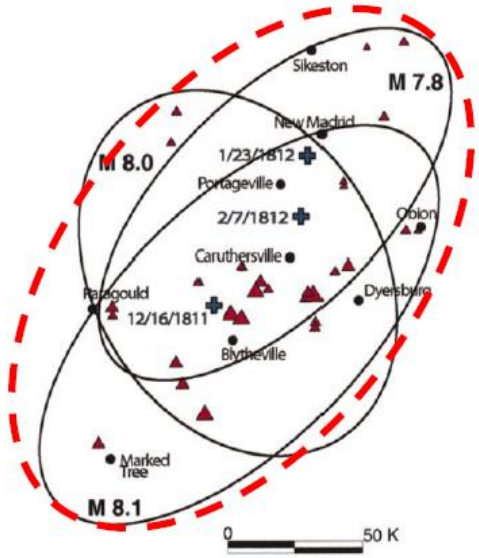

Figure 3. Reinterpretation of bounds of the liquefaction fields from the 1811-1812 New Madrid events as being induced by a single earthquake (adapted from Tuttle et al., 2002a).

The accuracy of paleoliquefaction interpretation is much more than an academic interest; the uncertainties of paleoliquefaction analyses significantly affect the computed seismic hazard in regions where they're relied upon. For example, the computed seismic hazard of the central U.S. is founded largely on the paleoliquefaction record of the NMSZ (Petersen et al., 2008) and is significantly influenced by the uncertainty of paleomagnitude estimates (Vidale et al., 2011). The potential consequences of such uncertainty were demonstrated during the 2010–2011 Canterbury (New Zealand) earthquake sequence (CES), which, due in part to the exceedance of design ground-motions, caused extensive damage to the city of Christchurch. In the 22 February 2011, M_w6.2 Christchurch earthquake, ground-motion displacement demands were approximately twice the seismic design level for many structures in the central business district (CBD) (Bradley and Cubrinovski, 2011), resulting in the majority requiring either demolition or extensive repair (Kam et al., 2011; Smyrou et al., 2011). Coinciding with the unanticipated ground motions, the CES induced widespread and recurrent liquefaction, with as many as 10 episodes of liquefaction documented at a single site over a 16 month period (Quigley et al., 2013).

In addition to demonstrating the importance of accurately assessing seismic hazards, the CES presents a unique opportunity to improve our capacity for interpreting seismic records from liquefaction evidence. As previously mentioned, this requires field investigation and interpretation followed by numerical back-analyses. Using liquefaction evidence from the CES, Part A of this report evaluated the accuracy of quantative back-analysis methods and explored the challenges and uncertainties of their application; this study is the first to assess the efficacy of these quantitative methods using modern earthquakes with known magnitudes. In addition, a large body of literature exists pertaining to the field investigation methods prerequisite for such

analyses. This includes overviews of field interpretation given by Obermeier et al. (2001; 2005) and the case studies presented by Obermeier and Dickenson (2000), Tuttle (2001), Talwani and Schaeffer (2001), Tuttle et al. (2002a; 2002b, 2005), and Cox et al. (2007), among others. Research focusing on the interpretation of recurrent liquefaction, however, is limited. Since the accuracy of interpretation is contingent upon differentiation of liquefaction episodes, a reliable method for their identification could help mitigate prevailing uncertainties and resolve paleoseismic mysteries. Several researchers have suggested from visual inspection of paleoliquefaction features in the NMSZ (Saucier, 1989; Tuttle et al., 2002a) and modern features in California (Sims and Garvin, 1995) that soil grains tend to sort by size within layers of liquefaction ejecta, fining both upwards and laterally from the source vent, and that such trends are an identifying feature of episodic liquefaction. Accordingly, the objective of this study is to determine whether recurrent liquefaction episodes can be discerned from the structure and grain size distribution of vented sediments by analyzing sites of recurrent liquefaction from the CES. This study is the first to quantitatively analyze particle size gradation trends within liquefaction structures in extensive detail and addresses a critical need in paleoliquefaction studies.

In the following, the geologic and seismologic setting of the CES is briefly summarized. This is followed by a description of the field investigation and sampling methodology. The morphology and grain size distribution patterns of blow structures are then analyzed in detail, with discussion of the implications for paleoseismicity studies.

2. Geologic and Seismologic Setting

The coastal city of Christchurch is located in the Canterbury Plains region of New Zealand's South Island and amongst the Heathcote, Avon, and Waimakariri rivers. The surficial geology of Christchurch and its environs is characterized by a history of coastline transgression and progradation, and consists predominantly of loosely-deposited estuarine and alluvial sediments (Brown et al., 1995). In addition, following establishment of Christchurch in the mid-1800's, river realignments and land reclamation projects resulted in infilling of many low-lying areas with loose, low-plasticity sediments (e.g., Wotherspoon et al., 2012). While the liquefaction susceptibility of the region's natural and artificial deposits had been recognized (Environment Canterbury [ECan], 2004), the only previously documented liquefaction occurred during the 1901 Cheviot earthquake in the village of Kaiapoi, north of Christchurch (e.g., Berrill et al., 1994). Paleoliquefaction features have recently been discovered (Bastin et al., 2012; Tuttle et al., 2012; Quigley et al., 2013) and could help elucidate the regions seismic history, unknown prior to 19th century settlement, but the source and size of the event(s) which induced these features are as of yet unknown.

The 2010-2011 CES initiated with the 4 September 2010, M_w7.1 Darfield earthquake and included twelve other $M_w \geq 5.0$ events epicentrally located within 20 km of Christchurch (GeoNet, 2012). While at least 10 of these events are known to have induced liquefaction (Quigley et al., 2013), the 22 February 2011, M_w6.2 Christchurch earthquake, with its rupture

plane located directly beneath the southernmost environs of Christchurch (e.g., Beavan et al., 2011), was by far the most damaging. An extensive body of literature exists pertaining to the CES, including numerous aspects of liquefaction incidence and prediction (e.g., Cubrinovski and Green, 2010; Cubrinovski et al., 2011a; 2011b; Orense et al., 2011; Green et al., 2011a; 2011b; Cubrinovski et al., 2012; Wotherspoon et al., 2012; Maurer et al., 2013; Robinson et al., 2013); the reader is referred to these works and others for a complete overview of the CES.

Of particular relevance to paleoliquefaction studies, the geomorphology of soil deposits, severity of liquefaction, and relative timing of the CES events make them directly analogous to paleoearthquake clusters that occurred in the NMSZ and elsewhere. As such, the CES provides a unique modern analog to recurrent paleoliquefaction evidence.

3. Methodology

Beginning in August 2011, a series of trenches were excavated at sites of known recurrent liquefaction distributed throughout eastern Christchurch and its environs. Episodic liquefaction was documented throughout the earthquake sequence from ground reconnaissance and high-resolution aerial imagery. As mapped in Figure 4, trenches were located in Ferrymead (FMD) near the Heathcote River, in South Kaiapoi (KAI) near the Kaiapoi River, a tributary to the Waimakariri River, and in Dallington (DAL) and Burwood (BUR), each in close proximity to the Avon River. Also shown in Figure 4 are the epicenters of CES events having $M_w \geq 4.5$; several notable events, including the M_w7.1 Darfield earthquake, plot beyond the extents of Fig. 4. High-resolution satellite images (captured 24 Feb 2011) of each investigate site are presented in Fig. 5; the presence of widespread and/or severe liquefaction is readily apparent in each case.

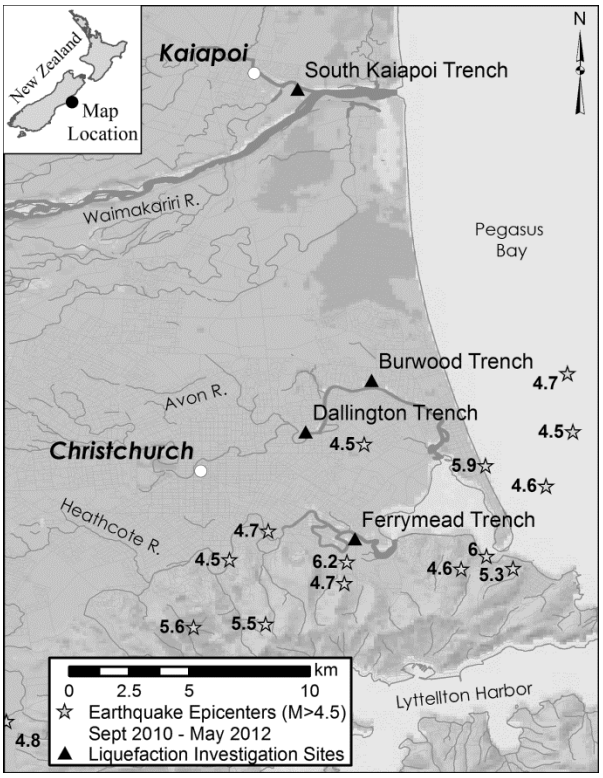

Figure 4. Liquefaction investigation sites and local earthquake epicenters, $M_w \geq 4.5$ (Sept. 2010 – May 2012). Note: M_w7.1 Darfield earthquake epicentrally located ~40 km west of central Christchurch.

Facilitated by their locations in pastures (FMD, KAI) and vacant residential properties abandoned early in the earthquake sequence (DAL, BUR), the investigated liquefaction features were free of anthropogenic disturbance, but open to the elements. With the exception of BUR, trenches cross-cut liquefaction features formed from multiple episodes of liquefaction venting onto the ground surface through a common dike. BUR is located at a site known to have liquefied multiple times, but is unique in that the liquefaction dike terminated beneath the ground surface, producing a buried lateral sill of liquefied material and resulting in a "blister" on the ground surface. Such features could be especially important in paleoseismic analyses because they are protected from erosion and may better preserve the seismic record. The authors are not aware of a modern feature of this type having been studied before. The structures of these liquefaction features were mapped in detail and extensive sampling of the ejecta was undertaken to analyze trends in particle size gradation via laser diffraction.

Figure 5. Satellite imagery (captured 24 Feb 2011) of liquefaction investigation sites located in (a) South Kaiapoi; (b) Burwood; (c) Dallington; and (d) Ferrymead. Imagery adapted from CGD (2012).

4. Results and Discussion

4.1 Internal Structure of Sandblow Deposits

In the KAI trench, mapped and photographed in Fig. 6, five distinct episodes of liquefaction were clearly evident, each separated by inter-event silt laminations (or "seams") approximately 1 cm thick. These silt seams, which cap individual layers of coarser ejecta up to 10 cm thick, suggest an interval of placid water deposition following a period of turbulent rupture. Silt seams were found to commonly contain 10 μm sized particles up to 5% by volume, and to have particle sizes less than 2 μm. Applying the fundamentals of Stoke's Law, and assuming spherical particles, the smallest of these grains is estimated to have a terminal settling velocity less than 1 cm/hr. This suggests that significant time was required for the silt seams to form, and that multiple silt seams within a blow structure are unlikely to have been produced by multiple

"pulses" of shaking during a single earthquake. As such, silt seams were found to be an identifying feature of episodic liquefaction.

In the DAL and FMD features, mapped in Figs. 7 and 8, three and four episodes of liquefaction were respectively discernible. In the BUR trench, mapped in Fig. 9, excavating through the center of the liquefaction blister revealed two distinct silt seams in the sill structure. Gradations of samples collected from the silt seams and coarse ejecta regions in the BUR feature are shown in Fig. 10. It can be seen that depositional sorting of the finer from the coarser grains occurred despite a lack of venting onto the ground surface. This significant observation indicates that it is possible to gather evidence of recurrent paleoliquefaction from these unique and important structures. In all investigation trenches, silt seam particle size gradations were compared to those in the underlying layer of coarser ejecta, with data pairs sampled at the same lateral distance from the vent. Sample pairs were compared by considering the ratio of effective particle size diameters D_5, D_{10}, D_{60}, and D_{90} in the silt seam to those in the underlying layer. Accordingly, ratios less than 1.0 indicate a finer particle size gradation in the silt seam. Considering sampling pairs at varying lateral distances from the vent, the average D_5, D_{10}, D_{60}, and D_{90} ratios were 0.52, 0.61, 0.68, and 0.80, respectively. Thus, silt seams were visually distinct due to their finer grain size distributions, particularly in the finest particle sizes, rather than the result of weathering or any other phenomena.

While episodic liquefaction was apparent in the DAL and FMD blow structures from the presence of progressive oxidation, flattened vegetation at the base of each ejecta layer, and distinct inter-event silt seams, the silt seams in these liquefaction features were significantly thinner (~2 mm) than those in the KAI and BUR structures (~8 mm), despite having per event ejecta layers of comparable or greater thickness. To investigate the correlation between silt seam thickness and source material characteristics, vertical boreholes were drilled in the floor of the DAL and KAI trenches to locate and sample the liquefied source strata; borings were not possible in the other trenches due to the presence of a high water table (FMD) and shallow hardpan (BUR).The locations of suspected source strata in the DAL and KAI features were corroborated using data from nearby in-situ penetration tests. The grain size distributions of liquefied source strata in the KAI and DAL trenches are shown in Fig. 11. The KAI source stratum was found to contain ~45% silt-size particles (<75 μm), while the source stratum of the DAL blow structure contained only ~14% silt-sized particles by volume. Thus, silt seam thickness is proportional to the fines content of the liquefied source stratum, and consequently, silt seams are not anticipated to form as the fines content of the liquefied stratum approaches small values. It is hypothesized that there is a lower-bound fines content at which particle sorting fails to produce a perceptible silt seam, or if formed, the seam is so thin that it is susceptible to erosion and may not be preserved in the geologic record. Given that the range of soils considered to be liquefiable is large (e.g., Numata and Mori, 2002) and encompasses soils containing less fines than some of the soils that liquefied in Christchurch (Fig. 12), silt seams cannot be relied upon to define recurrent paleoliquefaction. In the NMSZ, Tuttle et al. (2002a) trenched numerous paleoliquefaction features and observed that individual liquefaction units were capped by silt

only in some cases, and interpreted the deposition of fining-upward units as evidence of episodic liquefaction. Identifying particle size gradation trends in the absence of silt seams could therefore be critical for identifying recurrent liquefaction. In the following, the utility of particle size trends within the coarser fraction of ejecta underlying silt seams is explored.

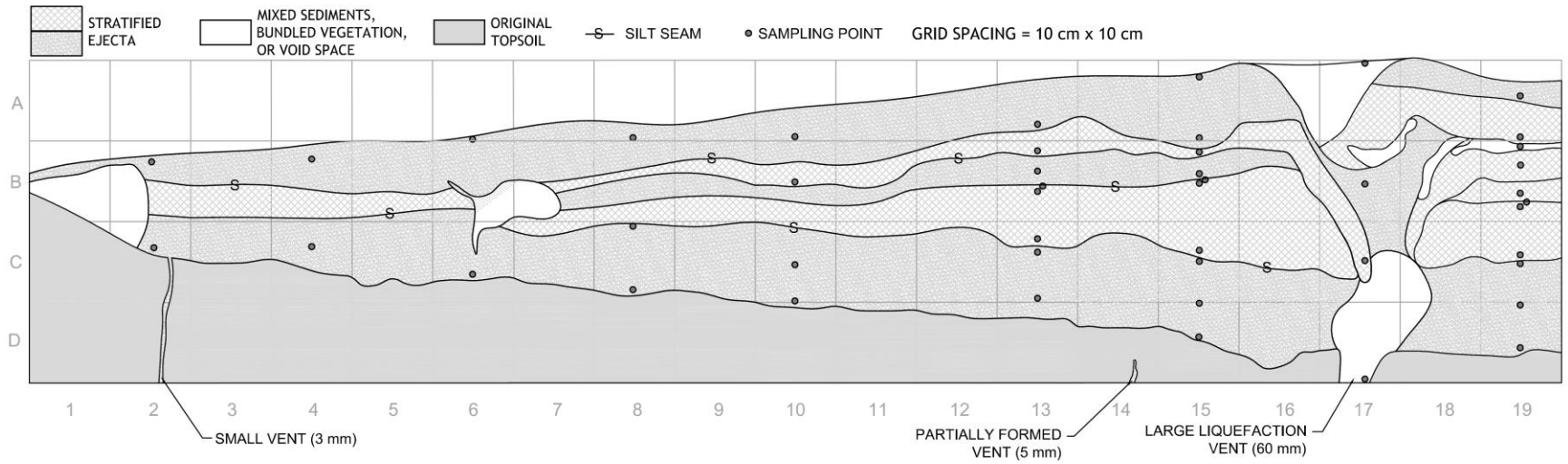

(a)

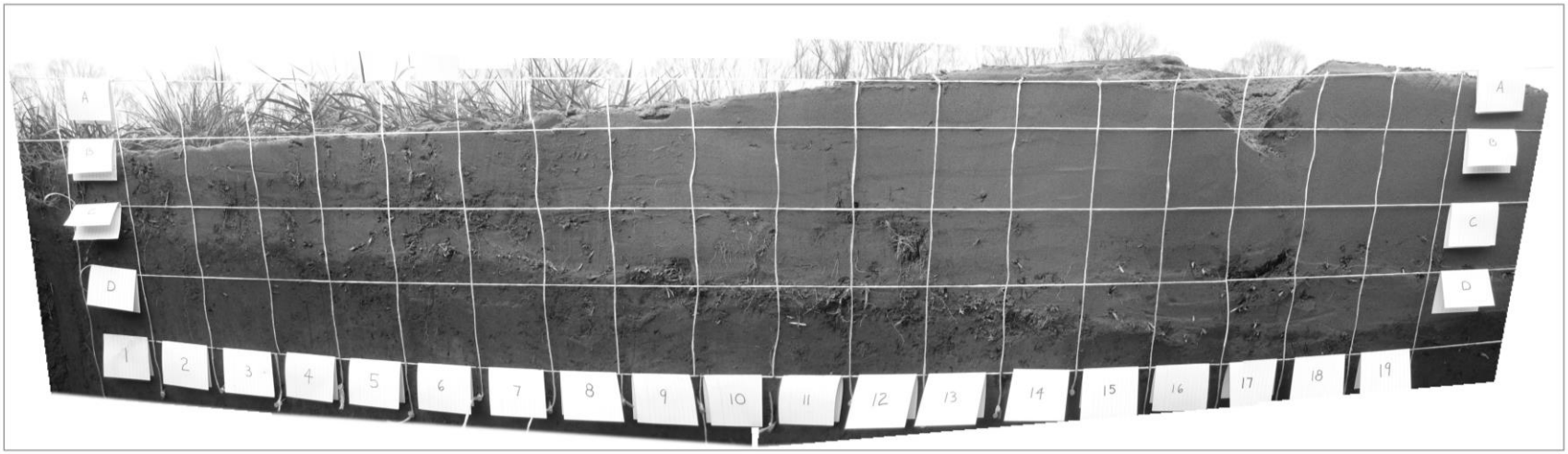

(b)

Figure 6. (a) Log of the eastern wall at the KAI trench showing at least 5 sand-venting episodes of liquefaction; sampling points identified in the log are discussed in the text. (b) Photograph of the eastern wall at the KAI trench prior to sampling (overlaid with 10 cm^2 grid).

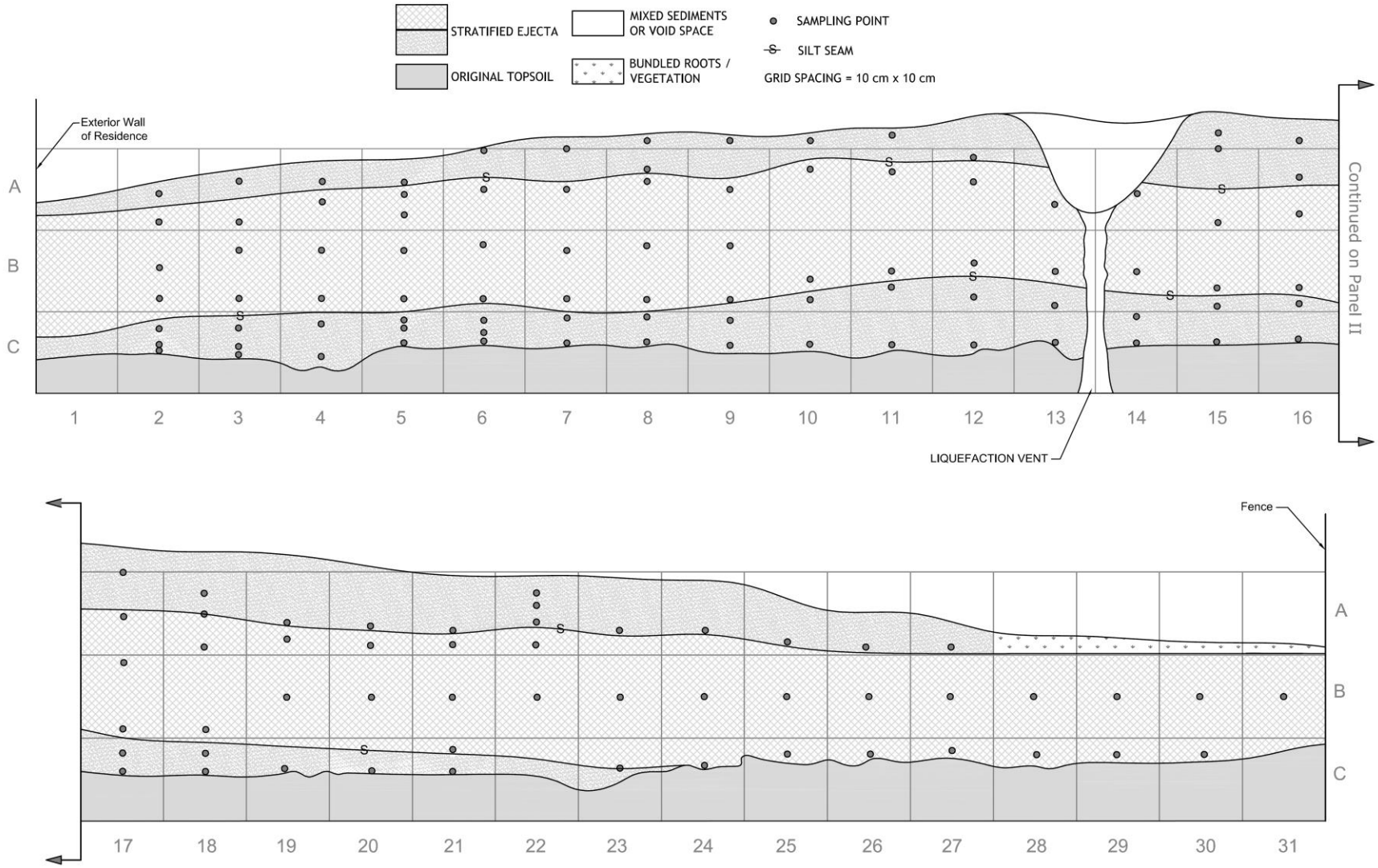

Figure 7. Log of the eastern wall at the DAL trench showing at least 3 sand-venting episodes of liquefaction; sampling points identified in the log are discussed in the text.

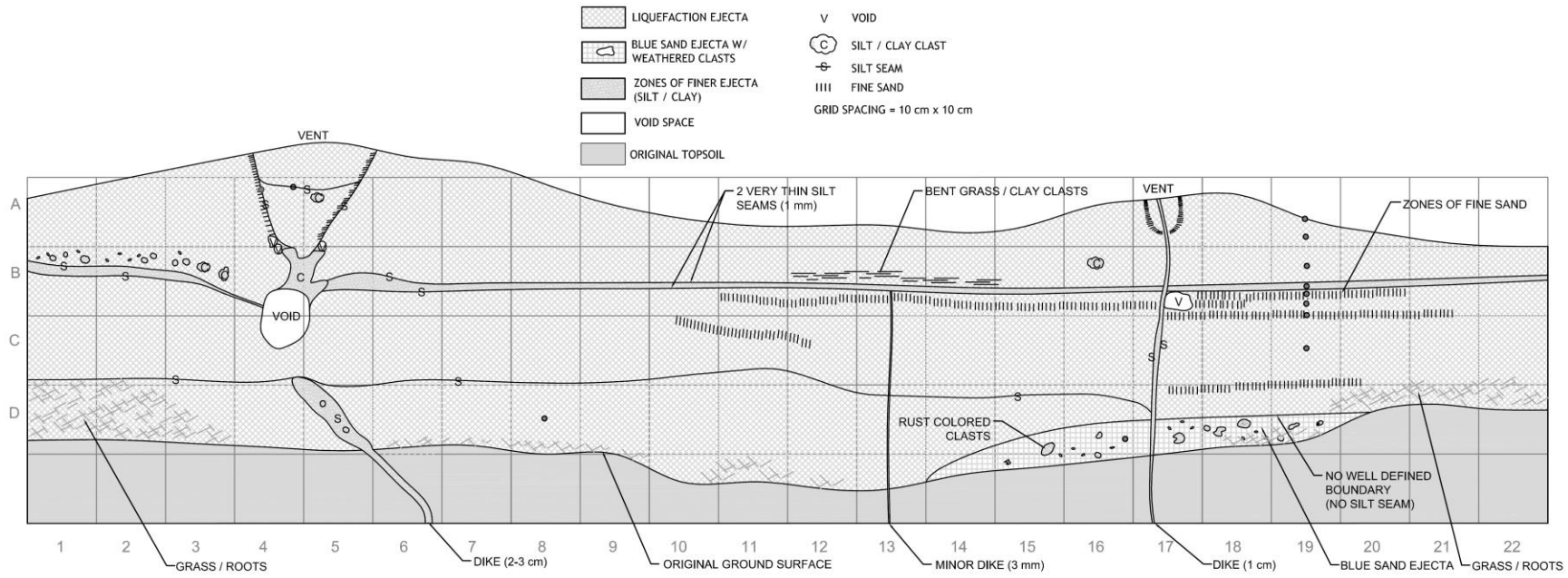

Figure 8. Log of the western wall at the FMD trench showing at least 4 sand-venting episodes of liquefaction; sampling points identified in the log are discussed in the text.

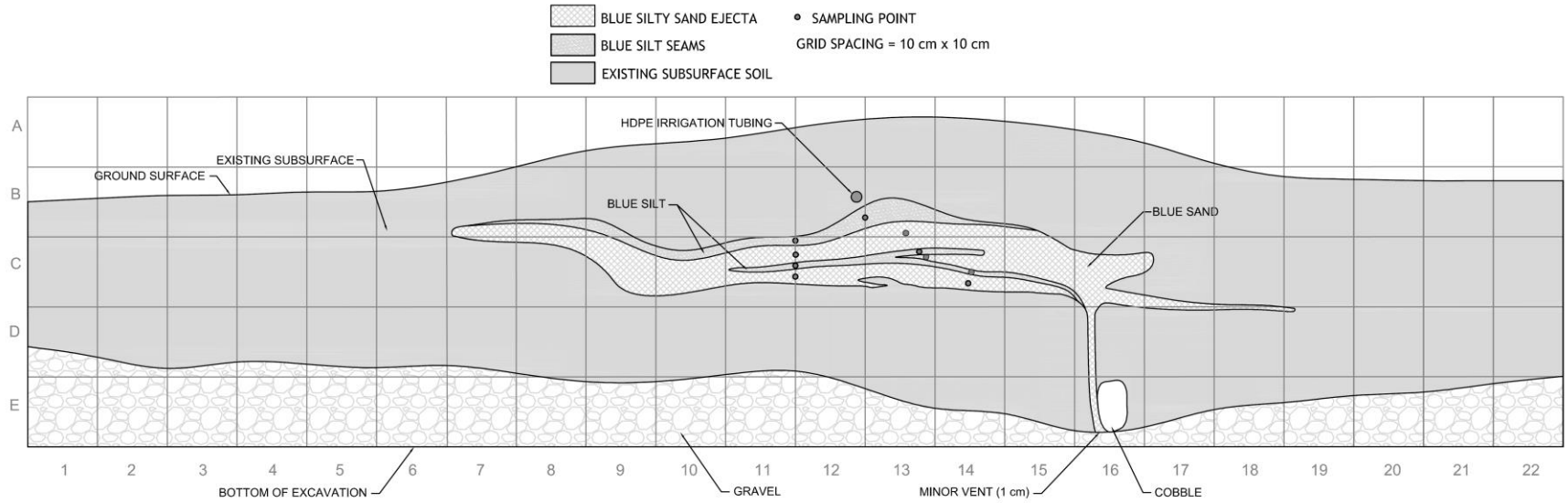

Figure 9. Log of the southwestern wall at the BUR trench showing depositional sorting and multiple episodes of liquefaction despite a lack of venting onto the ground surface. Photographs of the BUR trench are provided in the electronic supplement.

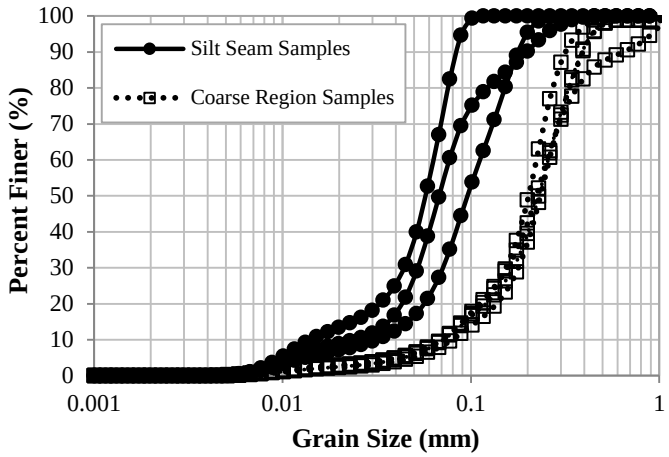

Figure 10. Comparison of silt-seam and coarse ejecta grain size distributions in the BUR trench.

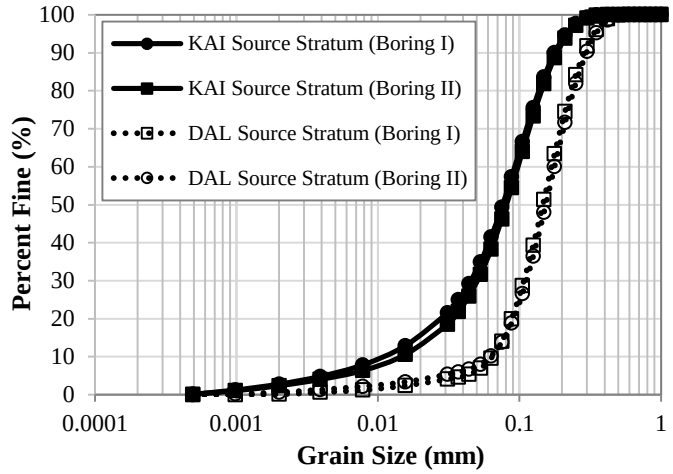

Figure 11. Grain size distributions of liquefied source strata beneath the KAI and DAL trenches.

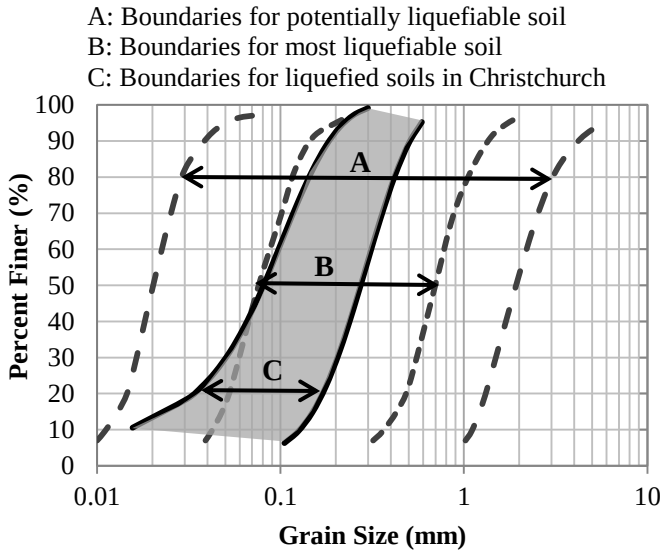

Figure 12. Grain size distributions of liquefied soils in Christchurch and Kaiapoi, with boundaries for 'most liquefiable' and 'potentially liquefiable' soils (Ishihara, 1985). It can be seen that many liquefiable soils have fewer fines than those in Christchurch. As such, some blow structures would likely lack silt seams.

4.2 Analysis of Grain Size Distribution Patterns

Analyzing more than 200 samples recovered from the base and top (immediately below silt seam) of individual blow units at varying distances from the vent, trends in the grain size distributions both vertically and laterally were investigated. To identify fining-upward trends, sample pairs were compared by considering the ratio of effective particle diameters D_5, D_{10}, D_{60}, and D_{90} in the upper-reaches of a blow unit to those at the base of the same unit. As such, ratios less than 1.0 indicate fining upwards within a depositional unit. Vertical trends are shown in Fig. 13 for the KAI (Fig 13a) and DAL (Figs. 13b, 13c) trenches. Owing to the large number of samples in the DAL feature, vertical trends are parsed into those of the first (oldest) and second ejecta layers. It can be seen in Fig. 13 that there are no consistent trends in either the KAI or DAL trenches. While some sample pairs indicate that ejecta is fining upwards, many show no spatial change in gradation, while others indicate that ejecta is finer at the base of a unit. Considering all sampling pairs in the KAI and DAL features, the average D_5, D_{10}, D_{60}, and D_{90} ratios were 0.96, 0.91, 0.94, and 0.96, respectively. If blow units were fining upwards as often expected, this ratio would be significantly less than one. Further, no clear pattern was identified in the fining-upward trends with lateral distance from the vent.

To identify fining-outward trends, the same effective particle diameters (i.e., D_5, D_{10}, D_{60}, and D_{90}) were plotted vs. lateral distance for each blow unit, along lines of constant relative elevation within the unit (top or bottom of layer). Lateral trends are shown for the KAI and DAL features in Figs. 14 and 15, respectively. In the KAI feature, trends were investigated on a total of three lateral lineations, contained within two different depositional units; in the DAL feature, trends were investigated on a total of five lateral lineations, contained within three depositional units. While some

units loosely suggest a trend of decreasing particle size with increasing lateral distance from the vent (e.g., Fig. 15c), other units showed no apparent trend (e.g., Fig 15a), or the opposite trend, with grain sizes loosely increasing with distance from the vent (e.g., Fig 14c). Further, there was no relationship between the presence of fining-outward trends and either the vertical location within a unit or the source stratum's gradation.

In summary, particle size gradation trends in both the vertical and lateral directions were unreliable for identifying episodes of liquefaction in the CES features. The lack of reliable trends may be due to heterogeneities in the source stratum, or to variations in the ejection velocity and mixing energy imparted during fluidization. In the absence of silt seams, it would be very difficult to discern recurrent liquefaction or to accurately define the number of liquefaction episodes in the features formed during the CES. As discussed previously, inaccurate field interpretation of recurrent liquefaction features could lead to erroneous estimates of the causative earthquake magnitude(s). Given that the features studied herein were very recently deposited and minimally disturbed by weathering, spatial trends in particle gradation may be unreliable indicators of episodic liquefaction in older, more disturbed paleoliquefaction features.

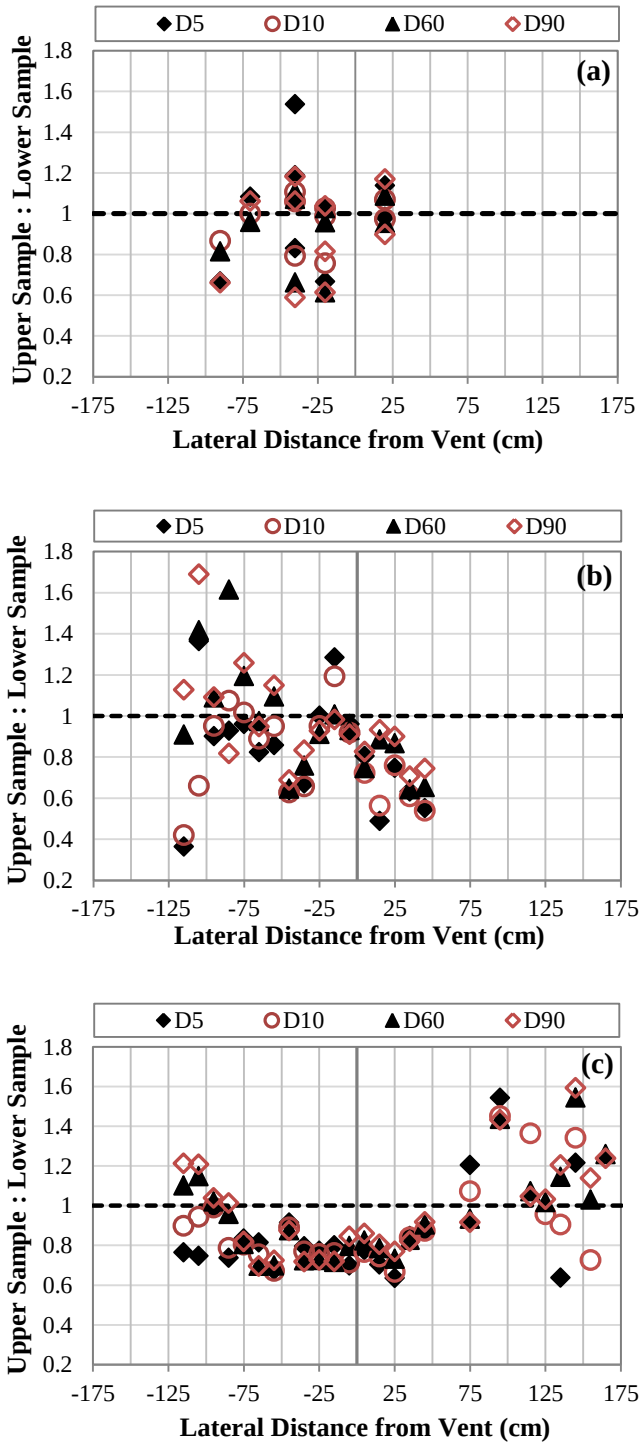

Figure 13. Analysis of particle size trends in the vertical direction for (a) KAI trench – all sample pairs, (b) DAL unit 1 (oldest ejecta layer); and (c) DAL unit 2 (2nd oldest ejecta layer). Data points represent the ratio of sample characteristics from the top of a depositional unit to those at the bottom. As such, values less than 1.0 indicate fining upwards within a unit.

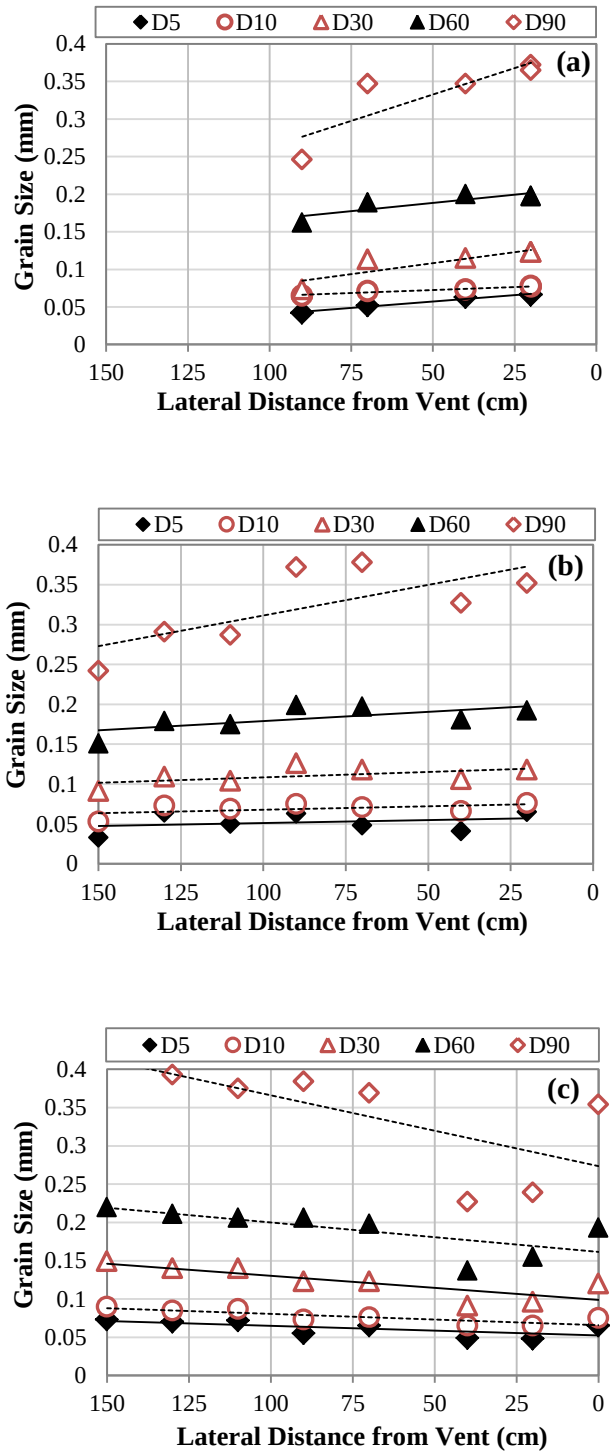

Figure 14. Analysis of particle size trends in the lateral direction for the KAI trench, along lineations of constant relative elevation: (a) base of first (oldest) unit; (b) top of first (oldest) unit; and (c) top of fifth (youngest) unit.

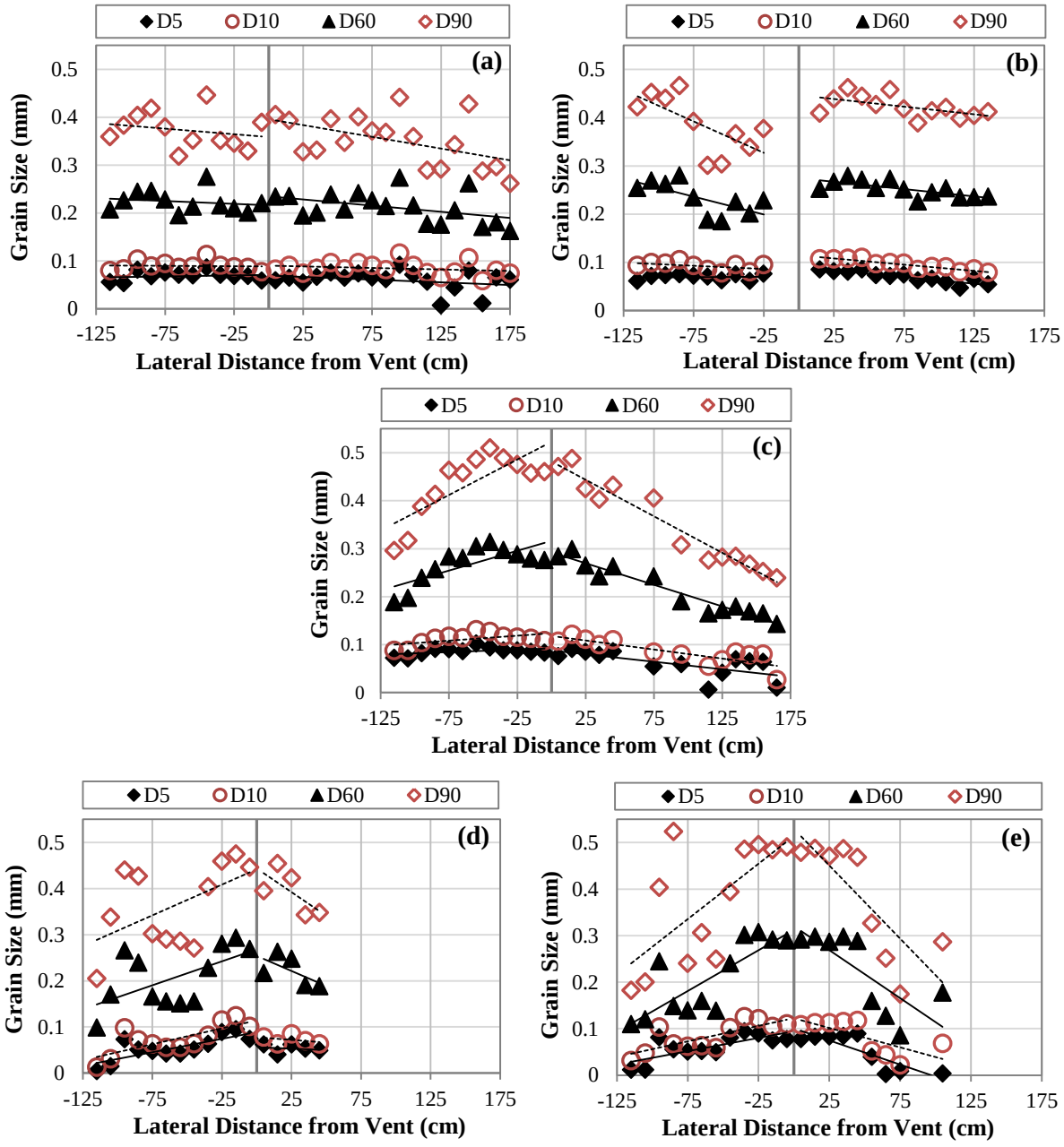

Figure 15. Analysis of particle size trends in the lateral direction for the DAL trench, along lineations of constant relative elevation: (a) base of first (oldest) unit; (b) top of first (oldest) unit; (c) base of second unit; (d) top of second unit; and (e) top of third (youngest) unit.

5. Conclusions

In regions of infrequent but potentially damaging seismicity, the computed seismic hazard is often heavily influenced by paleoliquefaction features, from which the magnitude recurrence rates of large prehistoric or pre-instrumental earthquakes are inferred. An accurate interpretation of the paleoseismic record becomes more difficult when these features are caused by earthquakes spaced closely in time. Accordingly, to better interpret paleoliquefaction evidence, a series of trenches were dug through recurrent liquefaction features formed during the 2010-2011 CES, with particular emphasis on discerning episodic liquefaction from spatial trends in particle size within the blow structures. Such trends were found to be unreliable as evidence for recurrent liquefaction and thus may be unreliable for paleoliquefaction analyses. Silt seams provide the most-definitive evidence for recurrent liquefaction, but their presence is dependent on the source stratum having sufficient fines, and their absence may therefore not disprove recurrent liquefaction. This study provided a modern analog to recurrent paleoliquefaction evidence, and has important implications for interpretation of seismic hazards in the central U.S. and elsewhere.

Part B References

Ambraseys, N.N., 1988. Engineering seismology. Earthquake Engineering and Structural Dynamics 17, 1-105.

Aydan, O., Ulusay, R., Kumsar, H., and Tuncay, E., 2000. Site investigation and engineering evaluation of the Duzce-Bolu earthquake of November 12, 1999. Turkish Earthquake Foundation, Istanbul. Report No. TDV/DR 09-51, 307 p.

Bastin, S., Quigley, M. and Bassett, K., 2012. Characterization of modern and paleo-liquefaction features in Christchurch following the 2010-2011 Canterbury earthquake sequence." [poster presentation] San Francisco, CA, USA: American Geophysical Union Fall Meeting (AGU), 3-7 Dec 2012.

Beavan, J., Fielding, E., Motagh, M., Samsonov, S., and Donnelly, N., 2011. Fault location and slip distribution of the 22 February 2011 M_w6.2 Christchurch, New Zealand, earthquake from geodetic data. Seismological Research Letters 82 (6), 789-799.

Berrill, J.B., Mulqueen, P.C., and Ooi, E.T.C., 1994. Liquefaction at Kaiapoi in the 1901 Cheviot, New Zealand, earthquake. Bulletin of the New Zealand National Society for Earthquake Engineering 27 (3), 178-189.

Bradley, B. A. and Cubrinovski, M., 2011. Near-source Strong Ground Motions Observed in the 22 February 2011 Christchurch Earthquake. Seismological Research Letters 82 (6), 853-865.

Brown, L.J., Beetham, R.D., Paterson, B.R., and Weeber, J.H., 1995. Geology of Christchurch, New Zealand. Environmental and Engineering Geoscience 1, 427–488.

CDG - Canterbury Geotechnical Database (2012) "Aerial Photography", Map Layer CGD0100 - 1 June 2012, retrieved [12/12] from https://canterburygeotechnicaldatabase. projectorbit.com

Cox, R.T., Hill, A.A., Larsen, D., Holzer, T., Forman, S.L., Noce, T., Gardner, C., and Morat, J., 2007. Seismotectonic implications of sand blows in the southern Mississippi embayment. Engineering Geology 89, 278-299.

Cubrinovski, M. and Green, R.A., eds., 2010. Geotechnical Reconnaissance of the 2010 Darfield (Canterbury) Earthquake, (contributing authors in alphabetical order: J. Allen, S. Ashford, E. Bowman, B. Bradley, B. Cox, M. Cubrinovski, R. Green, T. Hutchinson, E. Kavazanjian, R. Orense, M. Pender, M. Quigley, and L. Wotherspoon), Bulletin of the New Zealand Society for Earthquake Engineering 43(4), 243-320.

Cubrinovski, M, Bray, J.D., Taylor, M., Giorgini, S., Bradley, B., Wotherspoon, L., and Zupan J., 2011a. Soil liquefaction effects in the central business district during the February 2011 Christchurch earthquake. Seismological Research Letters 82(6), 893-904.

Cubrinovski, M., Bradley, B., Wotherspoon, L., Green, R., Bray, J., Woods, C., Pender, M., Allen, J., Bradshaw, A., Rix, G., Taylor, M., Robinson, K., Henderson, D., Giorgini, S., Ma, K., Winkley, A., Zupan, J., O'Rourke, T., DePascale, G., and Wells, D., 2011b. Geotechnical aspects of the 22 February 2011 Christchurch earthquake. Bulletin of the New Zealand Society for Earthquake Engineering 43(4), 205-226.

Cubrinovski, M., Robinson, K., Taylor, M., Hughes, M.M., and Orense, R., 2012. Lateral spreading and its impacts in urban areas in the 2010-2011 Christchurch earthquakes, New Zealand Journal of Geology and Geophysics 55(3), 255-269.

Environment Canterbury (ECan), 2004. Solid facts on Christchurch liquefaction. Environment Canterbury, Christchurch, New Zealand; http://ecan.govt.nz/publications/ General/soid-facts-christchurch-liquefaction.pdf.

Galli, P., 2000. New empirical relationships between magnitude and distance for liquefaction. Tectonophysics, 324, 169-187.

Green, R.A., Obermeier, S.F., and Olson, S.M., 2005, Engineering Geologic and Geotechnical Analysis of Paleoseismic Shaking Using Liquefaction Effects: Field Examples, Engineering Geology 76, 263-293.

Green, R.A., Allen, A., Wotherspoon, L., Cubrinovski, M., Bradley, B., Bradshaw, A., Cox, B., and Algie, T., 2011a. Performance of levees (stopbanks) during the 4 September M_w7.1 Darfield and 22 February 2011 M_w6.2 Christchurch, New Zealand, earthquakes. Seismological Research Letters 82(6), 939-949.

Green, R.A., Wood, C., Cox, B., Cubrinovski, M., Wotherspoon, L., Bradley, B., Algie, T., Allen, J., Bradshaw, A., and Rix, G., 2011b. Use of DCP and SASW Tests to Evaluate Liquefaction Potential: Predictions vs. Observations during the Recent New Zealand Earthquakes, Seismological Research Letters 82(6), 927-938.

Idriss, I.M. and Boulanger, R.W., 2006. Semi-empirical procedures for evaluating liquefaction potential during earthquakes. Soil Dynamics and Earthquake Engineering 26, 115-130.

Ishihara, K., 1985. Stability of natural deposits during earthquakes. Proceedings of the 11th International Conference on Soil Mechanics and Foundation Engineering, San Francisco, CA, USA, Aug. 1985, A.A. Balkema, Rotterdam, 1, 321-376.

Kam, W.Y., Akguzel, U., and Pampanin, S., 2011. 4 Weeks on: preliminary reconnaissance report from the Christchurch 22 Feb 2011 6.3M_w earthquake. Report, New Zealand Society of Earthquake Engineering, Wellington, New Zealand.

Kuribayahsi, E. and Tatsuoka, F., 1975. Brief review of liquefaction during earthquakes in Japan. Soils and Foundations 15(4), 81-92.

Maurer, B.W., Green, R.A., Cubrinovski, M., and Bradley, B., 2013. Evaluation of liquefaction potential index (LPI) for assessing liquefaction hazard: a case study in Christchurch, New Zealand. ASCE Journal of Geotechnical and Geoenvironmental Engineering, *in review*.

Moss, R.E.S, Seed, R.B., Kayen, R.E., Stewart, J.P., Der Kiureghian, A., and Cetin, K.O., 2006. CPT-based probabilistic and deterministic assessment of in situ seismic soil liquefaction potential. ASCE Journal of Geotechnical and Geoenvironmental Engineering, 132(8), 1032-1051.

Numata, A. and Mori, S., 2002. Grain Size Distribution of Erupted Sands Due to Liquefaction Journal of the Japanese Society of Civil Engineering, 722(61), 129-147.

Obermeier, S., 1989. The New Madrid earthquakes: an engineering-geologic interpretation of relict liquefaction features. U.S. Geological Survey Prof. Paper 1336-B, 114 p.

Obermeier, S.F. and Dickenson, S.E., 2000. Liquefaction evidence for the strength of ground motiosn resulting from the late Holocene Cascadia subduction earthquakes, with emphasis on the event of 1700 A.D. Bulletin of the Seismological Society of America 90(4), 876-896.

Obermeier, S.F., Pond, E.C., Olson, S.M. with contributions by Green, R.A., Mitchell, J.K., and Stark, T.D., 2001. Paleoliquefaction studies in continental settings: geologic and geotechnical factors in interpretations and back-analysis. U.S. Geological Survey Open-File Report 01-029.

Obermeier, S.F., Olson, S.M., and Green, R.A., 2005. Field occurrences of liquefaction-induced features: a primer for engineering and geologic analysis of paleoseismic shaking. Engineering Geology 76, 209-234.

Olson, S.M., Green, R.A., and Obermeier, S.F., 2005a. Revised magnitude bound relation for the Wabash Valley Seismic Zone of the central United States. Seismological Research Letters v. 76 (6), 756-771.

Olson, S.M., Green, R.A., and Obermeier, S.F., 2005b. Geotechnical analysis of paleoseismic shaking using liquefaction features: a major updating. Engineering Geology 76, 235-261.

Orense, R.P., Kiyota, T., Yamada, S., Cubrinovski, M., Hosono, Y., Okamura, M., and Yasuda, S., 2011. Comparison of liquefaction features observed during the 2010 and 2011 Canterbury earthquakes. Seismological Research Letters 82(6), 905-918.

Papadopoulos, G.A. and Lefkopoulos, G., 1993. Magnitude-distance relations for liquefaction in soil from earthquakes. Bulletin of the Seismological Society of America 83(3), 925-938.

Papathanassiou, G., Pavlides, S., Christaras, B., and Pitilakis, K., 2005. Liquefaction case histories and empirical relations of earthquake magnitude versus distance from the broader Aegean region. Journal of Geodynamics 40, 257-278.

Petersen, M., A., Frankel, S., Harmsen, C., Mueller, K., Haller, R., Wheeler, R., Wesson, Y., Zeng, O., Boyd, D., Perkins, N., Luco, E., Field, C.Wills, and Rukstales, K., 2008. Documentation for the 2008 update of the United States national seismic hazard maps, U. S. Geological Survey Open-File Report 2008-1128, 61 p.

Pirrotta, C., Barbano, M.S., Guarnieri, P., and Gerardi, F., 2007. A new dataset and empirical relationships between magnitude/intensity and epicentral distance for liquefaction in central-eastern Sicily. Annals of Geophysics 50(6), 763-774.

Quigley, M.C., Bastin, S., and Bradley, B.A., 2013. Recurrent liquefaction in Christchurch, New Zealand, during the Canterbury earthquake sequence. Geology 40 (1), 55-58.

Robertson, P.K. and Wride, C.E., 1998. Evaluating cyclic liquefaction potential using cone penetration test. Canadian Geotechnical Journal 35(3), 442-459.

Robinson, K., Cubrinovski, M., and Bradley, B.A., 2013. Comparison of actual and predicted measurements of liquefaction-induced lateral displacements from the 2010 Darfield and 2011

Christchurch Earthquakes, Proc. 2013 Conference of the New Zealand Society for Earthquake Engineering (NZSEE 2013), Wellington, New Zealand, 26-28 April, *in review*

Saucier, R.T., 1989. Evidence for episodic sand-blow activity during the 1811-1812 New Madrid (Missouri) earthquake series. Geology 17 (2), 103-106.

Sims, J.D., and Garvin, C.D., 1995. Recurrent liquefaction induced by the 1989 Loma Prieta earthquake and 1990 and 1991 aftershocks: implications for paleoseismicity studies. Bulletin of the Seismological Society of America 85 (1), 51-65.

Smyrou, E., Panagiota, T., Engin Bal, I., and Gazetas, G., 2011. Ground motions versus geotechnical and structural damage in the February 2011 Christchurch earthquake. Seismological Research Letters 82(6), 882-892.

Tuttle, M.P., 2001. The use of liquefaction features in paleoseismology: lessons learned in the New Madrid seismic zone, central United States. Journal of Seismology 5, 361-380.

Tuttle, M.P., Schweig, E.S., Sims, J.D., Lafferty, R.H., Wolf, L.W., and Haynes, M.L., 2002a. The earthquake potential of the New Madrid Seismic Zone. Bulletin of the Seismological Society of America 92 (6), 2080-2089.

Tuttle, M.P., Dyer-Williams, K., and Barstow, N.L., 2002b. Paleoliquefaction study of the Clarendon-Lindon fault system, western New York State. Tectonophysics 353, 263-286.

Tuttle, M.P., Schweig, E.S., Campbell, J., Thomas, P.M., Sims, J.D., and Lafferty, R.H., 2005. Evidence for New Madrid earthquakes in A.D. 300 and 2350 B.C.. Seismological Research Letters 76, 489-501.

Tuttle, M.P., 2012. Paleoliquefaction lessons learned from the 2010-2011 Canterbury, New Zealand, earthquakes. [abs]. In: Proceedings of the Geological Society of America Annual Meeting; 2012, Nov 4-7; Charlotte NC, USA.

Vidale, J., Atkinson, G., Green, R., Hetland, E., Grant-Ludwig, L., Mazzotti, S., Nishenko, S., and Sykes, L., 2011. Report of the independent expert panel on New Madrid Seismic Zone earthquake hazards as approved by NEPEC on April 16, 2011: U.S. Geological Survey, 26 p.

Wakamatsu, K., 1993. History of soil liquefaction in Japan and assessment of liquefaction potential based on geomorphology. A Thesis in the Department of Architecture Presented in Partial Fulfillment of the Requirements for the Degree of Doctor of Engineering, Waseda University, Tokyo, Japan.

Wotherspoon, L.M., Pender, M.J., and Orense, R.P. 2012. Relationship between observed liquefaction at Kaiapoi following the 2010 Darfield earthquake and former channels of the Waimakariri River, Engineering Geology 125, 45-55.

IV. Part C: Assessment of Aging Correction Factors for Liquefaction Resistance at Sites of Recurrent Liquefaction

Summary

Studies suggest the cyclic shear strength of sands may be reduced following recent liquefaction. As such, the severity of liquefaction manifestation may be greater than expected for sites of repeat liquefaction events spaced closely in time. Accordingly, to investigate short time-scale "aging-effects," an assessment of aging-correction factors was performed at sites of recurrent liquefaction during the Canterbury (NZ) earthquake sequence. Using an LPI framework, short time-scale aging correction factors were found to be plausible at sites with prior moderate-to-severe liquefaction. However, aging-effects were only perceptible at sites of marginal liquefaction (i.e., those that *just* liquefied), while at sites of more severe liquefaction likely to damage infrastructure, prior liquefaction had no measureable effect. A modified aging-relation is proposed herein and is presented for use with CRR-based triggering curves. Significant scatter exists in the dataset, however, and judicious use of aging corrections is thus advised.

1. Introduction

Increases in the shear strength and stiffness of sands with time have been widely investigated. These temporal gains, or "aging effects," are discernible from both in-situ penetration resistance (e.g., SPT, CPT) and liquefaction resistance (i.e., CRR), where the rate of increase in CRR exceeds that suggested by in-situ penetration data (e.g., Lewis et al., 1999; Arango et al., 2000; Leon et al., 2006). It has thus been recognized that aging effects may be resolved into gains measurable by large-strain penetration tests (e.g., Mitchell and Solymar, 1984; Mitchell, 1986; Mesri et al., 1990; Skempton, 1986; Kulhawy and Mayne, 1990) and gains in liquefaction resistance (i.e., cyclic shear strength) (e.g., Youd and Hoose, 1977; Youd and Perkins, 1978; Hayati et al., 2008; Hayati and Andrus, 2009; Ha et al., 2011; Kokusho et al., 2012), where the latter is influenced by small-strain soil fabric phenomena undetected at large-strain (e.g., Howie et al., 2012; Wang and Tsui, 2009; Roy et al., 1996). Because liquefaction triggering curves (SPT- and CPT-based) are developed from post-liquefaction penetration resistance of Holocene sands, evaluations of older deposits should account for the effects of aging using a framework consistent with both penetration indices and liquefaction resistance (Leon et al., 2006). The influence of aging on liquefaction resistance can be represented by the deposit resistance factor, K_{DR} (Hayati and Andrus, 2009), computed as the ratio of an older deposit's CRR to that of a deposit at a younger "reference age." As such, the age-corrected liquefaction resistance is determined as follows:

$$CRR_K = CRR \times K_{DR} \tag{1}$$

where CRR_K is the age-corrected CRR, and K_{DR} represents the influence of aging. The K_{DR} relations of Arrango et al. (2000) Hayati et al. (2008), and Hayati and Andrus (2009) are shown

in Fig. 1.

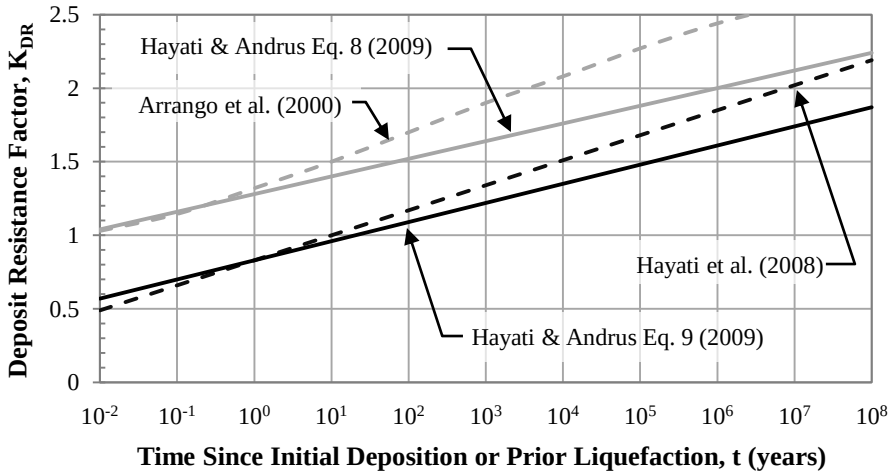

Figure 1. Comparison of four aging- relations (K_{DR}) for liquefaction resistance.

It can be seen in Fig. 1 that while the aging-relations have relatively similar slopes (0.09 to 0.17 gain in K_{DR} per log-cycle), their reference ages (i.e., K_{DR} = 1) range from 2 days to 23 years, reflecting different manners of development and different intended uses. For example, the relation given by Eq. 8 in Hayati and Andrus (2009) was developed from cyclic triaxial and cyclic simple shear tests. As such, the reference age is that of a freshly deposited laboratory specimen (~2 days), and the increase in liquefaction resistance is presented without a specific application or intended use. As noted, the liquefaction triggering curves commonly used in practice (e.g., Robertson and Wride, 1998; Idriss and Boulanger, 2006; Moss et al., 2006) are derived using a case-history database from Holocene deposits. Because the positions of the triggering curves are controlled by the youngest, most susceptible deposits, these CRR-based triggering curves likely have a reference age on the order of 1 to 100 years. Thus, lab-derived aging-relations cannot be directly applied to the triggering curves, as this would erroneously elevate the computed liquefaction resistance. For example, the relation of Arrango et al. (2000) would increase the computed CRR of deposits aged 1 and 10 years by 32% and 50%, respectively. While lab-derived K_{DR}-relations are not presented as corrections for triggering curves, they have been inappropriately used as such in the literature.

In contrast, the relation given by Eq. 9 in Hayati and Andrus (2009) (a refinement of Hayati et al., 2008) was developed from field and laboratory tests using CRR-based triggering curves. As such, the reference age found from data regression (23 years) is consistent with the likely reference age of the case-history database, and the K_{DR}-relation is therefore applicable to CRR-based triggering curves. Although principally developed to evaluate deposits older that the reference age (e.g., Pleistocene deposits), regression of these relations implies liquefaction resistance is reduced for deposits younger than the reference age (i.e., $K_{DR} < 1$). Of relevance to the objective of this study, the liquefaction resistance of a previously liquefied deposit is thus assumed to be reduced if the reference age is greater than the time since the deposit previously liquefied. As such, for sites of repeat liquefaction closely spaced in time, the susceptibility of liquefaction triggering and severity of liquefaction manifestation may be greater than predicted if the time since the previous occurrence of liquefaction is not appropriately taken into account.

Observations of the site-to-source distance of the most distal liquefaction site being

greater for aftershock events than for equivalent-magnitude mainshocks (Audemard and De Santis, 1991; Sims and Garvin, 1995; Green and Cubrinovski, 2010) may give credence to $K_{DR} < 1$ corrections. In Fig. 2, the Ambraseys (1988) "magnitude-bound" relations for epicentral distance and fault distance are shown with the global database of observations used in their development. Magnitude-bound curves are commonly used in paleoliquefaction studies to relate the site-to-source distance of the most distal liquefaction site to the causative earthquake magnitude. Also shown in Fig. 2 are observations from aftershock events following the 1989 Boca del Tucuyo (VE), 1991 Loma Prieta (USA), 2010 Darfield (NZ), and 2011 Christchurch (NZ) earthquakes; mainshock observations from these events are circled in red and are consistent with the Ambraseys (1988) database. It can be seen that aftershock observations deviate from those of mainshocks such that reliquefaction resistance appears to be reduced following prior liquefaction. In addition, Towhata et al. (2013) studied aging-effects using case-histories from the March 2011 M_w9.0 Tohoku (JPN) earthquake. Towhata et al. (2013) found the liquefaction resistance of natural alluvium to be approximately twice that of recent deposits that had liquefied in prior earthquakes. Furthermore, Ha et al. (2011) studied reliquefaction resistance of sands using 1 g laboratory shaking table tests. The tests showed that the number of cycles required for reliquefaction reduced significantly following the first liquefaction event as a result of destroying the aged soil-fabric.

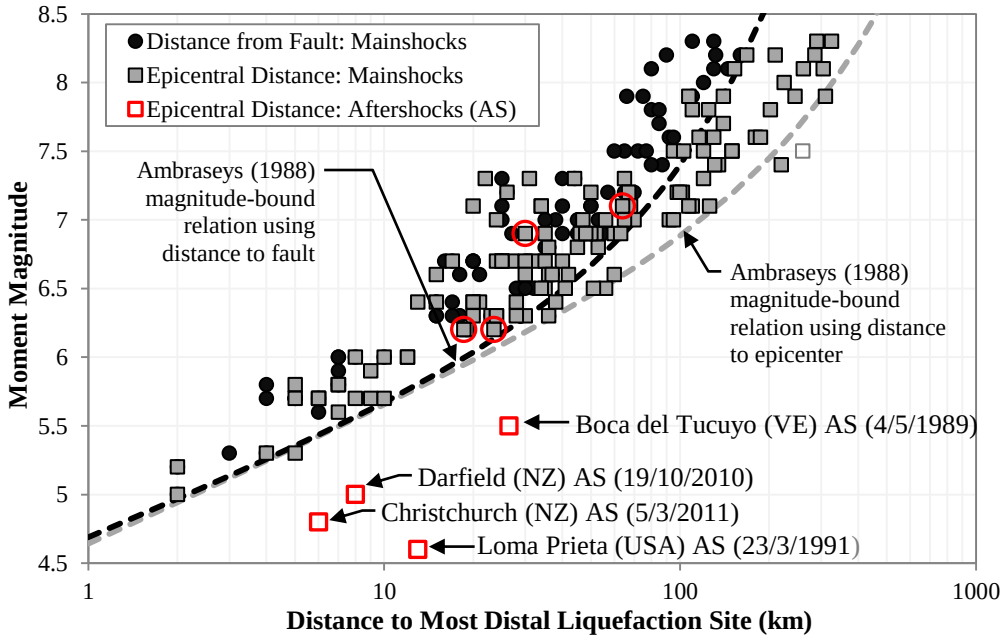

Figure 2. Magnitude-bound relations of Ambraseys (1988) with aftershock observations from four recent earthquakes; the four corresponding mainshock observations are circled in red.

Although aging mechanisms are not yet fully understood, recent studies suggest reliquefaction resistance is reduced after recent liquefaction, an observation with potential implications for seismic hazard assessment and recovery. Assessments of aging-correction factors are very limited, however, and their accuracy is thus highly uncertain. Accordingly, to evaluate whether aging-corrections are applicable when extrapolated to very short ages (i.e., days to months), the study presented herein evaluates sites of recurrent liquefaction during the 2010-2011 Canterbury (NZ) earthquake sequence. The aging relations of Hayati et al. (2008) and

Hayati and Andrus (2009) are applied within the framework of a liquefaction potential index (LPI) assessment to determine whether their use is consistent with the observed severity of liquefaction manifestation. Based on the results of this analysis, implications to liquefaction hazard assessment are discussed, and recommendations for aging correction factors are given.

2.0 Methodology

The 2010-2011 Canterbury (NZ) Earthquake Sequence (CES) resulted in a liquefaction dataset of unprecedented size and quality. The combination of well-documented liquefaction response, densely-recorded ground motions, and detailed subsurface characterization provides a unique opportunity to investigate short time-scale aging-effects on liquefaction (i.e., $K_{DR} < 1$), and moreover, to determine whether such effects increase liquefaction hazards for the built environment. The CES initiated with the 4 Sept. 2010, M_w7.1 Darfield earthquake and was punctuated by the 22 Feb. 2011, M_w6.2 Christchurch earthquake, which induced severe liquefaction throughout much of Christchurch. To assess whether prior liquefaction reduced reliquefaction resistance in the Christchurch earthquake, thus exacerbating damage to the built environment, a database of ~1200 investigation sites was assembled for analysis. This database consisted of post-liquefaction CPT soundings, observations of severity of liquefaction manifestation, and conditional PGA distributions for each investigation site.

The effects of aging on reliquefaction resistance were investigated using the liquefaction potential index (LPI) proposed by Iwasaki et al. (1978). While CRR-based triggering curves predict liquefaction in particular strata, they provide no objective characterization of the cumulative response of a soil deposit. LPI was proposed to fill this need and is computed as:

$$\mathrm{LPI} = \int_0^{20\,\mathrm{m}} \mathrm{F} \cdot \mathrm{w(z)}\, \mathrm{dz} \tag{2}$$

In Eq. 1, F = 1 – FS for FS ≤ 1 and F = 0 for FS > 1, where FS is the factor of safety against liquefaction computed by a liquefaction evaluation procedure (triggering curve), and w(z) is a depth weighting function given by w(z) = 10 – 0.5z, where z = depth in meters. Thus, it is assumed that the severity of liquefaction manifestation is proportional to the thickness of a liquefied layer, the proximity of the layer to the ground surface, and the amount by which FS is less than 1.0. Given this definition, LPI can range from 0 to 100. While LPI is by no means a perfect index, it has been shown to generally correlate well with the severity of surficial manifestation (Maurer et al. 2013). As such, LPI provides a reasonably consistent tool for examining trends in liquefaction hazard associated with aging-effects. In the following, the components of the liquefaction database and the computation of LPI are discussed in more detail.

2.1 CPT Soundings

Due to the severity and spatial extent of liquefaction damage, the New Zealand Earthquake Commission (EQC) funded a subsurface characterization program that produced extensive CPT sounding data. Approximately 1500 soundings were initially performed following the Darfield and Christchurch earthquakes and are utilized for this study. To identify soundings prematurely terminating on shallow gravels, the CPT database was geo-spatially analyzed using an Anselin Local Morans I analysis (Anselin, 1995) and soundings with anomalously shallow termination

depths were removed from the study, leaving ~1200 soundings. For further discussion of CPT depths and the geospatial analysis used herein, see Maurer et al. (2013).

2.2 Liquefaction Severity

Observations of liquefaction and the severity of manifestations were made by the authors for each of the CPT sounding locations following both the Darfield and Christchurch earthquakes. This was accomplished by ground reconnaissance and using high-resolution aerial and satellite imagery performed in the days immediately following each of the earthquakes. CPT sites were assigned one of six damage classifications: no liquefaction, marginal liquefaction, moderate liquefaction, severe liquefaction, lateral spreading, and severe lateral spreading, where the classifications describe the predominant damage mechanism and manifestation of liquefaction. The criteria for each classification are given by Maurer et al. (2013).

2.3 Estimation of a_{max} (PGA)

To evaluate the factor of safety against liquefaction using one of the simplified liquefaction evaluation procedures, the amplitude of cyclic loading is proportional to PGA at the ground surface, and the duration is related to the earthquake magnitude. PGAs were computed using the procedure discussed in detail by Bradley (2013), and used by Green et al. (2011) and Maurer et al. (2013). The Bradley (2013) procedure combines unconditional PGA distributions estimated by the Bradley (2013) GMPE, recorded PGAs from strong motion stations, and the spatial correlation of intra-event residuals to compute the conditional PGA distribution at sites of interest.

2.4 Liquefaction Evaluation, Aging Corrections, and LPI

Factors of safety against liquefaction were computed using the CPT-based liquefaction evaluation procedure of Idriss and Boulanger (2006), where the soil behavior type index, I_c, was used to identify non-liquefiable strata. Soils having $I_c > 2.6$ were considered too plastic to liquefy. Soil unit weights were estimated per the method of Robertson and Cabal (2010), and fines content (FC) was estimated using the Christchurch-soil-specific I_c-FC correlation developed by Robinson et al. (2013). The efficacies of the Hayati et al. (2008) and Hayati and Andrus (2009) K_{DR} relations were evaluated for the Christchurch earthquake using a time-since-last-disturbance (i.e., "age") of 171 days, where applicable. Of the several $M_w > 5.0$ aftershocks occurring prior to the Christchurch earthquake, one is known to have induced liquefaction on the periphery of the study area; a small number of investigation sites were affected by this event and were removed from the study due to the uncertain time-since-last-disturbance. Because the K_{DR} corrections of Hayati et al. (2008) and Hayati and Andrus (2009) are approximately equal for deposits aged 171 days, a common value of K_{DR} (0.78) is used in the evaluations presented

herein. Lastly, LPI values were computed at each study site for the Darfield and Christchurch earthquakes using Eq. 2.

3.0 Results & Discussion

To evaluate aging effects, the severity of liquefaction manifestation predicted by LPI is compared to that actually observed. If prior liquefaction reduced reliquefaction resistance during the Christchurch earthquake, there should be a shift toward under-predictions of liquefaction severity (i.e., liquefaction manifestations were worse than expected). For this analysis, the following LPI values are used to assess prediction accuracy: LPI < 5, No Liquefaction; 5 ≤ LPI < 8, Marginal Liquefaction; 8 ≤ LPI < 15, Moderate Liquefaction; LPI ≥ 15, Severe Liquefaction. Cases of lateral spreading were not considered for this study because (1) there are separate criteria for assessing its severity; and (2) LPI may inconsistently predict its occurrence (Maurer et al., 2013) making analysis of K_{DR} corrections difficult. For further discussion of the LPI hazard-scale used herein, see Maurer et al. (2013). To quantify the accuracy of LPI predictions, a prediction error (E) was computed using the LPI values assigned to each liquefaction classification, such that E = LPI – (min or max) of relevant range. For example, if the computed LPI is 15 for a site with marginal liquefaction, E = 15 – 8 = 7, whereas if the computed LPI is 6 for a site with severe liquefaction, E = 6 – 15 = -9. As such, positive errors indicate over-predictions of liquefaction severity, and conversely, negative errors indicate under-predictions.

In Fig. 3, the distribution of LPI prediction errors is shown for each earthquake, where K_{DR} corrections have not yet been applied; it can be seen that the severity of liquefaction manifestation was accurately predicted for the majority of study sites during both events. However, it is also evident that for the Christchurch earthquake, the severity of manifestation was under-predicted more often than for the Darfield earthquake (i.e., more sites had negative prediction errors). As the total number of cases per event is equal, and the distributions of over-predictions are similar, the increase in negative errors for the Christchurch earthquake is a result of fewer near-zero errors. This suggests that prior liquefaction may have reduced reliquefaction resistance during the Christchurch earthquake. However, this does not elucidate whether sites with under-predictions are those that had previously liquefied. Thus, of greater importance is the relative change in prediction error for individual sites, and moreover, whether this relative change is affected by prior liquefaction.

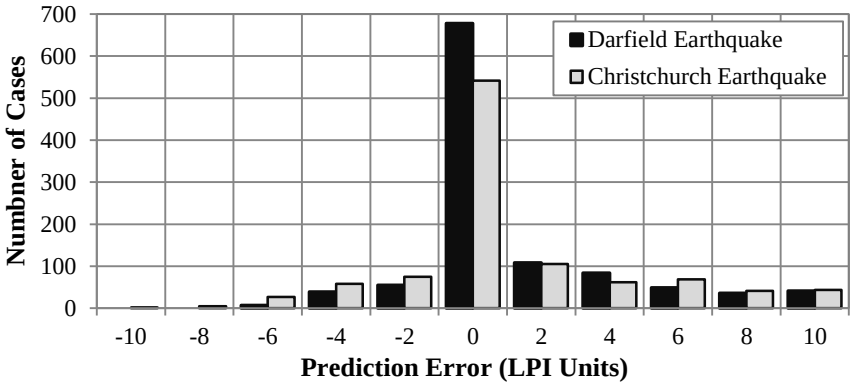

Figure 3. Distribution of LPI prediction errors for the Darfield and Christchurch earthquakes.

In Fig. 4, the change in LPI prediction error between the Darfield and Christchurch earthquakes (i.e., $E_{CHCH} - E_{DAR}$) is presented, where sites have been categorized by the observed severity of manifestation during the Darfield earthquake. Thus, data plotting below the $\Delta E = 0$ line indicates that as compared to the Darfield earthquake, the severity of manifestation was worse than predicted for the Christchurch earthquake. If prior liquefaction exacerbated liquefaction severity, a shift below the $\Delta E = 0$ line is expected with increasing prior liquefaction severity. Although the mean ΔE is less at sites with prior moderate/severe liquefaction relative to sites without prior manifestation, the difference between means is not statistically significant. While the results presented in Fig. 4 suggest $K_{DR} < 1$ corrections may not be warranted, several complicating factors have yet to be accounted for and are discussed as follows. First, as discussed by Maurer et al. (2013), LPI predictions may be inherently poor for some profiles. If the LPI framework does not accurately model liquefaction manifestation, then LPI values at these sites should not be used to access the plausibility of K_{DR} corrections. Further, to apply K_{DR} corrections, assumptions must be made regarding the prior liquefaction of soils. K_{DR} is applied only to strata that previously liquefied rather than to the entire profile, but when LPI predictions deviate from actual observations, it is difficult to identify the strata that actually liquefied. For example, if the computed LPI is 15 for a site with marginal liquefaction (i.e., liquefaction severity is over-predicted), then some soils predicted to liquefy may not have. As such, only sites where LPI accurately predicted the severity of manifestation during the Darfield earthquake are considered subsequently. In cases where LPI predictions agreed with observations, it is assumed that soils indeed liquefied during the Darfield earthquake if they were predicted to do so by the Idriss and Boulanger (2006) liquefaction evaluation procedure. Thus, the approach taken herein is to use only the highest quality data in lieu of the entire liquefaction database, thereby reducing uncertainties. Second, though the analysis shown in Fig. 4 accounts for the severity of liquefaction in the Darfield earthquake, the severity of the liquefaction induced by the Christchurch earthquake is not directly considered. Conceptually, aging-effects should be most perceptible at sites that moderately to severely liquefied during the Darfield earthquake and then only marginally liquefied during the Christchurch earthquake. This is because these soils may not have liquefied during the Christchurch earthquake if the soil structure was not completely

disrupted during the Darfield earthquake. Conversely, aging effects may be difficult to detect at sites that moderately to severely liquefied during both earthquakes. This is because the intensity of shaking during the Christchurch earthquake likely far exceeded the threshold level to trigger liquefaction regardless of whether the threshold was reduced due to the prior occurrence of liquefaction. Accordingly, the severity of liquefaction should be considered in both events.

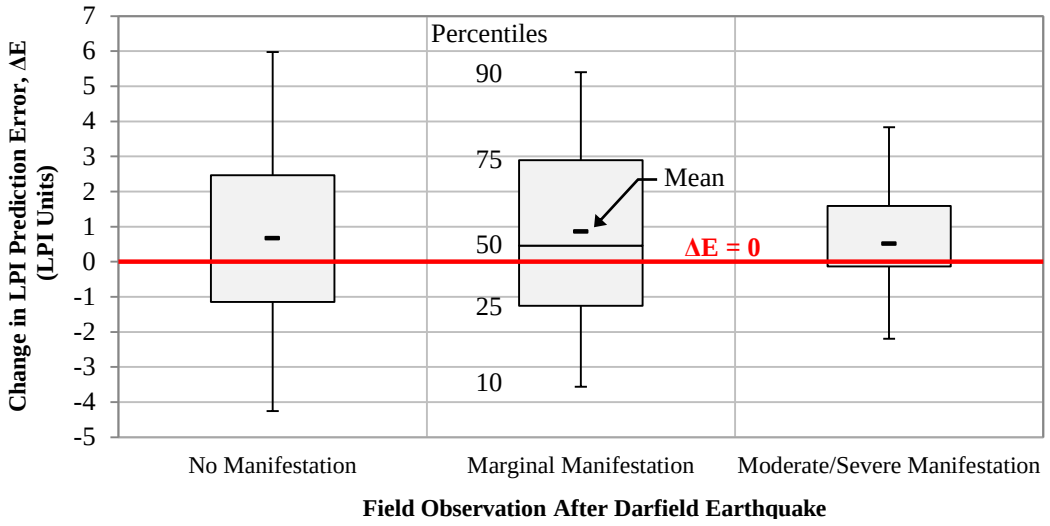

Figure 4. Change in LPI prediction error: $E_{CHCH} - E_{DAR}$

In Fig. 5, prediction errors for the Christchurch earthquake are shown as a function of the severity of manifestation in both events, where only sites at which manifestations were accurately predicted in the Darfield earthquake are considered. At sites with prior manifestation, a $K_{DR} = 0.78$ correction has been applied per the aforementioned assumptions. To evaluate the need for, and efficacy of, aging correction factors, results are shown with and without the K_{DR} correction. First, it may be seen in Fig. 5 that for 45 sites with marginal manifestations in the Darfield earthquake, application of the K_{DR} correction generally results in over-predictions of manifestation severity for the Christchurch earthquake. Furthermore, manifestations are generally not under-predicted when the K_{DR} correction is not applied. Thus, at sites with previous marginal manifestation, there is no apparent need for aging-corrections, and based on these results, the K_{DR} correction applied is problematic. These findings are not surprising given the ambiguous cause of marginal manifestations, characterized by a small amount of water or ejecta (a few cm thick at most). Such observations could result from elevated pore pressures even if liquefaction is not triggered, making it unclear whether K_{DR} corrections are applicable.

Next, for 8 sites with marginal manifestations in the Christchurch Earthquake that had prior moderate-to-severe liquefaction in the Darfield earthquake, manifestation severity was generally under-predicted when K_{DR} correction was not applied, and applying this correction typically improved prediction accuracy. It can also be seen in Fig. 5 that for 21 sites with moderate-to-severe manifestations in both events, K_{DR} corrections were not needed for accurate predictions, but are none-the-less plausible (i.e., their use did not reduce prediction accuracy).

Thus, either prior liquefaction had no effect, or its effects were imperceptible given the resolution of the LPI hazard-scale. In either case, prior liquefaction did not measurably exacerbate hazards at sites of moderate-to-severe liquefaction in the Christchurch earthquake. Returning to the former 8 sites with marginal manifestations, K_{DR} correction factors were back-calculated such that LPI predictions matched the lower (5), middle (7.5), and upper (8) values consistent with marginal manifestation (i.e., $5 \leq LPI < 8$). The range of back-calculated median K_{DR} values is shown in Fig. 6 along with the Hayati and Andrus (2009) K_{DR} relation and data (n = 24), and suggest that $K_{DR} < 1$ corrections are plausible. Using the combined 32 data-points, a modified K_{DR} aging-relation, applicable to CRR-based triggering curves, is shown in Fig. 6.

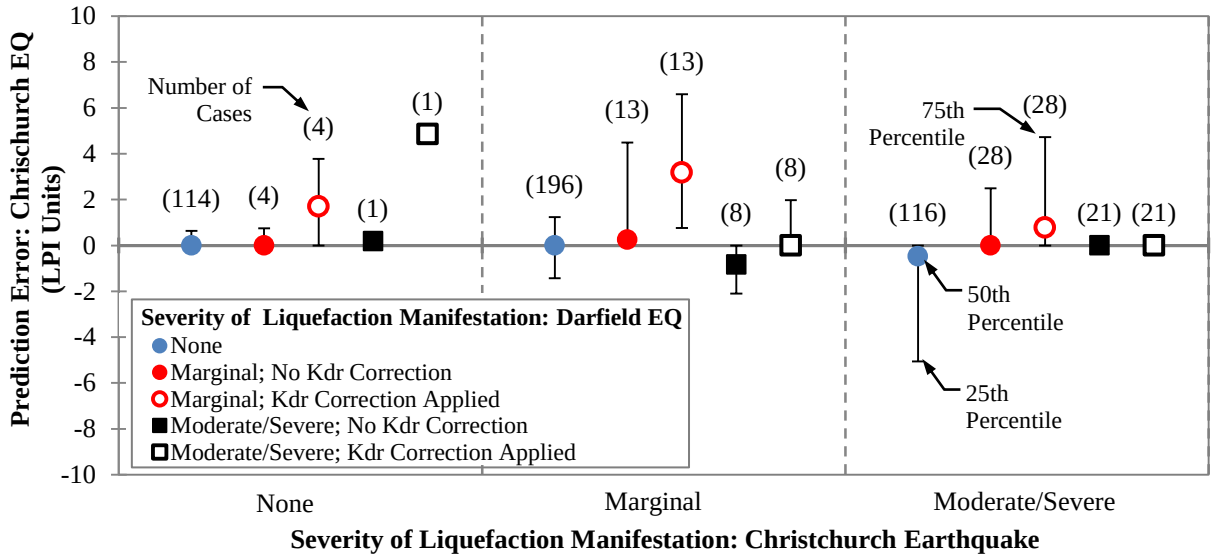

Figure 5. LPI prediction errors in the Christchurch earthquake, sorted by manifestation severity.

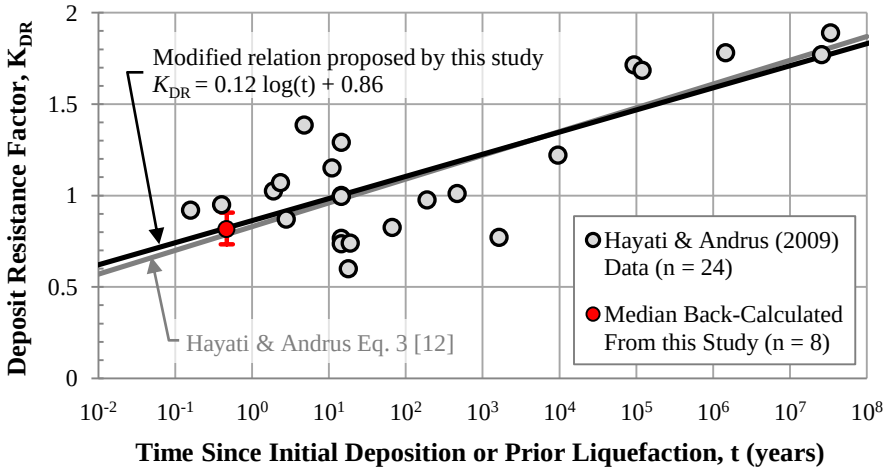

Figure 6. Time vs. K_{DR} correction factor

4.0 Conclusions

An assessment of aging-correction factors at sites of recurrent liquefaction was performed using data from the Canterbury earthquakes. Short time-scale aging correction factors for CRR-based triggering curves (i.e., $K_{DR} < 1$) were found to be plausible at sites with prior moderate-to-severe liquefaction. Aging relations such as that proposed by Hayati and Andrus (2009) may explain anomalies in published magnitude-bound data (Audemard and De Santis, 1991; Sims and Garvin, 1995; Green and Cubrinovski, 2010) and are consistent with laboratory observations (Ha et al, 2011). However, while $K_{DR} < 1$ correction factors were found to be plausible, post-liquefaction reductions in reliquefaction resistance did not exacerbate liquefaction hazard to the built-environment. In other words, aging effects were only perceptible at sites that moderately to severely liquefied during the Darfield earthquake that then marginally liquefied during the Christchurch earthquake. For sites that moderately to severely liquefied during both events, any reduction in the threshold to trigger liquefaction was indiscernible due to the intensity of shaking during the Christchurch earthquake. A modified K_{DR} relation was proposed based on data from Hayati and Andrus (2009), and is shown in Fig. 6. However, significant scatter still exists in the dataset, and judicious use of aging corrections is thus advised; continued research into aging-effects on liquefaction is warranted.

Part C References

Ambraseys, N.N., 1988. Engineering seismology. Earthquake Engineering and Structural Dynamics 17, 1-105.

Anselin, L., 1995. Local indicators of spatial association – LISA. Geographical Analysis 27(2), 93-115.

Arango, I., Lewis, M.R., and Kramer, C., 2000. Updated liquefaction potential analysis eliminates foundation retrofitting of two critical structures. Soil Dynamics and Earthquake Engineering 20, 17-25.

Audemard, F.A., and De Santis, F., 1991. Survey of liquefaction structures induced by recent moderate earthquakes. Bulletin of the International Association of Engineering Geology 44, 5-16.

Bradley, B.A., 2013. Site-specific and spatially distributed estimation of ground motion intensity in the 2010-2011 Canterbury earthquakes. Soil Dynamics and Earthquake Engineering. In Review.

Bradley, B.A., 2013. A New Zealand-specific pseudo-spectral acceleration ground-motion prediction equation for active shallow crustal earthquakes based on foreign models. Bulletin of the Seismological Society of America 103(3), 1801-1822.

Green, R.A., Allen, A., Wotherspoon, L., Cubrinovski, M., Bradley, B., Bradshaw, A., Cox, B., and Algie, T., 2011. Performance of levees (stopbanks) during the 4 September M_w7.1 Darfield and 22 February Christchurch, New Zealand earthquakes. Seismological Research Letters 82(6), 939-949.

Green, R.A. and Cubrinovski. M., eds., 2010. Geotechnical Reconnaissance of the 2010 Darfield (New Zealand) Earthquake. Report of the NSF-Sponsored GEER Team.

Ha, I.S., Olson, S.M., Seo, M.W., and Kim, M.M., 2011. Evaluation of reliquefaction resistance using shaking table tests. Soil Dynamics and Earthquake Engineering 31, 682-691.

Hayati, H., Andrus, R.D., Gassman, S.L., Hasek, M., Camp, W.M., and Talwani, P., 2008. Characterizing the liquefaction resistance of aged soils. Proceedings of Geotechnical Earthquake Engineering and Soil Dynamics IV, GSP No. 181, Zeng, D., Manzari, M., and Hilunen, D., eds., Reston, VA; 1-10.

Hayati, H. and Andrus, D., 2009. Updated liquefaction resistance correction factors for aged sands. Journal of Geotechnical and Geoenvironmental Engineering 135(11), 1683-1692.

Howie, J.A., Shozen, T., and Vaid, Y.P., 2002. Effect of Aging on stiffness of very loose sand. Canadian Geotechnical Journal 39(1), 149-156.

Idriss, I.M. and Boulanger, RW., 2006. Semi-empirical procedures for evaluating liquefaction potential during earthquakes. Soil Dynamics and Earthquake Engineering 26,115-130.

Iwasaki, T., Tatsuoka, F., Tokida, K., and Yasuda, S., 1978. A practical method for assessing soil liquefaction potential based on case studies at various sites in Japan. Proc. 2nd Int. Conf. on Microzonation, San Francisco, CA, USA; 885-896.

Kulhawy, F.H. and Mayne, P.W., 1990. Manual on estimating soil properties for foundation design. Final Report 1493-6, EL-6800, Electric Power Res. Inst., Palo Alto, CA.

Kokusho, T., Ito, F., Nagao, Y., and Green, R.A., 2012. Journal of Geotechnial and Geoenvironmental Engineering, 138(6), 747-756.

Leon, E., Gassman, S.L., and Talwani, P., 2006. Accounting for soil aging when assessing liquefaction potential. Journal of Geotechnical and Geoenvironmental Engineering 132(3), 363-377.

Lewis, M.R., Arango, I., Kimball, J.K., and Ross, T.E., 1999. Liquefaction resistance of old sand deposits. Proc.11th Panamerican Conf. on Soil Mech. And Geotechnical Engineering. Foz do Iguassu, Brazil; 821-829.

Maurer, B.W., Green, R.A., Cubrinovski, M., and Bradley, B.A., 2013. Evaluation of liquefaction potential index (LPI) for assessing liquefaction hazard: Case Study: Christchurch, New Zealand. Journal of Geotechnical and Geoenvironmental Engineering. In Review.

Mitchell, J.K., 1986. Practical problems from surprising soil behavior. Journal of Geotechnical Engineering 112(3), 259-289.

Mitchell, J.K. and Solymar, Z.V., 1984. Time-dependent strength gain in freshly deposited or densified sand. Journal of Geotechnical Engineering 110(11), 1559-1576.

Mesri, G., Feng, T.W., and Benak, J.M., 1990. Postdensification penetration resistance of clean sands. Journal of Geotechnical Engineering 116(7), 1095-1115.

Moss, R.E.S., Seed, R.B., Kayeb, R.E., Stewart, J.P., Der Kiureghian, A., and Cetin, K.O., 2006. CPT-based probabilistic and deterministic assessment of in situ seismic soil liquefaction potential. Journal of Geotechnical and Geoenvironmental Engineering 132(8), 1032-1051.

Robertson, P.K. and Wride, C.E., 1998. Evaluating cyclic liquefaction potential using cone penetration test. Canadian Geotechnical Journal 35(3), 442-459.

Robertson, P.K. and Cabal, K.L., 2010. Estimating soil unit weight from CPT. 2nd Int. Symposium on Cone Penetration Testing, Huntington Beach, CA, USA; paper #2-40.

Robinson, K., Cubrinovski, M., and Bradley, B.A., 2013. Sensitivity of predicted liquefaction-induced lateral displacements from the 2010 Darfield and 2011 Christchurch Earthquakes. Proc. New Zealand Soc. for Earthquake Eng. Annual Conf. 2013, Wellington, New Zealand; 8p.

Roy, D., Campanella, R.G., Byrne, P.M., and Hughes, J.M.O., 1996. Strain level and uncertainty of liquefaction related index tests. Uncertainty in the geologic environment: from theory to practice, GSP No. 58, Shackelford, C.D., Nelson, P.P., and Roth, M.J.S., eds., New York; 1149-1162.

Schmertmann, J.H., 1991. The mechanical aging of soils. Journal of Geotechnical and Geoenvironmental Engineering 117(9), 1288-1330.

Sims, J.D. and Garvin, C.D., 1995. Recurrent liquefaction induced by the Loma Prieta earthquake and 1990 and 1991 aftershocks: implications for paleoseismicity studies. Bulletin of the Seismological Society of America 85(1), 51-65.

Skempton, A.W., 1986. Standard penetration test procedures and the effects in sands of overburden pressure, relative density, particle size, aging, and overconsolidation. Geotechnique 36(3), 425-447.

Towhata, I., Maruyama, S., Kasuda, K., Koseki, J., Wakamatsu, K., Kiku, H., Kiyota, T., Yasuda, S., Taguchi, Y., and Aoyam,a S., 2013. Liquefaction in Kanto region during the East-Japan gigantic earthquake on March 11, 2011. Soils and Foundations. In Review.

Wang, Y.H. and Tsui, KY., 2009. Experimental characterization of dynamic property changes in aged sands. Journal of Geotechnical and Geoenvironmental Engineering 135(2), 259-270.

Youd, T.L. and Hoose, S.N., 1977. Liquefaction susceptibility and geologic setting. Proc. 6th World Conf.

on Earthquake Eng., New Delhi, India; 6: 37-42.
Youd, T.L. and Perkins, D.M., 1978. Mapping liquefaction-induced ground failure potential. Journal of Geotechnical Engineering 104, 433-446.

V. Publications resulting from Award No. G12AP20002

Green, R.A., Maurer, B.W., Wotherspoon, L., and Cubrinovski, M. (2013). "Implications from liquefaction observations in New Zealand for interpreting paleoliquefaction data in the central U.S." *Nature Communications. In Review.* (Journal Paper)

Green, R.A., Maurer, B.W., Wotherspoon, L., and Cubrinovski, M. (2013). "Recurrent liquefaction induced by the 2010-2011 Canterbury earthquake sequence: implications for paleoseismicity studies." *Engineering Geology*, Elsevier Science. *In Review.* (Journal Paper)

Green, R.A., Maurer, B.W., Wotherspoon, L., Cubrinovski, M., Quigley, M., Bastin, S. (2012). "Use of liquefaction observations in New Zealand for interpreting paleoliquefaction features in the NMSZ." *Seismological Research Letters*, 84(1): 153. (Conference Contribution – Oral Presentation)

Maurer, B.W., Green, R.A., Bradley, B., and Cubrinovski, M. (2013). "Evaluating the efficacy of paleoliquefaction analysis techniques using modern analogs." *Geological Society of America Southeastern Section 63rd Annual Meeting*, April 10-11, 2014, Blacksburg Virginia. *Submitted Abstract.* (Conference Contribution – Oral Presentation)

Maurer, B.W., Green, R.A., Bradley, B., and Cubrinovski, M. (2013). "Field assessment and updating of liquefaction-based paleomagnitude back-analysis methods: a case study of the 2010-2011 Canterbury earthquake sequence." *Engineering Geology*, Elsevier Science. *In Review.* (Journal Paper)

Maurer, B.W., Green, R.A., Cubrinovski, M., and Bradley, B. (2013). "Assessment of aging correction factors for liquefaction resistance at sites of recurrent liquefaction." *10th National Conference on Earthquake Engineering*, July 20-26, 2014, Anchorage Alaska. *In Review.* (Conference Contribution – Full Conference Paper)